EUROPEAN ORGANIZATION FOR NUCLEAR RESEARCH

CERN/SPSC 88–32
SPSC/R76
September, 30 1988

RESPONSE TO QUESTIONS OF SPSC FROM 25.7.1988 (SPSC/0348h)

WA80 Collaboration

GSI Darmstadt
R. Albrecht, R. Bock, H.H. Gutbrod, B.W. Kolb, I. Lund, H.R. Schmidt, T. Siemiarczuk

Lawrence Berkeley Laboratory
A. Franz, P. Jacobs, A.M. Poskanzer, H.G. Ritter

Lund University
G. Claesson, A. Eklund, S. Garpman, H.Å. Gustafsson, J. Idh, P. Kristiansson, A. Oskarsson, I. Otterlund, S. Persson, E. Stenlund

Münster University
P. Beckmann, F. Berger, G. Clewing, L. Dragon, R. Glasow, K.H. Kampert, H. Löhner, M. Purschke, T. Peitzmann, R. Santo, K. Steffens, D. Stüken

Oak Ridge National Laboratory
T.C. Awes, C. Baktash, R.L. Ferguson, I.Y. Lee, F.E. Obenshain, F. Plasil, S. Saini, S.P. Sorensen, M. Tincknell, G.R. Young

VECC–BARC Calcutta
B. Sinha, Y.P. Viyogi

Spokesman: H.H. Gutbrod

Response from WA80 to the questions asked by the SPSC in July 1988

Question 1:

Where is the excess of prompt photons expected at low $p_\perp$ ($p_\perp \leq 0.5$ GeV/c) or high $p_\perp$ ($p_\perp \geq 2$ GeV/c)? What is the expected modification of the γ/π^0 ratio and on which theoretical predictions are the expectations based?

Response to question 1:

There have been fewer theoretical investigations of the expected effect on the direct photon yield resulting from plasma formation than there have been for the corresponding effect on the lepton pair spectra. Both observables, however, are closely related to each other, because the same QCD-diagrams which generate the transverse momentum of lepton pairs also yield real photons with high transverse momentum. In the following we will discuss some specific, if qualitative, predictions in the literature concerning photon production. For early discussions on the hadroproduction of real and virtual photons we refer to a series of articles by *F. Halzen* and *D.M. Scott* [Ha78a,b, Ha80]. (Later these authors also considered direct photon production ($\gamma/\pi^0 \approx 0.3$–0.4) to be a signature of a QGP phase transition in high energy heavy ion collisions.) An unbiased review and discussion on experimental work on direct photon measurements up to 1984 can be found in Ref. [Fe84] by *T. Ferbel* and *W.R. Molzon*.

a) An early study was made by *Shuryak* [Sh78a,b] (see also [Sh74, Sh78c, Sh 78] for related and [Fe62, Fe76] by *Feinberg* for earlier work), who pointed out that the space-time region corresponding to production of particles of transverse mass, $m_\perp = \sqrt{p_\perp^2 + M^2}$, in the range 1 GeV $\leq m_\perp \ll \sqrt{s}$ is rather far from the collision point itself. Reactions taking place at small distances are well described by the parton model and perturbative QCD, for example Drell-Yan production and production of high-$p_\perp$ photons, jets and hadrons. He argues that reactions taking place at larger space-time distances would not be described by the parton model but could still be treated in perturbative QCD.

Shuryak makes the essential point that the known inability of, e.g., Drell-Yan calculations to describe the lepton pair mass region below ≈ 4 GeV/c^2 points to the need to consider processes occurring at later proper times to account for the observed yield, which exceeds the Drell-Yan prediction by 10–100 as lower masses are considered.

If after some proper time interval after the start of a hadronic collision, the system can be treated as being in local thermal equilibrium, it can then be described by a single parameter T which is a function of the space-time coordinates. The production rate for a penetrating particle can be written (see Eq.1 of Shuryak [Sh78a])

$$\sigma = \sigma_{inel} \cdot \int_{T_i}^{T_f} W_a(t)\, \phi(t)\, dt \tag{1}$$

were σ_{inel} is the basic inelastic cross section, $W_a(T)$ is the production rate per unit volume of plasma, expressed as a function of temperature T, and $\phi(T)$ is the so-called temperature 'profile function'. Formally,

$$\phi(T) = \int_{space-time} \delta\left(T(x,t) - T\right) d^3x dt \tag{2}$$

The function $\phi(T)$ scales as $A(s)/T^7$, where $A(s)$ collects the $\sqrt{s}$ dependence. The coefficient of T is actually equal to $(1 + 2/v_s^2)$ where v_s is the sound velocity in the plasma. A value $v_s^2 = 1/3$ for the velocity of sound is expected in the Landau picture for an ideal-gas equation of state, as discussed by Zhirov [Zh78], Shuryak [Sh78b] and McLerran and Toimela [Mc85]. This can be shown to be the case in either a thermodynamical picture in the scaling limit or in a hydrodynamical picture.

The sharpness of $\phi(T)$ with T obviously favors later stages (i.e., lower T space-time regions) of the reaction for production of particles. Shuryak [Sh78a] argues that even in spite of the resulting small Boltzmann factors, $\exp(-m_\perp/T)$, particles with transverse mass even up to 4–5 GeV are thus produced not via hard initial collisions but rather during the plasma stage. However, such a large $m_\perp$ scale allows using perturbative QCD (as α_s is then 'small') so that relations among production cross sections for lepton pairs, high-$p_\perp$ mesons and direct photons can be derived. Shuryak [Sh78a] then presents analytic expectations for lepton pair and direct photon production cross sections (see his equations 2,3) and points out that the ratio of direct photon/lepton pair cross sections should depend only logarithmically on $p_\perp$ under his assumptions about existence of an thermally equilibrated intermediate state. One is led based on these considerations to be careful not to restrict a study of direct photon production in heavy-ion collisions to only low-$p_\perp$ photons. This is most encouraging to an experimentalist seeking to find a way to investigate evidence for plasma formation without being confined to studying only low-$p_\perp$ physics, where the predictive power of QCD is small.

b) A general theoretical study of the emission rates for photons and lepton pairs from a quark-gluon plasma has been made by *McLerran* and *Toimela* [Mc85]. They

show that the rates can be calculated as the thermal expectation values of an electromagnetic current-current correlation function. This correlation function was shown by them to have an invariant-tensor decomposition with structure functions completely analogous to the familiar W_1 and W_2 of deep-inelastic scattering of leptons from hadronic targets. They derived the thermal scaling properties of these new structure functions and showed that at high plasma temperature, a weak-coupling expansion could be used to compute the thermal structure functions themselves. This then leads to analytic expressions for the emission rates which can be used to make quantitative estimates for the emission of real and virtual photons from a quark-gluon plasma. Although these authors then concentrated on an analysis of lepton pair emission, their general framework can be employed to study real photon emission also. McLerran and Toimela pointed out that thermal emission should be dominant in the range of 600 MeV $\leq m_\perp \leq$ 1–2 GeV and that the main spectrum from a plasma should exhibit a power-law dependence. For lepton pairs, the transverse mass spectrum should vary as $dN/dM^2\, dy\, dp_\perp^2 \sim 1/M_\perp^8$, and after integrating over $p_\perp$ should vary as $1/M^4$. They noted the existence of an exponential component in the transverse mass spectrum in addition to the power-law piece, if the phase transition is first-order. They also showed that for a first-order phase transition, there would probably be a strong increase in the photon and lepton pair emission rates as $\sqrt{s}$ or the projectile baryon number were raised through the threshold for plasma production.

This general theoretical treatment has formed the basis for a number of subsequent specific theoretical studies. Continuing from this framework, further specific studies of photon production for the case of nucleus-nucleus collisions have been presented by Hwa and Kajantie [Hw85] and by Sinha [Si83, Si85] and also Ref. [Ra87]. They have considered the problems specific to probing a quark-gluon plasma using lepton pairs and direct photons and have suggested prescriptions that one might follow in preparing and analyzing an experiment.

c) *Hwa* and *Kajantie* [Hw85] concentrate on connecting information about photon spectra (for either real or virtual photons) to information about the putative thermalized state formed in nucleus-nucleus collisions. They point out that if one makes the standard assumptions about a plasma state, namely that it has become thermalized, expands isentropically and exhibits similarity flow in the central rapidity region (i.e., is boost invariant there), then one can use the pion rapidity density as a measure of the entropy density as a function of rapidity. This provides a natural quantity by which to scale the observed cross sections for real and virtual photon production in order to bring out effects that must be due to the formation of a thermalized plasma state. In order to establish the existence of plasma, it is necessary to vary the masses of the nuclei involved and $\sqrt{s}$, all of which vary the (conserved) total entropy in any plasma state formed. The above scaling with the pion rapidity density provides a natural measure with which to relate different measurements.

Hwa and Kajantie then propose the following series of experimental investigations to 'diagnose' quark matter.

1. One would first want to study high $M_\perp$ photons ($M_\perp \geq 5$ GeV) to check that perturbative QCD calculations can reproduce the yield, using structure functions appropriate for nuclei. As lower $M_\perp$ is approached, one looks for an excess not described by this direct mechanism.

2. Next, one would like to look at the virtual photon yield to see that the excess depends only on $M_\perp$ and not M or $p_\perp$ separately.

   The expected yield for photons from quark matter should decrease as a power of $M_\perp$, for $M_\perp$ values in the range of $T_c \leq M_\perp/k \leq T_i$, and decrease exponentially for $M_\perp/k \gg T_i$. Here k is 5.5 for virtual photons and 3.5 for real photons, T_c is the critical temperature separating the quark-gluon plasma and hadron-gas phases, and T_i is the initial temperature reached in the reaction at some initial proper time, τ_i at which the thermodynamic description is first reasonable to use. To illustrate these limits with numerical values, Hwa and Kajantie suggest the case of $^{16}O+(heavy target)$ such that $dN^\pi/d\eta$ is 42, which corresponds roughly to the charged-particle pseudo-rapidity density observed in the WA80 experiment for E/A=200 GeV ^{16}O + Au average events at η=3. They then suggest the following values: (i) initial: $\tau = 0.1$ fm, $T = 320$ MeV, $\varepsilon = 17$ GeV/fm^3; (ii) end of quark phase/start of mixed phase: $\tau = 0.8$ fm, $T = T_c = 160$ MeV, $\varepsilon = 1.4$ GeV/fm^3; (iii) end of mixed phase/start of hadronic phase: $\tau = 9.8$ fm, $T = 160$ MeV, $\varepsilon = 0.1$ GeV/fm^3; and (iv) end of hadronic phase: $\tau = 14$ fm, $T = m_\pi = 140$ MeV, $\varepsilon = 12\ m_\pi^4$.

   They note that the mixed phase lasts for such a long proper time because the velocity of sound is zero in that phase, so the transverse rarefaction wave cannot propagate; the longitudinal expansion is solely responsible for reducing the energy density in this phase. In the hadronic phase, the transverse rarefaction wave again propagates, spoiling the longitudinal-boost-invariant pattern.

   With these values for T_i and T_c, one should look for real photons from plasma to follow a power law in the range of 0.56 GeV to 1.12 GeV (if one observes the above inequality strictly) and one should look for an exponential fall-off of the spectrum with larger $p_\perp$. To observe the latter requires measurements up to $p_\perp = 2$ GeV/c or more. Obviously, a larger range needs to be covered in order to have a sample of events at very high $M_\perp$ to check the connection to perturbative QCD and initial hard-scattering and at lower $M_\perp$ to check the yield expected from hadron gas phase, as well as to allow for a large range of possible T_c, T_i values. This result again points to the need to cover $p_\perp$ values for real photons up to several GeV/c, as well as below 1 GeV/c.

3. One can then look for an increase of the first and second moments of the $p_\perp$ distribution as a function of the pion rapidity density. If quark matter is formed,

a scaling with the square of the pion rapidity density is expected. If this is found, one can then search for adiabatically expanding quark matter by seeing if the numerical predictions made based on those assumptions indeed agree with observed cross sections. Hwa and Kajantie point out that the dependence on T_i becomes weaker with increasing T_i; the dependence finally vanishes for very large T_i, although it is not clear that such T_i can be reached experimentally.

Hwa and Kajantie [Hw85] also point out that the basic equations governing the production of virtual and real photons are quite similar for the two physically different regimes of direct and thermal production. The product of structure functions in the equation for direct production is replaced by the entropy squared (or the square of the pion rapidity density) of the expanding thermalized system. This again reflects the point made by Shuryak [Sh78a, Sh78b] and also by Zhirov [Zh78], that perturbative QCD can be used to calculate cross sections in both cases, but the space-time region available for formation of real and virtual photons must be accounted for differently, resulting in differing production rates.

Hwa and Kajantie [Hw85] point out that the main experimental controls that one has available are the masses of the interacting nuclei, $\sqrt{s}$, and the pion rapidity density. The pion rapidity density provides an experimental control of the system's entropy, which should be a constant of the motion during the expansion of the plasma. The other variables allow the variation of the initial temperature of the system. It is known from the early heavy-ion experiments at the SPS that varying $\sqrt{s}$ provides the best method to vary the energy density and thus the initial temperature. The observed large range of transverse energies reflects mainly the geometry of the collision. In contrast, the initial comparisons at bombarding energies of $E/A = 60$ and 200 GeV of transverse energy and entropy density (given as *charged particle rapidity density*/$A^{2/3}$ by the WA80 collaboration), showed that the larger bombarding energy led to roughly a factor of two increase in energy density and entropy density. It thus is important to be able to vary the range of temperatures studied by using more than one bombarding energy. We have requested $E/A = 60$, 120 and 200 GeV, which spans the useful range delivered by the SPS for heavy-ion beams.

d) The work of *Sinha* [Si83, Si85] and of *Raha* and Sinha [Ra87] has concentrated on studying the behavior of the ratios of the invariant cross sections for real photon, μ-pair and π^0 production. Following on the work of Domokos and Goldman [Do81], the production rates of photons, lepton pairs and mesons are determined by integrating the basic production cross sections over the thermal history of the reaction. The photon and μ-pair production cross sections are found to scale as T^4, as expected for a Stefan-Boltzmann gas. In addition, their ratio is found to be constant (with a value around 100 - see Eq. 9 of Sinha 83) for the plasma phase. The production of μ-pairs from the hadronic phase is expected to rise more rapidly with T than T^4,

whereas the production of photons will depend on the density of π -mesons, which does scale as T^4. The ratio of photon to μ-pair cross sections is thus expected to fall rapidly with increasing T of the fireball produced until a transition to a plasma state is reached. At that point the basic production cross sections for photons and μ-pairs will be given by the Born level QCD graphs (to first order), meaning that the cross section ratio will exhibit a constant behavior with further increases in T.

Sinha [Si83, Si85] points out that the above result is independent of the space-time evolution of the plasma or of its baryonic chemical potential. Thus he proposes it as a universal signal of quark-gluon plasma formation that may be used to examine either the baryon free central region or the baryon rich high/low rapidity region. Sinha and Raha [Ra87, Si86] examine the behavior of the γ/π^0 and the γ/μ-pair ratio as a function of $p_\perp$ of the particles in question. Nearly the entire variation with $p_\perp$ is predicted by them to take place for $p_\perp$ values less than 2 GeV/c, with a much greater variation with $p_\perp$ expected for a system in a hadronic or mixed phase. They also do not expect a marked change in the $p_\perp$ behavior of the γ/π^0 ratio in going from a mixed phase to a plasma phase, predicting only about a factor of two, in contrast to the several orders of magnitude change predicted for the γ/μ-pair ratio. These authors thus suggest measuring both the μ-pair and the direct photon cross sections as a function of $p_\perp$ in the range from 0–5 GeV/c. They suggest that measuring the behavior across this whole region is the best way to demonstrate the existence of a plasma; i.e., the production ratio must be independent of temperature not only for a small region of phase space. From a comparison the ratio $\pi^0/\mu^+\mu^-$ with $\mu^+\mu^-/\gamma$ they extract a ratio $\gamma/\pi^0 \approx 0.3$–0.4 for $p_\perp \geq 3$–4 GeV/c for a QGP formation. They also point out the need to make measurements up to about $p_\perp = 5$ GeV/c, in order to have a connection to cross sections that should be calculable assuming direct production described by perturbative QCD.

Summary of a) - d):

To summarize, the theoretical work suggests the following properties for an experiment measuring direct photon emission in nucleus-nucleus collisions.

1. It should cover a range in $p_\perp$ from at least 0.5 GeV/c to 4–5 GeV/c in order to measure the cross sections from hadron-gas, mixed and plasma phases and be able to relate these in the same experiment to cross sections calculable as direct processes in perturbative QCD. The ability to measure absolute cross sections is needed to test specific predictions regarding rates, and to make comparisons with measurements of lepton pair production cross sections. It should be expected that photons arising from plasma appear at $p_\perp$ values even as large as 1–3 GeV/c. It is expected that the 'window' in $p_\perp$ for real photons from a plasma state is in the range of 0.5–3 GeV/c, to be above the hadron gas background and clearly below the QCD hard-scattering region.

2. The experiment should be able to acquire sufficient statistics to distinguish a power law spectrum, expected for emission from plasma at temperatures between the initial and critical temperatures, and the exponential spectrum expected from mixed phase emission.

3. The experiment should be able to measure charged particle rapidity densities, in order to have a handle on the entropy if a plasma is formed, and should have an independent means of selecting central collisions, such as a Zero-Degree-Calorimeter. Cross sections normalized by the square of the pion rapidity density are expected to depend only on $M_\perp$ and T_i for plasma emission; for T_i large enough the result should only depend on $M_\perp$ (doubtful at SPS energies).

4. The experiment should have a means of varying the initial temperature of any plasma phase, in order to observe the expected scaling behaviour for a high-temperature plasma, as well as any transition to behavior characteristic of a thermalized system. The apparent best method for doing this is to vary the center-of-mass energy by a sizeable step, such as a factor of two, based on earlier results from the CERN and AGS heavy-ion programs. An additional check of this is to vary the projectile mass, again preferably by a factor of two or more.

5. The experiment should be able to measure prompt photons above background in the suggested 'plasma window' (i.e. 0.5–3 GeV/c) down to the 'no-plasma' level of $\gamma/\pi^0 \leq 0.05$ [Ba86].

Question 2:

What is the p and $p_\perp$ range (for γ's, π^0's, η's) accessible with the present experimental set-up?

Response to question 2:

2.1 Design Considerations

The SAPHIR detector (an artist's view is shown in Fig. 1) was designed to measure photons and π^0's of transverse momenta larger than 1 GeV/c in the rapidity region corresponding to the effective center of mass of asymmetric nuclear collisions at E/A = 60 and 200 GeV. In the selected rapidity region $1.5 \leq \eta \leq 2.2$ a good π^0-mass resolution requires both a good energy resolution as well as a good spatial resolution. The error in the invariant mass can be written as:

$$\frac{\sigma_{M_{\rm inv}}}{M_{\rm inv}} = \sqrt{\left(\frac{\sigma_{E_1}}{2E_1}\right)^2 + \left(\frac{\sigma_{E_2}}{2E_2}\right)^2 + \left(\frac{\sigma_\psi}{2 \cdot \tan(\psi_{12}/2.)}\right)^2} \qquad (3)$$

E_1, E_2 : *decay photon energies*
ψ_{12} : *decay photon opening angle.*

Fig. 2 displays the contributions of the 'energy term' and the 'angular term' to the total error as a function of $E(\pi^0)$ (assuming symmetric decays) and $p_\perp(\pi^0)$ for different rapidities. In the present set-up and the investigated $p_\perp$ region one finds the total resolution to be close to the minimum of the summed contributions. (However, if one wants to focus on larger rapidities, e.g. when studying equal mass collisions like Pb on Pb, then the spatial resolution gets the dominant factor in the π^0-mass resolution, whereas for smaller rapidities, e.g. when measuring at low $\sqrt{s}$, the energy resolution must be as good as possible.)

A good spatial resolution is coupled to a small Moliere-radius, $R_M \sim X_0$ (X_0 = radiation length) of the detector and a fine sampling of the shower profile. A small Moliere radius is also needed to keep the shower-size small in view of the large particle density encountered in nuclear collisions. The lead-glass detector SAPHIR based on the GAMS design represents the optimal solution for detecting photons in the rapidity window chosen. With it's granularity it provides good spatial resolution, a good energy resolution, it allows a lateral shower profile fitting, it permits fast timing for a hardware trigger, suppression of soft particles by the Cherenkov threshold (E^p_{thresh} = 230 MeV), and of charged particles by a 98 % efficient charged particle veto detector

Table 1: SAPHIR construction items and performance

Material:	1278 lead glass modules SF5
Module cross section:	$35 \times 35\,\mathrm{mm}^2$
Module length:	460 mm $\equiv$ 18 radiation lengths
	(98 % containment for 30 GeV photons)
Total (rectangular) area:	$98 \times 171.5\ \mathrm{cm}^2$
Energy resolution:	$\sigma_E = E\,(6/\sqrt{E/\mathrm{GeV}} + 0.4)\%$
Spatial resolution:	$\sigma_x \leq 3mm$ for perpendicular incidence
	$\leq 5\,mm$ for 15^0 inclined incidence
Minimal shower distance:*	$57\,mm$ on average
Gain stability:	$(0.5 \pm 0.6)\%$
Dynamic range:	0.05 to 25 GeV
Minimum ionizing signal:	540 MeV photon equivalent

* will be lowered to $\approx 35\ mm$ in future shower fitting procedures currently under development.

in front. (We are well aware that an additional longitudinal shower sampling would be very advantageous if there is no loss in resolution. This information is in part accessible because of the non-projective geometry of the detector surface relative to the position of the target.)

Alternative designs have been studied and prototypes built. Among the homogeneous materials, BGO and NaI have been ruled out not only because of their price (about 20 times the price of lead-glass for a corresponding acceptance), but also by the long decay time and the high efficiency for low energy photons. Scintillator glass is only three times slower than lead-glass but has a larger radiation length which, at constant distance, translates to a worse position resolution and to a higher probability for overlapping showers for a given particle density. Among the sampling calorimeters the 'high density projection chamber' (HPC) has been looked at, but due to the low rate and the poor energy resolution it has been considered not adequate for the task in a fixed target experiment at this rapidity and energy. For the future lead-beams photon measurements at larger rapidities are being discussed, and high rate sampling EM-calorimeters of the 'Spaghetti' and the 'Lasagne' type are studied for a position resolution of about 1 mm as well as simple depth sampling calorimeters.

The construction items and performance values that have been achieved with the SAPHIR detector are listed in Table 1. They are found to be mostly in agreement with the design specifications. Geometrical details of the present set-up are shown in Fig. 3. Table 2 shows a compilation of the present cuts and limits that have been used in the SAPHIR data analysis.

The details leading to these restrictions in the acceptance are presented in the following.

Table 2: Momentum ranges used in current SAPHIR data analysis

momentum range of γ's:	$0.4 \leq$	p	≤ 25	GeV/c
$p_\perp$-range of γ's at 12^0:	$0.083 \leq$	$p_\perp$	≤ 5.2	GeV/c
$p_\perp$-range of γ's at 25^0:	$0.169 \leq$	$p_\perp$	≤ 10.6	GeV/c
$p_\perp$-range of π^0 (center):		$p_\perp$	≥ 0.4	GeV/c
$p_\perp$-range of η (center):		$p_\perp$	≥ 2.0	GeV/c

2.2 Calibration and energy resolution

A detector depth of 18 radiation lengths was chosen in order to provide a containment of more than 98 % of an electromagnetic shower of 30 GeV, so that shower leakage is expected to have negligible influence on the energy resolution. On the other hand, the length of the lead glass towers does not lead to a too large Cherenkov light absorption. Thus the energy resolution is mainly due to statistical fluctuations in the detection process.

Measurements with electron beams have been carried out at DESY with a prototype detector and at the X1-beamline spectrometer at the CERN-SPS with the complete SAPHIR. At X1, each lead glass module was calibrated with a 10 GeV electron beam. In addition, data were taken with 4 and 20 GeV electrons and, in order to investigate the response to hadronic showers and minimum ionizing particles, with a mixed hadron beam (p and π^+). Electron beams down to 1 GeV available at DESY allowed to check especially the low energy calibration.

The calibration function, shown in Fig. 4 turned out to deviate from a strictly linear behaviour for low energy electrons due to the influence of light absorption and threshold effects. Low energy showers do not penetrate as deep into the detector as high energetic do, so that the mean distance the Cherenkov light has to travel to the phototube and thereby the absorption loss increases. The energy response of the detector could be well parameterized with the empirical power law of the form:

$$R(E) = a \cdot E^{1+\delta} + b \tag{4}$$

In our case a parameter $\delta = 0.02$ was found.

The absolute energy calibration is maintained over the long running periods by a N_2 laser based reference system accompanied with a set of three ^{241}Am doped NaI(Tl) light pulsers serving as a light standard as well as by a cosmic-ray monitor identifying the minimum ionizing μ's. This cross checking is done, because NaI crystals are well known to get deteriorated on a time scale of several month by radiation damage and water admission. The redundant information also allows to check the quality of the reference system itself. It was found to be stable to a level of $\sigma = 0.22\,\%$ over a period of 420 hours (see Fig. 5).

Electromagnetic showers were found to spread over up to 16 modules with a light distribution depending strongly on the hit position relative to the module boundaries as well as on the angle of incidence. For a central position and normal angle of incidence, 80 % of the energy is contained in the hit module itself, decreasing to about 40 % for the marginal positions on the module front face. The shape of the shower light distribution depends only weakly on the energy E of the incident particle. E is calculated from the sum of the signals with a resolution of:

$$\frac{\sigma}{E} = 0.4\,\% + \frac{6\,\%}{\sqrt{E/\,\mathrm{GeV}}} \tag{5}$$

revealing the dominant influence of the Poisson law for particle number fluctuations via the energy dependence.

Figure 6 shows the spectral shape of electromagnetic and hadronic showers and their minimum ionizing signals. Since the depth of lead glass corresponds to only one interaction length for hadrons, their shower signals fluctuate strongly and are in general much lower than the signals from electromagnetic showers of comparable energies. The pulse height generated by minimum ionizing particles is equivalent to a photon shower of about 540 MeV.

2.3 Position resolution

The high granularity of the lead glass allows to obtain the position of incidence from the light distribution in the involved modules. This calculation is done in the following steps:

The center of gravity, x_p, of the pulse height distribution is computed. This is a biased estimate of the actual center of gravity, x_s, of the shower, because the modular structure of the detector is folded in. The relation between x_p and x_s can be approximated as:

$$x_s = a_1 \cdot \mathrm{arsinh}\left(\frac{x_p}{a_2}\right) \tag{6}$$

for perpendicular incidence, as was already pointed out by [Ak77]. For the needs of the WA80 experiment this correction function could be generalized for non-perpendicular incidence. Taking into account the position offset between the center of gravity x_s and the point of impact x_i, the position can be obtained from the function:

$$x_i = a_1 \cdot \mathrm{arsinh}\left(\frac{x_p - a_3}{a_2}\right) + a_4 \tag{7}$$

using the first moment x_p of the pulse height distribution. Results are shown in figure 7. The a_i are smoothly varying functions of the angle of incidence. Using this approximation as a starting point, the final position value is found by fitting a

simulated shower light distribution to the measured shower. The fitting is also part of the particle identification algorithm. This procedure yields a position resolution of 5 mm for an angle of incidence of 15 degrees, which represents the worst case, improving to about 3 mm for perpendicular incidence.

2.4 Photon identification

The lateral size of the lead-glass modules corresponds to $(0.8 \times 0.8)R_M$, so that electromagnetic showers deposit their energy into more than one module. A typical hit pattern of a central 200 AGeV O+Au event is shown in Fig. 8. The relative amount of the contained energy depends on the total shower-energy, angle of incidence, and on the hit position relative to the module boundaries. An area of adjacent modules with a photomultiplier signal above threshold ($\simeq$ 40 MeV) is called a 'cluster'. Each event is analysed in the following way:

i) The pulse height of the modules distribution is subdivided into clusters;

ii) Clusters are classified as charged or neutral hits via the assignment made by the charged particle veto detector (detection efficiency is $\simeq$ 98%);

iii) If a cluster consists out of at least 3 modules with a corresponding minimum photon energy $\sum_i E_i \geq 400$ MeV, its pulse-height distribution within the cluster is compared with that of a calculated model shower via a χ^2-test. This procedure allows to distinguish a single electromagnetic- from a hadronic shower as well as from the overlap of two showers of any combination (hadronic and electromagnetic).

The calculation of the reference distribution of showers is based on the parametrisation of T. Gabriel [Ga80] for electromagnetic showers. It has been checked to be consistent with the measured energy deposition of electrons from the calibration runs taken at DESY and at the $X1$ beamline at the CERN SPS. In the fitting-algorithm which compares the two showers, a combination of a gradient search and a parabolic extrapolation of χ^2 is applied. This procedure of shower comparison breaks down at very low cluster energies where only few modules are involved in the shower development. Thus, a lower limit on photon energies of $E^{\gamma}_{min} = 400$ MeV has been imposed on all the data. Multiplicity distributions of reconstructed photons are shown in Fig. 9 together with the total number observed hits in SAPHIR from O + Au collisions at 200 AGeV.

The photon reconstruction efficiency, ε_γ, is determined from the actual data by calculating the invariant mass, $M_{\gamma\gamma}$, of one photon - called the trigger-photon - and *all* other groups of particles in the same event. The trigger-photon has to fulfill

the requirement to appear as a well isolated shower with a minimum transverse momentum of 0.5 GeV/c ($\hat{=}$ energy $\approx$ 2 GeV). For $\varepsilon_\gamma = 100\%$ one would expect to observe a π^0-peak only in the mass spectrum filled by the group of $\gamma-\gamma$ combinations; the appearance of a distinct π^0-mass peak in the combinations of the trigger-photon with any other group of particles would reveal false assignments of 'real' photons. For example, one immediate source of 'misidentification' is the conversion of a decay photon in dead material in front of the detector. Such a converted decay photon - classified thereby as *charged* EM-shower - would still combine with the second decay photon to the π^0 mass. With the realistic assumption that the photon identification is not biased for the π^0 decay photons, the reconstruction efficiency is then determined by the ratio of the π^0 peak areas $A_{\gamma,m}$ taken from the different invariant mass spectra with the particle combinations γ, m:

$$\varepsilon_\gamma = \frac{A_{\gamma,\gamma}}{\sum_m A_{\gamma,m}} \tag{8}$$

with $A_{\gamma,m}$ being the π^0 peak area for the combinations of the trigger-photons γ with particles of type m.

In Fig. 10 ε_γ is shown as a function of $p_\perp$ for events of 200 AGeV O + Au, selected for peripheral and central collisions, respectively. A principle limit of reconstruction efficiency is given by the loss of photons due to conversion in dead material in front of the detector (vacuum chamber, streamer tubes, target, and air) which amounts to 6 % (4.4 %) for the Au (C) target. This theoretical limit is not totally reached in the present analysis of the data; for low multiplicity events and $p_\perp \geq 1$ GeV/c one reads a average value of $\varepsilon_\gamma = 0.863 \pm 0.012$, while selection of high multiplicity data reduces the efficiency to 0.778 ± 0.015. This effect can be understood by the higher multiplicities of charged particles and photons on SAPHIR's surface, which increases the overlap probability of two showers and thereby the probability of misidentifications. In addition, a slight increase of ε_γ towards lower $p_\perp$-values is observed. This can again be understood in the same way as before, namely for high energetic photons the energy is spread over more SAPHIR modules (up to 16 modules depending on angle of incidence and hit position relative to the module boundaries), hence the possibility for shower overlap or for accidental identification as a charged particle increases. In the present analysis a conservatively large and safe region around an electromagnetic shower was demanded to be free of any charge signal. The efficiency is therefore expected to reach a higher level when more sophisticated shower-analysis techniques are applied, which are currently being developed.

2.5 Hadron misidentification

This subject is currently under detailed investigation, both by using measured hadron-data from calibration runs as well as by means of Monte-Carlo simulations. The

simulations are being carried out with the GEANT-package and the computer code for hadronic shower simulation of T. Gabriel [Ga80].

According to the interaction length of SAPHIR ($\simeq 1\lambda$) about 40% of charged hadrons deposit only their minimum-ionizing energy (1 MIP $\cong$ 540 MeV γ-energy equivalent) in the detector, the remaining 60% of high energy hadrons begin to start a hadronic shower in the lead-glass with largely fluctuating energy deposition (see Fig. 11). This simulated response is then run through the same chain of programs (shower-analysis, etc.) as is done with real data.

Hadrons entering the finely granulated lead glass array are then rejected by the following methods:

- The investigation of the lateral shower distribution in the range $1 \leq p_{hadr} \leq 10$ GeV/c reveals that in the worst case 15 % of the hadrons starting a shower are compatible with an electromagnetic shower. This is mainly due to fluctuations in the hadronic shower development leading to a large π^0 fraction and thereby to a large amount of EM-energy in the hadron induced shower. A momentum dependent correction function $f(p)$ was determined which describes the probability of hadron 'leak-through' in the EM-shower requirements of the shower algorithm. It is found to decreases with decreasing hadron momentum p and, for example is $f(10\ \text{GeV/c}) = 0.15$.

- The energy deposition of hadronic showers within the detector depth of one interaction length is on the average 13 % of full energy. The corresponding response function $h(p)$ was deduced and is applied for the background estimation.

- Charged hadrons are detected by the multiplicity arrays in front of SAPHIR with an efficiency of 98 %.

The largest contribution to the photon contamination originates from charged pions. Their response is essentially given by the charged particle distribution measured with SAPHIR. This distribution needs to be corrected for photon conversion, i.e. diminished by 6 % of the inclusive photon yield. It is then further reduced according to a factor $0.02 \cdot f(p)$ taking into account the 2 % inefficiency of the charged particle veto and the misidentification probability due to shower fluctuations. The resulting distribution is shown in figure 12 labeled $(\pi^+ + \pi^-)$ and falls at least 3 orders of magnitude below the inclusive photon signal.

The proton response is estimated by taking the NA35 results [St88] for proton cross section in heavy ion reactions at midrapidity, folding these with the hadron response function $h(p)$ in SAPHIR and multiplying again by $0.02 \cdot f(p)$, see figure 12 curve labeled (p).

The neutron production rate is taken to be equal to the proton rate. The neutron

signal faking a photon is therefore 50 times more frequent than the proton signal because of the missing charge veto. Nevertheless, the neutron curve (n) is still found below the charged pion signal in figure 12.

We are aware of an uncertainty as large as a factor 5 in this estimate of the baryon contamination. This is mainly due to the rather uncertain proton cross sections. Nevertheless, we can conclude from the above analysis, that the amount of fake photons originating from misidentified hadrons is negligibly small, i.e. $\leq 0.1\,\%$ of N_γ^{incl} (see equation 18, chapter 4.1) above $p_\perp \simeq 0.5\,\mathrm{GeV/c}$.

2.6 π^0-reconstruction and acceptance calculations

The π^0 meson decays with a branching ratio of $(98 \pm 0.03)\%$ in two photons. It is a pseudo-scalar particle, so there is no preferred direction of the photons in it's own rest frame. Thus, a Monte Carlo can simply consider an isotropic distribution in the π^0's rest frame and then calculate the corresponding energies and the opening angle of the decay photons in the lab. system where they fulfill the following equation:

$$m = \sqrt{2 \cdot E_1 \cdot E_2 \cdot (1 - \cos\psi_{12})} \tag{9}$$

m : *π^0 rest mass*
E_1, E_2 : *decay photon energy*
ψ_{12} : *decay photon opening angle.*

A 100 % efficient reconstruction of π^0's according to Eq. 9 is only possible if both photons were recorded in each event, hence requiring an ideal 4π detector with no low energy threshold for photons. However, a real detector still permits to reconstruct a certain amount of the decaying mesons. Knowing the low energy cutoff of this detector and its geometry, one then can make precise corrections for the 'lost' decays.

There are two competing ways to lose showers:

- asymmetric decays and/or low energy π^0's get lost due to the low energy threshold of the detector and by their large opening angles of the decay photons, while
- symmetric decays and/or high energy π^0's get lost due to the minimum shower separation distance.

As the rapidity, Y, and $p_\perp$ decrease, the asymmetry cutoff hurts more, while as Y and $p_\perp$ increase, the two-shower cutoff hurts more. Thus, one needs to build a system, where the two problems do not exclude all acceptances.

The acceptance we will define here as:

$$A = \frac{\text{number of decays where both photons are detected}}{\text{number of parents for all azimuths}} \tag{10}$$

and is shown in Fig. 13 for the present SAPHIR set-up in form of linear contour lines for π^0 and η mesons in the polar angle ϑ versus $p_\perp$ plane. For π^0's it is found to be maximal in the $p_\perp$ region above $\simeq 1\,\mathrm{GeV/c}$ up to 4–6 GeV/c, depending on the polar angle ϑ. In this region more than 88 % of all π^0's heading the detector surface can be identified. Figure 13c shows the same acceptance integrated over the solid angle of the detector.

The influence of the low energy cutoff of 400 MeV in the photon energy to the acceptance is shown in Fig. 14, where the distribution in energy asymmetry, defined as

$$\alpha = \frac{|\,E_1 - E_2\,|}{E_1 + E_2} \tag{11}$$

is plotted for different rapidities and transverse momenta. Each plot has three curves. The solid one shows the distribution in α for all decays at the given Y and $p_\perp$. The dashed line shows the distribution in α for decays where both photons are accepted, and the dashed-dotted line shows the α-distribution of the decays lost due to the 400 MeV low-energy cutoff. As expected, the cutoff takes away only the most asymmetric decays, but where it starts discarding events as a function of α is quite dependent on Y, $p_\perp$ and the parent's mass. The plots are given normalized per 0.04 unit bin in α, so that the integral of the distribution is unity. The ratio between the dashed and solid lines is then the acceptance for that value of Y , $p_\perp$, and α. The maximum value of α where both photons can be observed, can be written as

$$\alpha_{max} = 1 - 2 \cdot \frac{E^{\gamma}_{cut}}{E_{\pi^0,\eta}} \tag{12}$$

Above this value *all* events are lost. The smooth decrease in acceptance towards α_{max} at values of low $p_\perp$ is due to the enlarged opening angle ψ_{12} which increases the probability for loosing one of the two decay photons. Thus, it is obvious that the energy threshold always provides a clean cut bias against the asymmetric decays, while the larger opening angle leads to a smooth decrease of the acceptance.

The upper limit of the π^0 (and η) momentum range is determined by the minimum resolvable shower distance of the detector. The minimum opening angle of a meson decaying into two photons is given by

$$\psi_{min} = 2 \cdot \arctan\left(\frac{m_0}{p}\right) \tag{13}$$

and is shown in Fig. 15 for π^0 and η mesons. Expressed in terms of the detector distance, D, from the target and the minimum resolvable shower distance, d_{min}, it can be written as

$$p_{max} = 2 \cdot m_0 \cdot \frac{D}{d_{min}} \tag{14}$$

This formula is strictly true only for symmetric decays, asymmetric decays can still be observed with reduced acceptance up to higher momenta. With the present configuration of the detector ($D = 3.425\,\mathrm{m}$) and a conservative value for the minimum two-shower separation distance by 57 mm, this results in $p^{\pi^0}_{max} \simeq 16\,\mathrm{GeV}$. This upper limit is clearly visible in the two-dimensional acceptance plot in Fig. 13.

The hadron misidentification does not play a role for the reconstruction of π^0-spectra, because a hadron misidentified as a photon can never contribute to the π^0-peak in the invariant mass spectrum, it influences only the shape of the combinatorial background. However, the photon reconstruction efficiency, ε_γ, changes the contents of the π^0-peak. In first order approximation the π^0-reconstruction efficiency, ε_{π^0}, is influenced by this effect quadratically, i.e. $\varepsilon_{\pi^0} \simeq \varepsilon_\gamma \cdot \varepsilon_\gamma$. The spectra of reconstructed π^0's (and η's) as well as the observed γ/π^0-ratio need to be corrected for this inefficiency as a function of $p_\perp$.

Figure 16 displays invariant mass spectra in different bins of $p_\perp(\gamma\gamma)$ for 200 AGeV $^{16}\mathrm{O} + \mathrm{Au}$ collisions, selected for central and peripheral reactions, respectively. The widths of the π^0 peaks of 5–8 $\mathrm{MeV/c^2}$ are consistent with the energy and position resolution of SAPHIR (see Fig. 2). By fitting the combinatorial background via a third order polynomial and subtracting this background from the mass spectrum the number of π^0s measured in the corresponding $p_\perp$-bin is obtained. The resulting π^0 transverse momentum distribution has to be corrected with the $p_\perp$ acceptance function in order to obtain the final π^0 $p_\perp$-spectrum. Table 3 shows a compilation of the number of photons, π^0's and η's measured and reconstructed, respectively, from the total amount of $2.1 \cdot 10^6$ events.

2.7 η-reconstruction

The discussion in the previous section about the π^0 reconstruction and acceptance calculation applies as well for the heavier η-meson. The only difference is the ≈ 4 times heavier rest mass of the η meson, which increases the average opening angle ψ_{12} roughly by the same factor, according to Eq. 13. In the present set-up, this results in a strongly reduced geometrical acceptance at low values of $p_\perp$ (Fig. 13), i.e. the acceptance is negligible below $p_\perp = 1\,\mathrm{GeV/c}$. Merging of the two decay photons into one single shower does not occur in the $p_\perp$-range up to about 20 GeV/c (center of SAPHIR-I).

We have been able to identify η-mesons from collisions of 200 AGeV O+Au in the $p_\perp$ bin 2.0 GeV/c $\leq p_\perp \leq$ 2.4 GeV/c (Fig. 17). At lower $p_\perp$ the present acceptance is too poor, so that a distinct η-peak cannot be observed above the combinatorial background in the invariant mass plot, whereas at higher $p_\perp$ the present statistics is too poor. In the $p_\perp$-region under consideration here, about 300 η's have been identified (see Table 3) using the full sample of $2.1 \cdot 10^6$ events, translating to an

η/π^0-ratio of $(77 \pm 24)\%$.

Table 3: Approximate statistics of photons ($E_\gamma \geq 400\,\mathrm{MeV}$), π^0's ($p_\perp \geq 0.5\,\mathrm{GeV/c}$), and η's ($2.0\,\mathrm{GeV/c} \leq p_\perp \leq 2.4\,\mathrm{GeV/c}$) measured with SAPHIR for $^{16}\mathrm{O}$ + Au reactions at 200 AGeV.

# evts:	*Total* ($2.1 \cdot 10^6$)	*Peripheral* ($0.46 \cdot 10^6$)	*Central* ($1.47 \cdot 10^6$)
photons	$7.2 \cdot 10^6$	$908 \cdot 10^3$	$6.8 \cdot 10^6$
π^0's	$290 \cdot 10^3$	$42 \cdot 10^3$	$220 \cdot 10^3$
η's	300	—	—

Question 3:

If the signals were to be found at low $p_\perp$, is it possible to observe signal in the charged to neutral ratio ($\pi^\pm/\pi^0$) as proposed in paper by Halzen and Liu?

Response to question 3:

We would like to point out that this question needs a small modification to avoid a misunderstanding: the proposed charged to neutral ratio does not refer to the ratio between $\pi^\pm/\pi^0$, but rather $\pi^\pm/apparent\ \pi^0$, as explained next.

If direct photons are produced abundantly from quark matter, especially at low $p_\perp$, then it may be possible to obtain experimental evidence for such photons indirectly by calorimetric measurements as suggested by Halzen and Liu [Ha82]. According to these authors, the energy fraction deposited into photons from quark matter may be as large as 25–40% of the total radiated energy. Evidence for such photons would be signalled by a ratio for electromagnetic to hadronic energy observed in the calorimeters, which was larger than expected based on isospin equality between the pions. Such an analysis can be made using the present calorimeters of WA80 and is planned for the data which have been obtained already. The procedure would be to compare the ratio of electromagnetic to hadronic energy for the most violent events with those events in which quark matter would not be expected. It should be remarked that the WA80 calorimeters were specifically designed with an EM section of 15 radiation lengths to obtain good separation of electromagnetic energy by insuring nearly complete containment of the electromagnetic energy within the EM section.

The major source of uncertainty in such an analysis would arise from the variation of the fraction of the hadronic energy deposited in the electromagnetic section of the calorimeters with incident particle energy. The ratio of apparent electromagnetic to hadronic energy might vary therefore due to simple variations in the pion spectra with event type. Although such an analysis might provide indirect evidence for increased direct photon emission, it would be important to verify this by comparison of the neutral spectra, as measured with SAPHIR in WA80, to charged pion spectra. Furthermore, the number of photons and reconstructed π^0's in SAPHIR compared with the number of charged particles measured in front of SAPHIR provides independent information. However, as is the case for the extraction of the EM/hadronic-energy, there is no direct possibility to distinguish between $\pi^\pm$ and charged baryons. For a correction of this effect one could apply cross section ratios of π^-/p, as they have been measured already.

Question 4:

Evaluation of the number of direct photons (N_γ^{direct}) as function of $p_\perp$:

$$\begin{aligned} N_\gamma^{direct} \;=\; N_\gamma^{obs} &- \frac{N_{\pi^0}^{obs}}{\varepsilon_{\pi^0}} \cdot \textit{prob. } (1\ \gamma \textit{ from } \pi^0) \\ &- \frac{N_\eta^{obs}}{\varepsilon_\eta} \cdot \textit{prob. } (1\ \gamma \textit{ from } \eta) \\ &- \frac{N_X^{obs}}{\varepsilon_X} \cdot \textit{prob. } (1\ \gamma \textit{ from } X, X = \eta', \omega ...) \\ &- \textit{BGD from misidentified hadrons} \\ &- \textit{BGD from beam halo} \end{aligned} \tag{15}$$

What are the errors (stat. and system.) contributing to each term for p, ^{16}O and ^{32}S data? (p-N data are expected to be the reference data sample where no excess of direct photons is expected).

What is the resulting total error on the γ/π^0 ratio?

Since there is a difference expected between various types of collisions (including central and non-central) is the procedure simplified by that effect? (Cancellation of system. errors?)

Response to question 4:

4.1 Calculation of the γ/π^0-ratio

The observation of direct photons is usually obscured by photons from meson decays and other background faking a single photon signal. Thus the quality of the direct photon signal depends sensitively on the quality of the meson reconstruction and the background evaluation. In the $p_\perp$ range $0.5 \leq p_\perp \leq 5$ GeV/c under consideration here the $\gamma\gamma$ invariant mass resolution depends on both the energy and the position resolution which in our experiment is achieved with sufficient accuracy by employing a finely granulated lead glass array. Moreover, the thorough analysis of the lateral shower development in such an array in combination with a highly efficient charged particle discrimination allows a reduction of hadronic background to a large extent. Direct photons can hardly be determined on an event by event basis if the number of detected photons is larger than roughly 5 because of combinatorial ambiguities which could only be resolved through complete event reconstruction. This, however, is not feasible in the high multiplicity environment of heavy ion reactions and, indeed, we never intended to pursue the event by event method. We rather restricted ourselves from the beginning to a reasonable photon $p_\perp$ range ($p_{\perp,\gamma} \geq 0.5$ GeV/c), which

allows a sufficient signal-to-background level in the π^0 invariant mass peak, and relied on an accurate definition of interesting event classes by means of calorimetry and multiplicity measurements. Thus the γ/π^0 ratio as a function of $p_\perp$ is determined on a statistical basis for certain event classes. We use the following detailed prescription which is well known from the literature (e.g. [Fe84]).

In our analysis we first determine the true π^0 yield (N_{π^0}) as a function of $p_\perp$ from the observed π^0 yield ($N_{\pi^0}^{obs}$) by taking into account the momentum dependent quantities:

- $A(\pi^0 \to \gamma\gamma)$ = detector acceptance for photon pairs from π^0 decay,
- ε_γ = reconstruction efficiency for photons, including conversion losses.

We define

$$\varepsilon_{\pi^0} = A(\pi^0 \to \gamma_1\gamma_2) \cdot \varepsilon_{\gamma_1} \cdot \varepsilon_{\gamma_2} \tag{16}$$

and obtain

$$N_{\pi^0} = N_{\pi^0}^{obs}/\varepsilon_{\pi^0}. \tag{17}$$

Next, we determine from the observed $p_\perp$ dependent photon yield (N_γ^{obs}) the inclusive photon yield (N_γ^{incl}) by taking the photon reconstruction efficiency into account:

$$N_\gamma^{incl} = N_\gamma^{obs}/\varepsilon_\gamma. \tag{18}$$

(Remark: the effect of the photon reconstruction efficiency, ε_γ, has been neglected in the formula of question 4.) N_γ^{incl} contains photons from meson decay and fake photons from beam halo or hadron misidentification, which obscure the direct photon signal N_γ^{dir}.

In order to disentangle the various contributions we write the full expression for the observed photon yield N_γ^{obs}:

$$\begin{aligned} N_\gamma^{obs} \;=\; & N_\gamma^{dir} \cdot \varepsilon_\gamma \;+\; N_{\pi^0} \cdot P(\pi^0 \to \gamma) \cdot \varepsilon_\gamma \;+\; N_\eta \cdot P(\eta \to \gamma) \cdot \varepsilon_\gamma \;+ \\ & N_X \cdot P(X \to \gamma) \cdot \varepsilon_\gamma \;+ \\ & N_{halo} \cdot P(halo \cong \gamma) \;+\; N_{hadr} \cdot P(hadr \cong \gamma) \end{aligned} \tag{19}$$

$P(y \to \gamma); y = \pi^0, \eta, X;$ denotes the probability for finding within the detector acceptance a photon from the decay of particle of type y having the yield N_y. Type X includes all heavier mesons like η', ω , ... which are not considered explicitly. $P(halo \cong \gamma)$ and $P(hadr \cong \gamma)$ denote the probability for finding a fake photon originating from beam halo or hadrons which appear with their respective yield N_{halo} and N_{hadr}. Equation 19 transforms into the following ratio which contains the wanted quantity, namely N_γ^{dir}/N_{π^0}:

$$\frac{N_\gamma^{incl}}{N_{\pi^0}} = \frac{N_\gamma^{obs}}{\varepsilon_\gamma \cdot N_{\pi^0}}$$
$$= \frac{N_\gamma^{dir}}{N_{\pi^0}} + P(\pi^0 \to \gamma) + \frac{N_\eta}{N_{\pi^0}} \cdot P(\eta \to \gamma) + \frac{N_X}{N_{\pi^0}} \cdot P(X \to \gamma) +$$
$$\frac{1}{\varepsilon_\gamma \cdot N_{\pi^0}} \cdot \{N_{halo} \cdot P(halo \cong \gamma) + N_{hadr} \cdot P(hadr \cong \gamma)\}. \qquad (20)$$

This ratio is shown in Fig. 18 together with the contribution of π^0 and η decay photons obtained from Monte Carlo calculations. A detailed discussion of the individual terms is given in the following sections.

4.1.1 Photon reconstruction efficiency

The photon reconstruction efficiency is determined from the measured data as described in the response to question 2 (section 2.4 Photon identification). It was found to vary from 0.863 ± 0.012 at low multiplicities to 0.778 ± 0.015 at high multiplicities for O + Au data and $p_{\perp,\gamma} \geq 1$ GeV/c.

4.1.2 Background from π^0 and η mesons:

The probabilities $P(\pi^0 \to \gamma)$ and $P(\eta \to \gamma)$ are determined by Monte Carlo simulation with realistic input data for detector geometry and resolution as well as production cross sections given by N_{π^0} and N_η. Instead of applying model calculations or using production cross-sections from other experiments (i.e. from different reactions, and/or deriving π^0-distributions from $\pi^\pm$ distributions) in order to determine N_{π^0} and N_η, SAPHIR measures neutral pions and η's directly. In Fig. 19 π^0 $p_\perp$-spectra are displayed a) for different systems and b) for central and peripheral collisions. The ratio of the latter two spectra (Fig. 20) shows clearly their difference in shape, which has to enter properly into the Monte Carlo calculations. This allows a reliable normalization and makes the background calculation to a high degree model independent.

The inputs to the Monte Carlo calculation are then:

- the measured π^0 $p_\perp$-distribution corrected for geometrical acceptance and the influence of the γ reconstruction efficiency, i.e. $N_{\pi^0}(p_\perp)$;
- the measured η/π^0-ratio (again with consideration of acceptance and reconstruction efficiency), i.e. $\frac{N_\eta}{N_{\pi^0}}$($2 \leq p_\perp \leq 2.4$ GeV/c). This ratio was taken from the analysis of the total amount of data (minimum bias) because of the better statistics and was assumed not to change as a function of impact parameter. (The validity of this assumption will be checked by higher statistics data of the

requested beam time.) From the η/π^0 ratio and the known π^0 $p_\perp$-distribution the η $p_\perp$-distribution is calculated by assuming the well known $m_\perp$ scaling (see also [Ak86]), i.e. the ratio $\frac{N_\eta}{N_{\pi^0}}$ is taken to be constant as a function of $m_\perp = \sqrt{p_\perp^2 + m^2}$. (This assumption is a direct consequence of the picture of a common thermodynamical mechanism of mass production and formation of the $p_\perp$-distributions.);

- a limited extrapolation of the measured ϑ distribution of π^0 and η outside of the solid angle of the detector. This extrapolation is taken from the FRITIOF model and is checked to be consistent with data over the measured region.

The output of this Monte Carlo simulation gives at present the background $p_\perp$-distribution of decay photons from π^0 and η mesons (i.e. $P(\pi^0 \to \gamma)$ and $P(\eta \to \gamma)$) contributing to the inclusive γ/π^0 ratio.

4.1.3 Other photon sources:

An important aspect and great advantage of identifying π^0's and η's within the same apparatus is, that heavier particle resonances contribute only very little to the 'direct' (i.e. after correcting for photons from the π^0 and η mesons) photon yield. This is because these resonances primarily decay via the π^0 and η meson channel (e.g. $\eta' \to \pi^0\pi^0\eta$) and therefore do not have to be considered as they are already contained in the measured π^0 and η distributions. Hence, only radiative decays of such particles have to be taken into account. The most important candidates of this group are $\omega \to \pi^0\gamma$ (8.7 %), $\eta' \to \rho\gamma$ (30 %), and $\eta' \to \omega\gamma$ (2.7 %). An estimate of these sources according to the literature [An82] adds an additional contribution of $\frac{N_X}{N_{\pi^0}} \cdot P(X \to \gamma) < 0.03$ to the inclusive γ/π^0 ratio (however, mainly at low values of $p_\perp$ because of their unfavorable decay kinematics). More elaborate studies of this type of background are currently under way.

4.1.4 Background from beam halo:

Special care was taken to reduce the background from interactions other than in the target. Very thin beam counters and efficient halo detectors are employed, all embedded in vacuum. Thin targets and a thin aluminum target chamber followed by a carbon fibre vacuum tube assured a low conversion probability ($\approx 6\,\%$). Target-in/out measurements were routinely done and results are shown in figure 21 for secondary proton beams and primary oxygen beams.

The background from beam halo is suppressed by a factor of more than 10^4 for the primary beam of oxygen and is lower by more than a factor of 10^3 for the secondary proton beam. We therefore conclude that the contribution from halo can be neglected, because $N_{halo} \ll N_\gamma^{obs}$ and no further detailed estimate of the probability $P(halo \cong \gamma)$ for a halo particle faking a photon is necessary.

4.1.5 Background from unidentified hadrons:

Hadrons entering the finely granulated lead glass array are efficiently rejected as discussed in the response to question 2 (section 2.5 Hadron misidentification).

Repeating the result of the total hadronic contribution ($\pi^{\pm}$, p, n) to the inclusive photon spectrum we find:

$$N_{hadr} \cdot P(hadr \cong \gamma) \leq 10^{-3} \cdot N_{\gamma}^{incl}, \tag{21}$$

so that the explicit correction can be neglected.

Summarizing sections 4.1.1 - 4.1.5, we obtain from equation 20 the final expression for the direct photon signal:

$$\left(\frac{\gamma}{\pi^0}\right)^{dir} = \frac{N_{\gamma}^{dir}}{N_{\pi^0}}(p_{\perp}) = \frac{N_{\gamma}^{incl}}{N_{\pi^0}} - P(\pi^0 \rightarrow \gamma) - \frac{N_{\eta}}{N_{\pi^0}} \cdot P(\eta \rightarrow \gamma) - \frac{N_X}{N_{\pi^0}} \cdot P(X \rightarrow \gamma) \tag{22}$$

Figure 18 shows the experimental $\frac{N_{\gamma}^{incl}}{N_{\pi^0}}$ data points with error bars containing statistical errors and the error of < 2 % due to the uncertainty in photon reconstruction efficiency. In comparison, the solid histogram shows $P(\pi^0 \rightarrow \gamma)$, whereas the dotted histogram contains the sum of $P(\pi^0 \rightarrow \gamma)$ and $\frac{N_{\eta}}{N_{\pi^0}} \cdot P(\eta \rightarrow \gamma)$. Also included in the latter histogram is the current statistical Monte Carlo error, which can be improved easily, and the uncertainty in the measured η production cross section.

We observe agreement within error limits of this histogram with the inclusive photon data points above $p_{\perp} = 1$ GeV/c for peripheral reactions (figure 18b), but a clear enhancement of the inclusive yield in central reactions (figure 18a), which even exceeds the possible 3 % fake photons from heavier meson decays ($\frac{N_X}{N_{\pi^0}} \cdot P(X \rightarrow \gamma) < 0.03$) and therefore has to be attributed to the direct photon yield.

An estimate of systematic errors is given in the following sections.

4.1.6 $m_{\perp}$ scaling:

Since there is some indication from recent experiments [Ak86] that $m_{\perp}$ scaling might be violated at low values of $p_{\perp}$ ($p_{\perp} < 1$ GeV/c), there is a possible overestimate of the η contamination $N_{\eta} \cdot P(\eta \rightarrow \gamma)$ in this region. This could explain the slight overestimate of the Monte Carlo background in the peripheral data at low $p_{\perp}$ in figure 18.

From this point of view, a careful measurement of the η $p_{\perp}$-distribution is necessary.

4.1.7 Extrapolation of ϑ distributions:

Another source of systematic error is the extrapolation of the angular distribution of π^0's and η's into regions outside the solid angle of the detector. Because of the steepness of this distribution, this assumption contributes mainly to the systematic error at low $p_\perp$ ($\leq$ 1 GeV/c). The full ϑ-distribution is the only non-measured input to the Monte Carlo simulating the contributions of the different terms in equation 19. It is taken from the Lund Monte Carlo version FRITIOF and has been checked to be consistent with experimental data over the angular region covered by SAPHIR. The influence of the assumed angular distributions to the observed γ/π^0 ratio has been checked by suppressing a certain amount of mesons produced by the model as a function of ϑ. We estimate the resulting uncertainty in $\frac{N_\gamma^{dir}}{N_{\pi^0}}$ to be at most 0.01.

4.1.8 Nonlinearities in the detector response:

Different from ionization detectors, the response of Cherenkov counters is extremely linear, as is due to the purely statistical process of photon production, e.g. there is no quenching or other similar effects. The only possible source of non-linearity therefore is the photomultiplier response function, the ADC, and possible light absorption effects in the lead-glass. Furthermore, special care was taken in the fabrication of the phototube bases where each base was adjusted to the tube to assure best linearity.

The energy linearity of SAPHIR has been studied with a N_2-laser based reference system with variable light intensity. One reference tube was used as a measure of the laser intensity and was compared with the observed laser signal from each SAPHIR module. The resulting curves were then corrected by polynomials up to the tenth order to obtain a straight line response. Application of this correction leads to a remaining non-linearity of $<$ 0.3 % over the full dynamic range of the detector. The overall effect of phototube nonlinearities and energy calibration errors has in addition been studied by investigating the position of the π^0 invariant mass peak as a function of the photon energy which was scanned in small steps of 200 MeV. Within the statistical sensitivity of the procedure of $\sigma_{lin} = \pm 0.76\,\%$ no dependence on photon energy was found.

Although non-linearities are found to be quite small, their effect becomes amplified by the steepness of the $p_\perp$ spectra. The effect on the γ/π^0 ratio can be estimated by assuming purely exponential π^0 and photon $p_\perp$-spectra with equal slope parameters of roughly 0.2 GeV/c, yielding a $p_\perp$-dependent error on $\frac{N_\gamma^{incl}}{N_{\pi^0}}$ of:

$$\sigma = \sigma_{lin} \cdot p_\perp/(0.2GeV/c) \cdot \frac{N_\gamma^{incl}}{N_{\pi^0}} \qquad (23)$$

For example, taking the data point at 2 GeV/c an upper error limit of 0.04 is found. This error is certainly overestimated because the 'worst-case' non-linearity of 0.76 % (measured over the whole dynamic range) is in this case assumed to distort the energy

scale by it's full amount whereas the π^0 and photon energies differ mostly by a factor of two only. In the near future a full Monte Carlo simulation will be applied taking into account the accepted asymmetry range of the π^0's as a function of $p_\perp$.

4.2 Summary of resulting errors on the γ/π^0-ratio

The absolute systematic and statistical errors (σ) entering the γ/π^0 determination are, according to the discussion above, given in the following table, which also includes the origin of the respective errors:

Acceptance calculation:	$\approx$0.01	(geometry + MC statistics)
Extrapolation of ϑ distribution:	$\leq$0.01	(event gen. + MC statistics)
Reconstruction efficiencies:	$<$0.02	(exp. statistics)
Nonlinearity:	$<$0.04	(exp. + MC statistics)
Exp. η/π^0 ratio:	$\approx$0.05	(exp. statistics)
Beam halo and hadrons:	negligible	
Exp. $\frac{N_\gamma^{incl}}{N_{\pi^0}}$ $(1 \leq p_\perp \leq 2.4\,\mathrm{GeV/c})$		
in 200 MeV/c bins:	$\approx$0.10	(exp. statistics for peripheral/central selections)
	$\approx$0.05	(exp. statistics for total minimum mias data set)

Assuming all sources to contribute independently, we arrive at a total error (statistical and systematic):

$\sigma\left(\frac{N_\gamma^{dir}}{N_{\pi^0}}\right) \approx 0.12$ for central/peripheral and

$\sigma\left(\frac{N_\gamma^{dir}}{N_{\pi^0}}\right) \approx 0.08$ for full data set.

It has to be noted, that the largest contribution to this error stems from experimental statistics, whereas all other contributions add up to an error of 0.07. We also note, that this is a worst case estimate with rather advanced but not yet fully sophisticated analysis techniques which are still being developed.

The above results were derived from $^{16}O + Au$ data, but similar results are expected from the proton or ^{32}S induced reactions, since roughly the same amount of photons has been measured in these reactions.

4.3 Analysis of p + nucleus and ^{32}S + nucleus-data

Previous proton data are analyzed and inclusive photon- and π^0 spectra are published [Al88, Lö88]. Only the last proton run in May allows us to go for direct γ's with reasonable statistics. The ^{32}S data are being processed and a new shower fitting algorithm is applied which improves the γ reconstruction efficiency (seen to be multiplicity dependent, see Fig. 10). The minimum two-shower separation is to improve

from the present 57 mm to about 35 mm. This was considered desirable to respond to the higher particle density in $^{32}S + Au$ compared with $^{16}O + Au$.

4.4 Analysis of central and non-central reactions

As already mentioned in section 4.1.5, an excess of single photons above all possible sources of photon contamination has been observed in central $^{16}O + Au$ data, but not in peripheral reactions. The comparison of a photon signal from different event classes simplifies the analysis in that sense, that uncertainties due to non-linearities in the detector response and acceptance and geometry automatically cancel out. Also the uncertainties in the contributions due to η's and other heavier mesons would cancel out if we assume a production mechanism independent of the type of reaction. This assumption is, however, not yet verified and will be one of the tasks of our experiment, especially the verification of $m_\perp$ scaling in central and peripheral reactions. Also the photon reconstruction efficiency is found to be multiplicity dependent, mainly due to a rather conservative method of charge assignment. This will be improved in the future by more sophisticated analysis techniques.

The influence of systematic errors can significantly be reduced by comparing central and peripheral reactions, however, the results are mostly suffering from statistical errors. The comparison of central and peripheral data serves, of course, as a basis to separate well known hadron physics from the new physics in dense nuclear matter, and therefore is a necessary requirement in addition to the proton induced reactions.

Question 5:

From the measured errors demonstrate the improvement expected with SAPHIR-II and the requested running time of the different contributions to N^{γ}_{direct}.

Response to question 5:

As pointed out in response to question 2, we found the lead glass detector to be the optimal detector for gamma detection and π^0 reconstruction to be employed in the rapidity region of $1.5 \leq \eta \leq 2.2$. Therefore we decided to base an increase in detection efficiency in that rapidity interval on the same technology. (For larger rapidities we are pursuing an R&D program which will be reflected in the future lead beam proposal.)

We consider it feasible to finance and construct in the next 16 month 1000 new lead glass modules. The additional SAPHIR-II will increase the detection efficiency for η's substantially and will improve the acceptance for π^0's at $p_\perp \leq 1\,\mathrm{GeV/c}$. The following simulations and studies will show the new limits based on the performance of and experience with SAPHIR-I.

In figure 22 we show the geometrical layout of the two SAPHIR in an L-shape which reduces the low efficiency border area and enhances the acceptance for decays with large opening angles as e.g. for η's. (Should we succeed in getting about 1000 additional modules from our Indian collaborators then we would form a U-shaped geometry.) In Figure 23a and 23b, we show the acceptance of SAPHIR I+II in the ϑ versus $p_\perp$ plane for π^0's (a) and η's (b) in comparison with the SAPHIR I. In Figure 24 the projected acceptance values onto the $p_\perp$ axis are shown.

Assuming the same integrated luminosity, the basic improvement in counting statistic is given by the ratios of the efficiencies quoted in the response to question 3. We plan to obtain improved information only on a few specific systems in order to invest the beamtime most efficiently. These systems are S+Au, S+Al, p+Au and p+C. They are chosen to provide presently the best chance at the SPS to create a plasma (S+Au), provide specific reference cases where such formation is less likely or will occur with rather different characteristics (S+Al, p+Au, p+C). The proton induced reactions can be tied to existing data on direct photons at high $p_\perp$ that have been reproduced by second order QCD calculations (p+C, comparison to published NA3 results [Ba86].)

Since we want to reach $p_\perp$-values for π^0's of about 4 GeV/c, we need to increase the statistic of reconstructed π^0's (with respect to the O+Au data, where we took 2.1 million events) by a factor of 100. This would allow:

- to determine experimentally the gamma reconstruction efficiency out to at least 3 GeV/c;
- to measure the η/π^0-ratio to about $\pm 3\,\%$ accuracy at $2 \leq p_\perp \leq 3$ GeV/c reducing its error contributing to γ/π^0 to 0.005 for Minimum Bias data;
- to study selected classes of events with good statistics, like peripheral and central collisions, or even within central collisions further subselected event classes.

with the following errors:

Acceptance calculation:	$\approx$0.01	(geometry + MC statistics)
Reconstruction efficiencies:	$<$0.01	(exp. statistics)
Nonlinearity:	$<$0.03	(exp. + MC statistics)
Exp. η/π^0 ratio:	$\approx$0.015	(exp. statistics)
Exp. $\frac{N_\gamma^{incl}}{N_{\pi^0}}$ $(1 \leq p_\perp \leq 2.4$ GeV/c) in 200 MeV/c bins:	$\approx$0.01	(exp. statistics for peripheral/central selections)

arriving at a total error (stat. and syst.) of 0.04.

A factor of 100 in statistics is to be achieved in the following way , similar to what was presented in our Addendum to M406:

- a factor of two (or somewhat more) from the larger solid angle and the improved acceptance of SAPHIR I+II
- a factor of about 3 due to increased data taking rate and hardened trigger conditions
- a factor of $\approx$ 1.6 due to the higher multiplicity with the sulfur beam
- a factor of 10 in beamtime = $5 \times 10 = 50$ days for S + Au.

Question 6:

$\pi^0 - \pi^0$ interferometry: Demonstrate that the resolution of SAPHIR is adequate to measure the source size. Is $\pi^0 - \pi^0$ interferometry sensitive to HBT correlations or does it basically reflect resonance decay?

Response to question 6:

6.1 Resolution and source size:

We have calculated the response of SAPHIR to a larger source size, as shown in Fig. 25 All three simulations were done with the following assumption: a pion source of radius 5 fm emits π^0's with $p_\perp \geq 1$ GeV/c with an exponential distribution employing an inverse slope of 200 MeV (this parameter is not critical). Furthermore, the angular distribution of the pions is assumed to isotropic over the solid angle of SAPHIR.

In the upper case of figure 25 these pions are looked at with a perfectly ideal detector having only the solid angle of SAPHIR. The correlation function in Q is calculated for these events as well as for a background of mixed events. In the second case in figure 25 the pions decay and the photon energies are smeared out by the energy resolution of SAPHIR ($\sigma_E/E = 6\%/\sqrt{E} + 0.4\%$). The position resolution σ_x is folded in, too. Furthermore, as with the real data, an opening angle between the two photons of less than 2.3° is excluded in order to avoid any overlapping between photon showers. These selected photons are used to reconstruct π^0's, which in turn are used as described above to construct the Q function and the background correlation. The mixed events are also subject to the opening angle restriction. The lower case in figure 25 is identical to the one just mentioned but the energy resolution has been worsened to ($\sigma_E/E = 12\%/\sqrt{E} + 0.4\%$).

The fit parameter are from a comparison of the real and background spectra with the 'Maximum Likelihood' method, i.e. there is no χ^2, but the negative log of the Likelihood function per degree of freedom. This method was chosen in order to weight the values at small ΔQ properly. The fit values are indicated in the figures. As the resolution becomes worse only the chaoticity parameter λ really changes, whereas the radius parameter decreases only a little.

6.2 HBT or Resonance Decay:

Anderson and Hoffmann [An86], and Bowler [Bo86] discuss the resonance decay in the framework of their models, especially the Bose-Einstein symmetrization of particles produced by one string. This may be related to e^+e^- physics or two jets in hadron collisions. In nuclear collisions the particle pairs considered should mainly come from different interactions. They discuss a possible suppression of the correlation due to resonance decay which is just not observed in the experiments they compare with.

We looked into a possible effect from the three-pion-decay of the η and compared the rates:
In the case of O + Au 200 AGeV with $p_\perp(\pi^0) \geq 1$ GeV, we expect from Monte Carlo simulations in the data sample analyzed about 4(!) pion-pairs from η decay (all 4 photons detected by SAPHIR). The measured correlation,however, corresponds to 641 pion-pairs. We conclude therefore from our MC-simulations based on the measured η/π^0 ratio in O + Au reactions show that resonance η-decay pions are negligible in this context.

However, we would like to point out a more crucial problem of this analysis: the false pions from the combinatorial background. As we measure photons ,which mostly originate from π^0's, we can only do multi-photon correlation studies. These photons carry through correlations from the pions. As long as the peak to background ratio for the photon pairs in the pion peak is large, we can consider this analysis a true HBT study with identified particles. When the peak to background ratio gets small, the value of Q is no longer well defined in terms of a 'two pion variable'. The fact that we do see a rise in the Q-spectrum compared to the mixed event background even with a high contribution of fake, 'combinatorial' pions is a hint that we observe a collective phenomenon which involves the multi-pion state as a whole (so do Bose-Einstein effects). 'Individual' processes, like decay pions from η's, should give no contributions, if false pions are considered.

Question 7:

Running time and beam requests:

a) 60 and 120 GeV/N for ^{32}S in addition to 200 GeV/N:

- *What are the important physics results so far obtained from comparisons of different beam energies?*
- *What is the physics motivation for running at different energies of the ^{32}S-beam?*
- *What are the expected errors (stat. and system.) for the proposed running-periods?*

b) Justification of the requested p-beam with low extraction from the machine.

Response to question 7:

Part a):

Part a) first subquestion:

There are three principal results that have come out of the comparisons to date of the runs with ^{16}O at $E/A = 60$ and 200 GeV, and with the AGS beams at $E/A = 14.5$ GeV. These are:

1. The observed average energy densities, as inferred from the transverse energy spectra, increase from a value of 0.7 GeV/fm^3 at 14.5 AGeV, to 1.4 GeV/fm^3 at 60 AGeV and 2.7 GeV/fm^3 at 200 AGeV.

2. There appears to be complete 'stopping' at $E/A = 14.5$ GeV for ^{28}Si beams once a target as thick as copper ($A = 64$) is used. At SPS energies of $E/A = 60$ and 200 GeV, there does not appear to be any longer complete stopping, and the fraction of 'stopped energy' decreases in going from 60 to 200 AGeV. There is presently an intensive effort to quantify the degree of observed stopping.
   Although transparency apparently sets in at SPS energies, the charged particle rapidity distributions do not yet exhibit the expected boost-invariant plateau at central rapidity suggested by Bjorken; it is not expected that this will appear until CM-energies at least 3–4 times larger are available to provide the needed rapidity interval.

3. The range of 'entropy densities', defined as the ratio of *charged particle rapidity density* divided by $A^{2/3}$, which can be reached in a given experiment increases by roughly a factor of two in going from $E/A = 60$ to 200 GeV. This directly determines how much 'reach' one has in a study of, e.g., mean $p_\perp$ as a function of entropy density.

4. The mean $p_\perp$ of photons is different for the same number of participants at the two energies. (see Fig. 26) This could be seen as an indication of a collective, hydrodynamical flow phenomenon of the pions as predicted by several authors (see also response to question 1, and e.g. Ref. [Da83, Bl87]). This effect should be more pronounced at larger participant volumes .

Part a) second subquestion:

We have requested the 3 different beam energies in order to have experimental control of the energy density in the participant zone; this provides the basic ability to vary the initial temperature of any thermalized system produced, as discussed above in the response to the first question. We thus feel this provides the best opportunity to observe variations in the behavior of real photon emission that might signal a transition to a thermalized state or plasma. Direct γ's can be looked for at lower energy density within the same experimental set-up and most systematic errors avoided.

part a) third subquestion:

Based on the experience of two approximately twenty days running periods with sulfur and oxygen, we estimate the quality of the data at 60 and 120 AGeV to be better in statistics by a factor of at least four (twice the spill length and twice the solid angle), i.e. we aim at a γ/π^0-ratio with a statistical error of 4–5 % for Minimum Bias data. In a comparison with data taken at other energies the systematic errors would nearly cancel in the ratios of γ/π^0 and η/π^0.

Part b):

See also the response to Question 5 above.

Technically, there is a little proton admixture in the secondary or even tertiary beam of 60 GeV/c, which we have tried to use in 1986. Typically, for $\approx 4{\cdot}10^6$ particles hitting the target area only 50000 protons were contained in the beam. When we have been running during a MD-time at an extraction energy of 120 GeV proton energy and focused a secondary beam of 60 GeV onto our target, the proton content in the beam was close to 80%, and of course the spill length was 8 sec instead of 2 sec. Altogether this gives a factor of 200 shorter beamtime when one runs with a beam

of $4 \cdot 10^6$ particles per 8-sec-spill under much better background conditions. If one wants to compare ion reactions with proton induced reactions the proton running time needs to be increased by the ratio of cross section between the oxygen and the proton reactions, at least!

References

Ak77: Akopdjanov et al., Nucl. Instr. and Meth. 140, 441 (1977)

Ak86: T. Akesson, et al., Phys. Lett. 178B, 447 (1986)

Al88: R. Albrecht, et al., WA80-Collaboration, Phys. Lett. 201B, 390 (1988)

An82: E. Anassontzis et al., Z. Phys. C13, 277 (1982)

An86: B. Andersson and W. Hofmann, Phys. Lett. B169, 364 (1986)

Ba86: J. Badier, et al., NA3 Collaboration, Z. Phys. C31, 341 (1986)

Bl87: J.P. Blaizot and J.Y. Ollitrault, Phys. Lett. 191B, 21 (1987)

Bo86: M.G. Bowler, Phys. Lett. 180B, 299 (1986)

Da83: M. Danos and J. Rafelski, Phys. Rev. D27, 671 (1983)

Do81: G. Domokos and J.I. Goldman, Phys. Rev. D23, 203 (1981)

Fe62: E.L. Feinberg, Izv. Akad. Nauk. Ser. Fiz. 26, 622 (1962)

Fe76: E.L. Feinberg, Nuovo Cimento 34A, 391 (1976)

Fe84: T. Ferbel and W.R. Molzon, Rev. Mod. Phys. 56, 181 (1984)

Ga80: T. Gabriel, private communication

Ha78a: F. Halzen and D.M.Scott, Phys. Rev. Lett. 40, 1117 (1978)

Ha78b: F. Halzen and D.M.Scott, Phys. Rev. D18, 3378 (1978)

Ha80: F. Halzen and D.M.Scott, Phys. Rev. D21, 1320 (1980)

Ha82: F. Halzen and H.M. Liu, Phys. Rev. D25, 1842 (1982)

Hw85: R.C. Hwa and K. Kajantie, Phys. Rev. D32, 1109 (1985)

Hi88: S. Hirasawa, Morihiro Kadoya and Tadashi Miyazaki, Science University of Tokyo Preprint 88-0382

Lö88 H. Löhner, et al., WA80 collaboration, Z. Phys. C38, 97 (1988)

Mc85: L.D. McLerran and T. Toimela, Phys. Rev. D31, 545 (1985)

Ow87: J.F. Owens, Rev. Mod. Phys. 59, 465 (1987)

Ra87: S. Raha and B. Sinha, Phys. Rev. Lett. 58, 101 (1987)

Re87: K. Redlich, Phys. Rev. D36, 3378 (1987)

Sh74: E.V. Shuryak, Yad. Fiz. 20, 549 (1974); Sov. J. Nucl. Phys. 20, 295 (1975)

Sh78a: E.V. Shuryak, Phys. Lett. 78B, 150 (1978)

Sc78b: E.V. Shuryak, Zh. Eksp. Teor. Fiz. 74, 408 (1978); Sov. Phys. JETP 47, 212 (1978)

Sh78c: E.V. Shuryak, Yad. Fiz. 28, 796 (1978); Sov. J. Nucl. Phys. 28, 3 (1978)

Si83: B. Sinha, Phys. Lett. 128B, 91 (1983)

Si85: B. Sinha, Phys. Lett. 157B,221 (1985); Phys. Lett. 160B, 287 (1985)

Si86: B. Sinha, Nucl. Phys. A459, 717 (1986)

St88: H. Ströbele et al., NA35-Collaboration, Z. Phys. C38 89, (1988), and private communication

Yo87: R. Yoshida, T. Miyazaki and M. Kadoya, Phys. Rev. D35, 388 (1987)

Zh78: O.V. Zhirov, Yad. Fiz. 30, 1098 (1978); Sov. J. Nucl. Phys. 30, 571 (1979)

Figure Captions

Figure 1: Artists view of the front face of SAPHIR I.

Figure 2: Influence of the energy resolution (dashed line) and the spatial resolution (dashed-dotted line) on the $\gamma\gamma$ invariant mass resolution (solid line) as function of $E(\pi^0) = E(\gamma_1) + E(\gamma_2)$. Assumed are symmetric decays of the π^0 meson (i.e. $E(\gamma_1) = E(\gamma_2)$) and a position resolution of 3.5 m at distance of the detector of $D = 3.425$ m. The different $p_\perp$-scales are obtained using different η-regions.

Figure 3: Geometrical details of the SAPHIR I setup. Shown are contours of the active area of SAPHIR-I.

Figure 4: Energy calibration function based on calibration runs at DESY and at the X1 beamline spectrometer at the SPS. The dashed line represents a linear function, the full line represents a polynomial parametrization.

Figure 5: Gain stability measurement of the laser reference system during the ^{16}O run in 1986.

Figure 6: Spectra of photons, hadrons and minimum ionizing particles in SAPHIR for $^{16}\mathrm{O} + \mathrm{C}$ at 200 AGeV.

Figure 7: True versus calculated position of showers in SAPHIR.

Figure 8: Single event display in SAPHIR-I of a typical event from the reaction $^{16}\mathrm{O} + \mathrm{Au}$ at 200 A GeV. Indicated are the shower light distributions caused by different particles. Electromagnetic showers are identified by their shower shape.

Figure 9: Multipliciy distributions of hits (i.e. 'clusters') and reconstructed photons measured in SAPHIR for $^{16}\mathrm{O} + \mathrm{Au}$ collisions at 200 AGeV selected for central and peripheral reactions.

Figure 10: γ-reconstruction efficiency, ε_γ for $^{16}\mathrm{O} + \mathrm{Au}$ as function of $p_\perp$ and charged particle multiplicity N_c. The dashed lines indicate the extrapolation to $p_\perp$ values above 0.8 GeV/c. For the low multiplicity a value of 0.863 ± 0.012 and for the high multiplicity a value of 0.778 ± 0.015 is used. ε_γ is determined from the data according to Eq. 8.

Figure 11: Measured hadron response in SAPHIR at different energies. The minimum ionizing peak corresponds to a photon energy equivalent of 540 MeV.

Figure 12: Contributions of fake γ's to the γ $p_\perp$ spectrum. The contribution is separated for light baryons n, p and charged light mesons π^-, π^+. The results are based on experimental data and Monte Carlo simulations in order

to determine the probability for misidentifying hadrons as photons. Protons and neutrons are calculated assuming equal cross sections. However, neutrons are faking the photon signal with 50 times higher probability, because of the missing charged particle veto (98 %).

Figure 13: π^0- and η-acceptances for SAPHIR I as function of ϑ and $p_\perp$ using a low energy cutoff of 400 MeV and a minimum distance of two showers of 57 mm corresponding to 1.5 module units. The 3.36 m is measured along the beam-axis and corresponds to the distance $D = 3.425$ of the detector surface to the target. Part c of the figure shows the acceptance after integrating over the ϑ region of the detector.

Figure 14: Effect of the geometry and low energy cutoff on asymmetric π^0 decays in SAPHIR-I.

Figure 15: Minimum opening angle $\psi_{\min}$ between two γ's as a function of $p_\perp$. $\psi_{\min}$ is determined by $\psi_{\min} = 2. * \arctan(m_0/p)$ where m_0 is the meson rest mass and p the momentum.

Figure 16: $\gamma\gamma$ invariant mass spectrum showing the π^0 -peak for different bins in $p_\perp(\gamma\gamma)$. Shown are data of ^{16}O+Au selected for central and peripheral collisions, respectively.

Figure 17: $\gamma\gamma$ invariant mass spectrum showing the π^0- and η-peak. The small inset shows the mass region around the η-peak.

Figure 18: γ/π^0 ratio for central and peripheral reactions of $^{16}\mathrm{O} + \mathrm{Au}$. The upper curves show the inclusive ratio and it's statisitical errors, the full-line histogram shows the background to this ratio due to photons from the π^0 decay, and the dashed line histogram shows the sum of decay photons from the π^0 and η meson together with the statistical errors from the Monte Carlo simulations and from the measured π^0/η-ratio.

Figure 19: a) Invariant π^0 $p_\perp$ distributions for different reactions
b) invariant π^0 $p_\perp$ distributions for the reaction $^{16}\mathrm{O} + \mathrm{Au}$ differenciated by centrality.

Figure 20: Cross section ratio of π^0_{central} divided by $\pi^0_{\mathrm{peripheral}}$ as a function of $p_\perp$.

Figure 21: Target-in/out measurements in SAPHIR for proton and ^{16}O induced reactions. The left two columns show the spectra of all particles hitting the detector, while the right ones show only the reconstructed photons.

Figure 22: Schematic drawing of the SAPHIR I+ II setup.

Figure 23: Acceptance for a) $\pi^0 \rightarrow \gamma\gamma$ and b) $\eta \rightarrow \gamma\gamma$ for SAPHIR I and SAPHIR I+II (both at a distance D of 4 m from the target) as function of ϑ and $p_\perp$.

Figure 24: ϑ integrated acceptance for $\eta, \pi^0 \rightarrow \gamma\gamma$ for SAPHIR I and SAPHIR I+II at $D = 4\,\mathrm{m}$ as function of $p_\perp$.

Figure 25: Monte Carlo simulation to study the effect of the energy resolution in SAPHIR to $\pi^0\pi^0$ correlations. The dashed line in the upper histogram shows for comparison the expected distribution of a 1 fm source. The parameters are fit results (Maximum Likelihood).

Figure 26: Mean transverse momentum ($< p_\perp >_{\gamma,400}$, for definition see [Al88]) of inclusive photons as a function of the Zero Degree Energy normalized to the beam energy for different reaction systems.

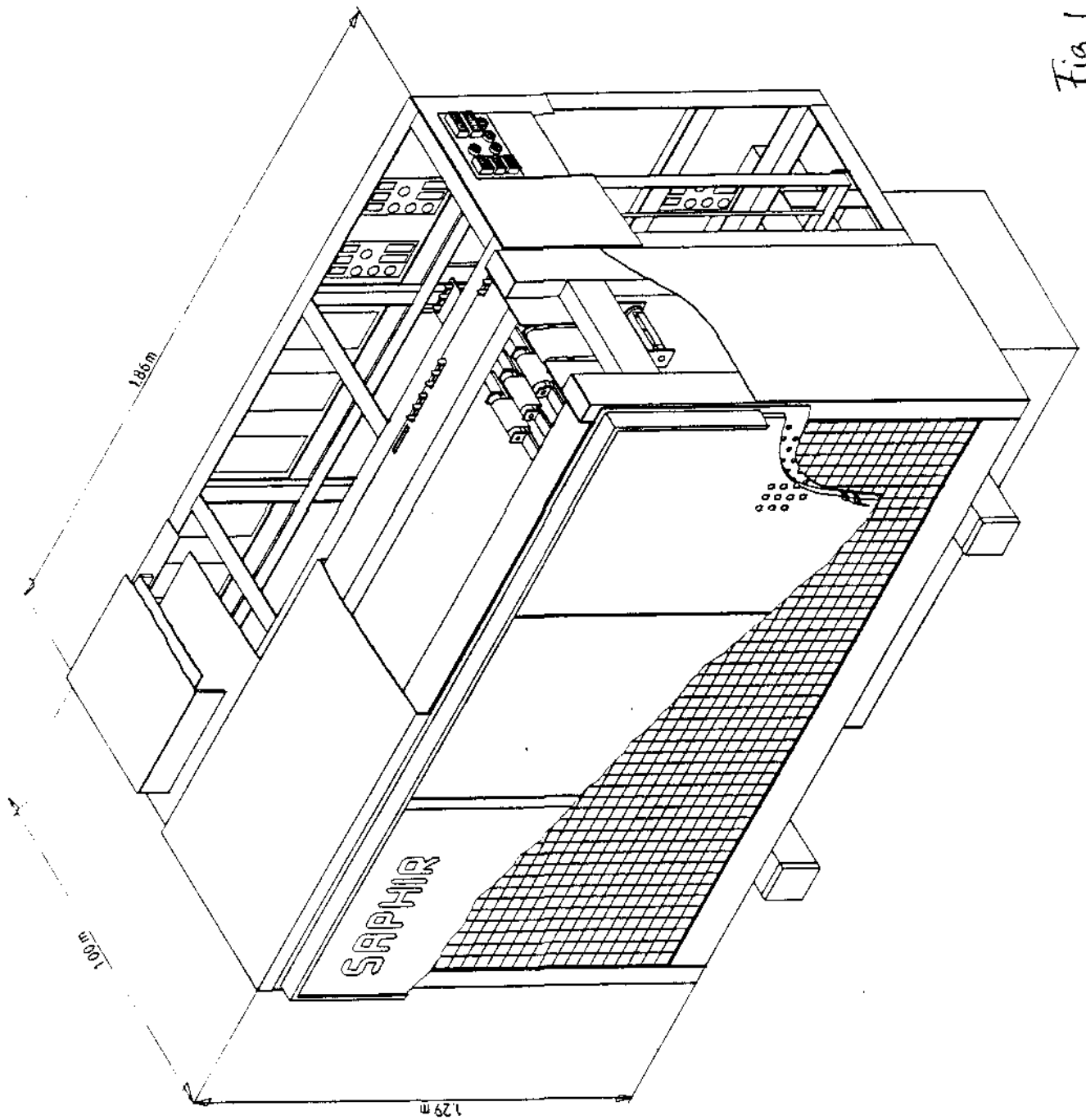

Fig 1

Fig 1

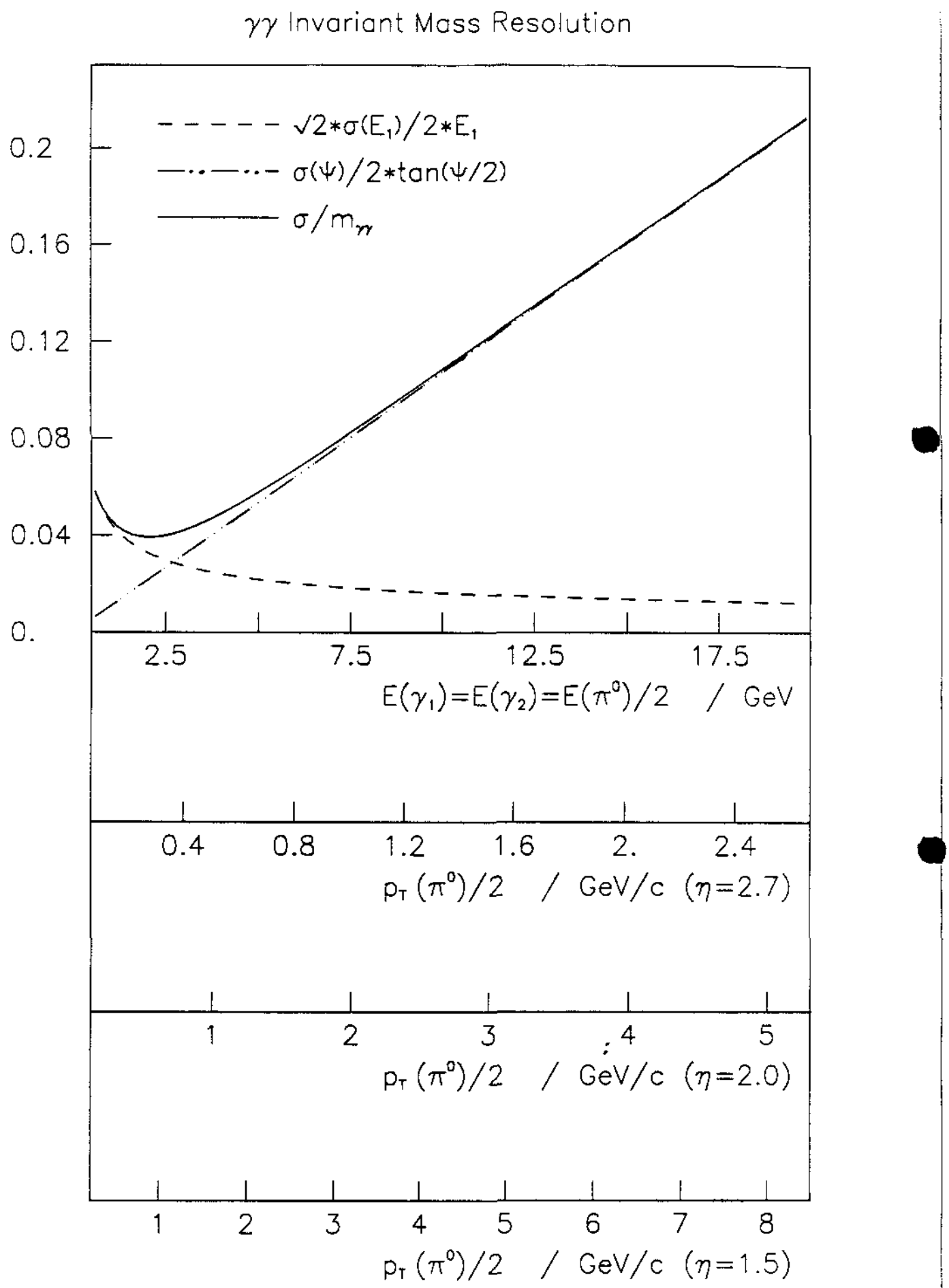
γγ Invariant Mass Resolution
√2*σ(E1)/2*E1
σ(Ψ)/2*tan(Ψ/2)
σ/mγγ
0.2
0.16
0.12
0.08
0.04
0.
2.5
7.5
12.5
17.5
E(γ1)=E(γ2)=E(π0)/2 / GeV
0.4
0.8
1.2
1.6
2.
2.4
pT (π0)/2 / GeV/c (η=2.7)
1
2
3
4
5
pT (π0)/2 / GeV/c (η=2.0)
1
2
3
4
5
6
7
8
pT (π0)/2 / GeV/c (η=1.5)

Fig 2

SAPHIR 12 degree position

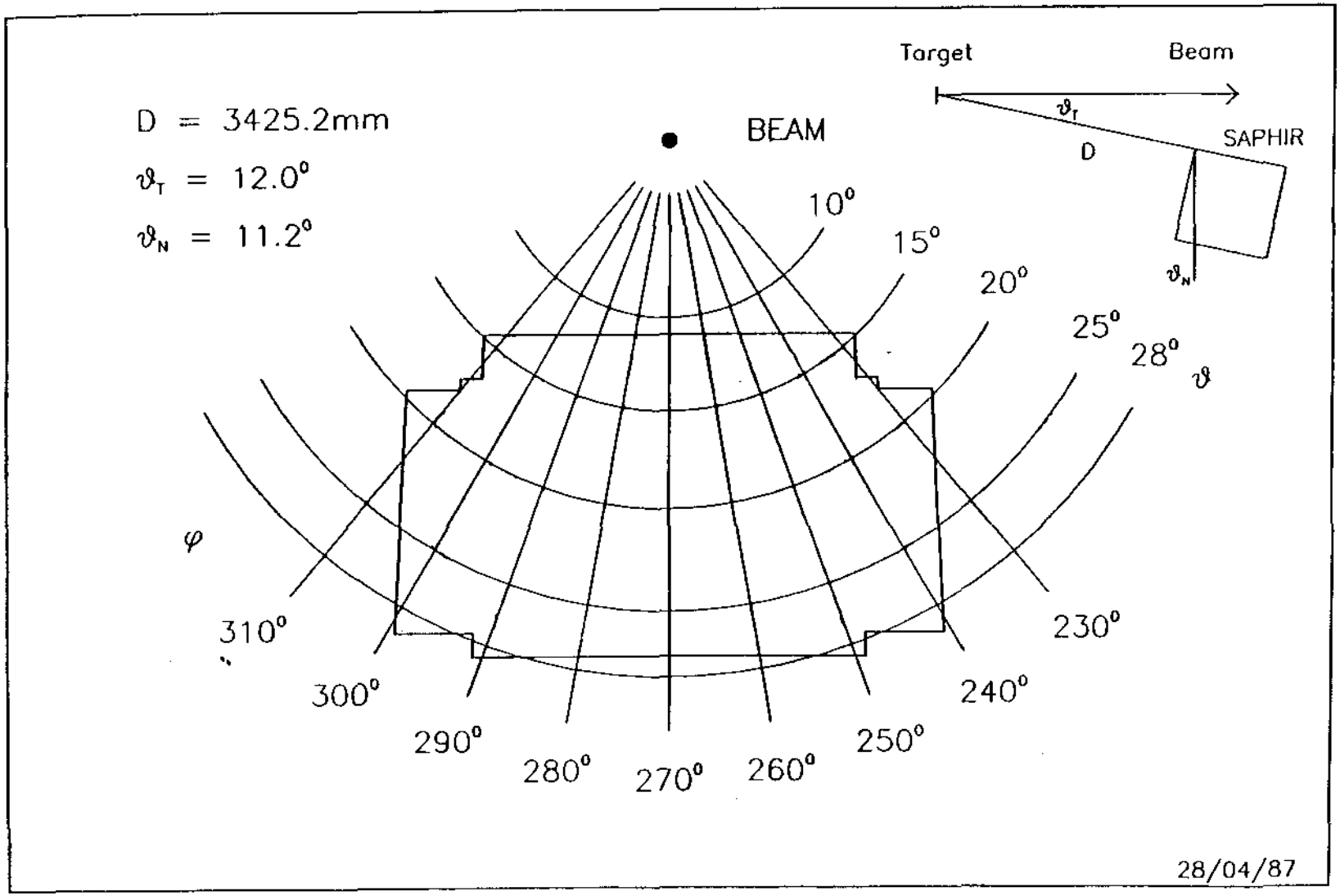

sweet spot : $\Delta\varphi = \pm 29^\circ$, $13.5^\circ \leq \vartheta \leq 26.0^\circ$,

ϑ = polar angle, φ = azimuthal angle, Ω = solid angle

Fig 3

Fig 3

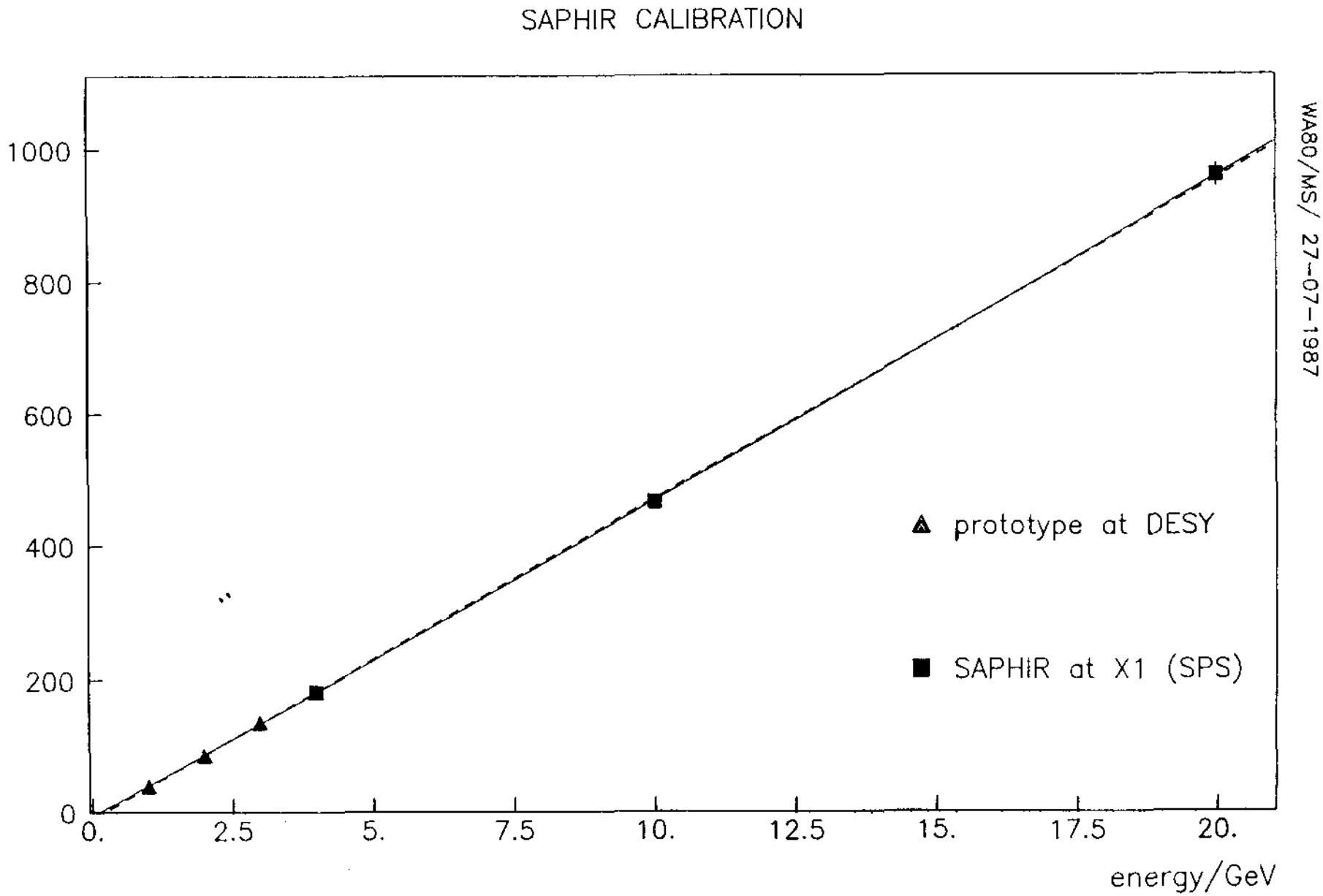

calibration law (dashed line: linear – full line: potential)

Fig 4

Fig 4

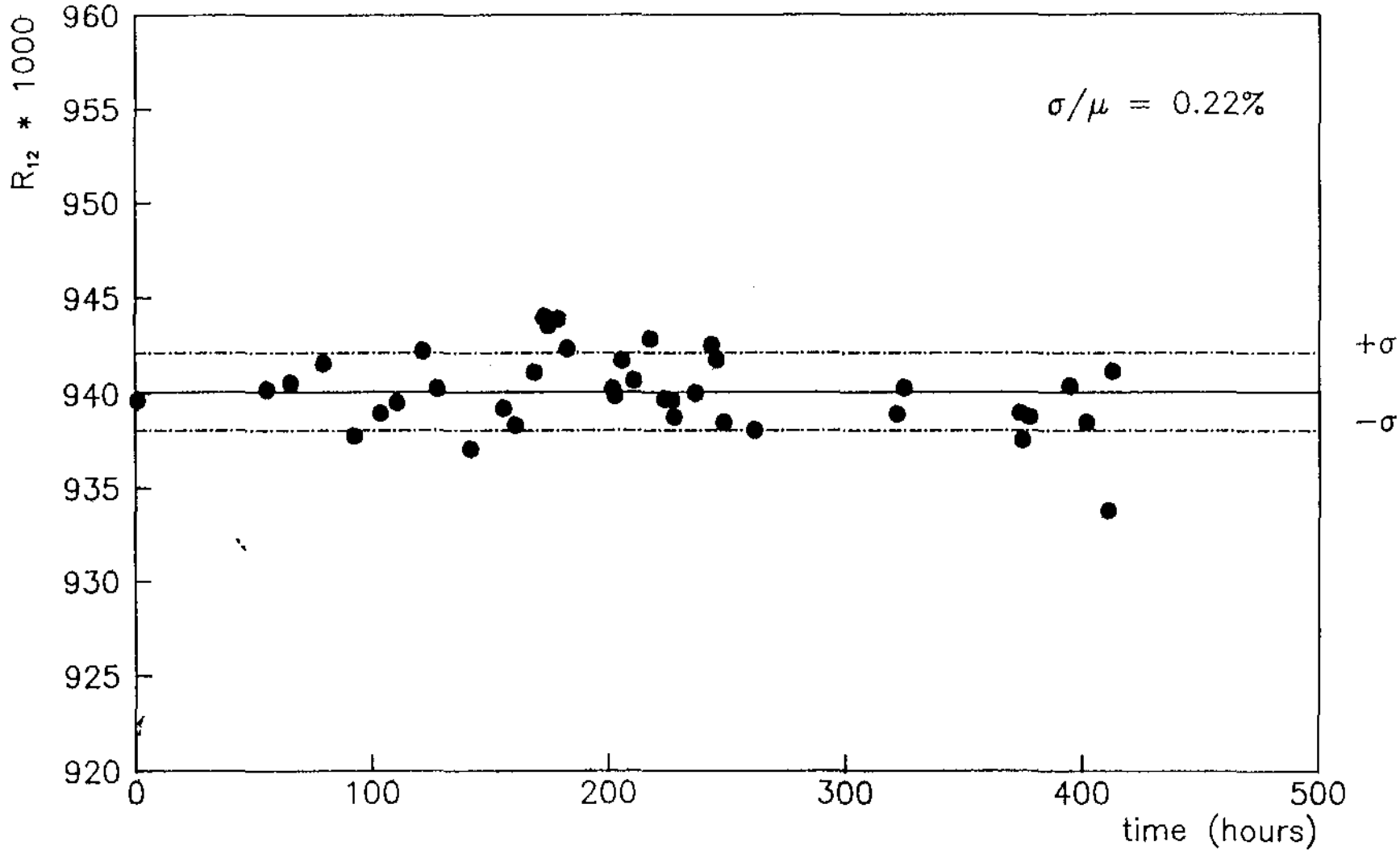
960
955
950
945
940
935
930
925
920
R_{12} * 1000
σ/μ = 0.22%
+σ
−σ
0
100
200
300
400
500
time (hours)

Fig 5

Fig 5

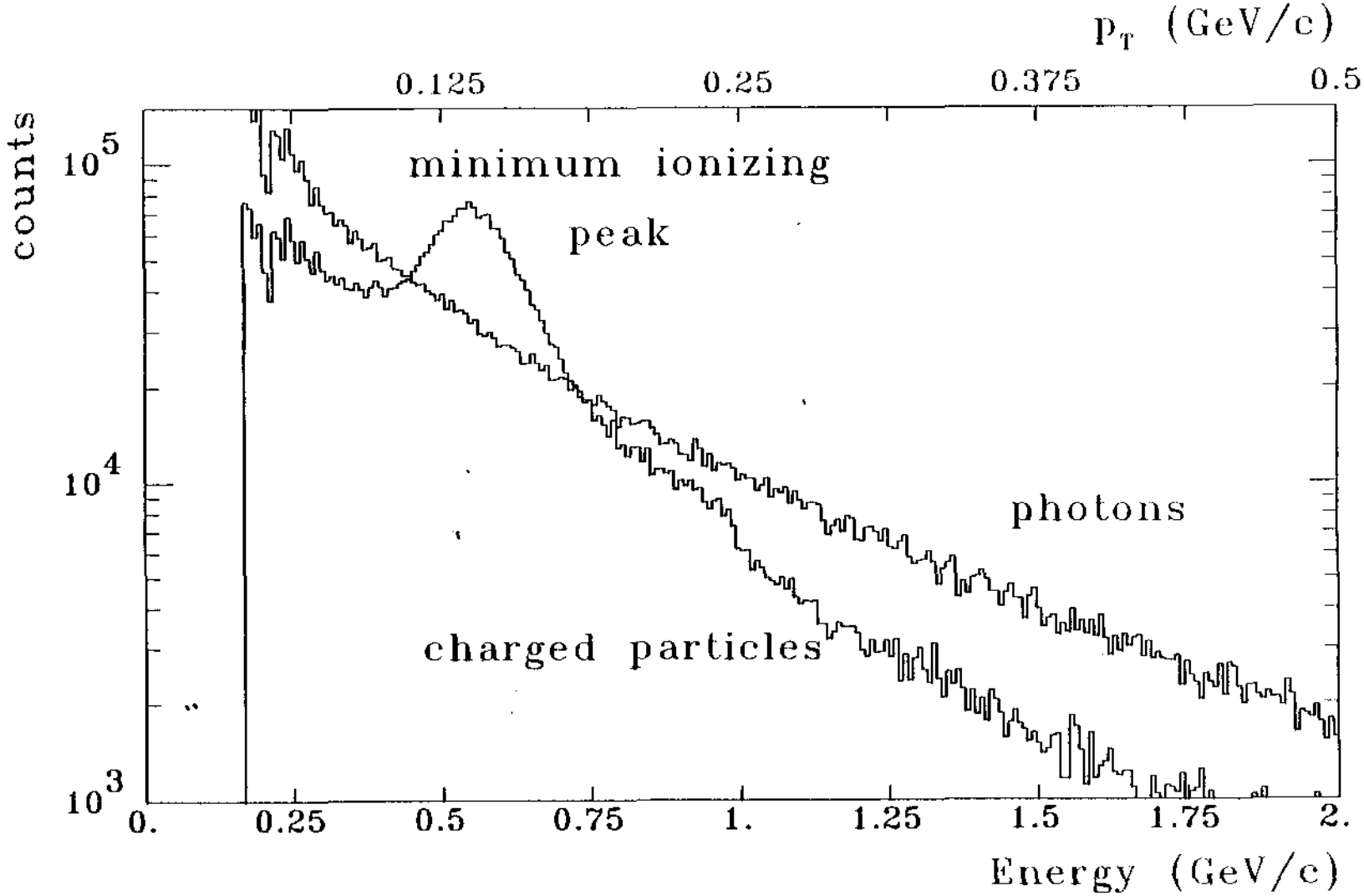
p_T (GeV/c)
0.125
0.25
0.375
0.5
counts
10^5
10^4
10^3
minimum ionizing
peak
photons
charged particles
0.
0.25
0.5
0.75
1.
1.25
1.5
1.75
2.
Energy (GeV/c)

Fig 6

Fig 6

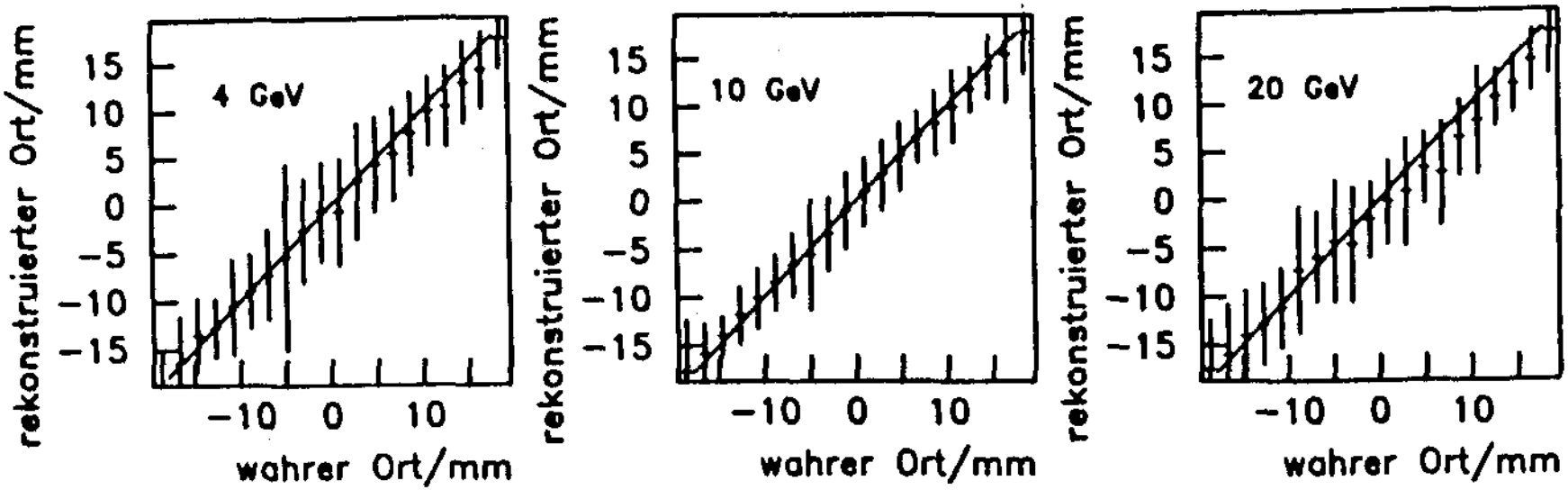
4 GeV
10 GeV
20 GeV
rekonstruierter Ort/mm
wahrer Ort/mm
15
10
5
0
−5
−10
−15
−10
0
10

Fig 7

Fig 7

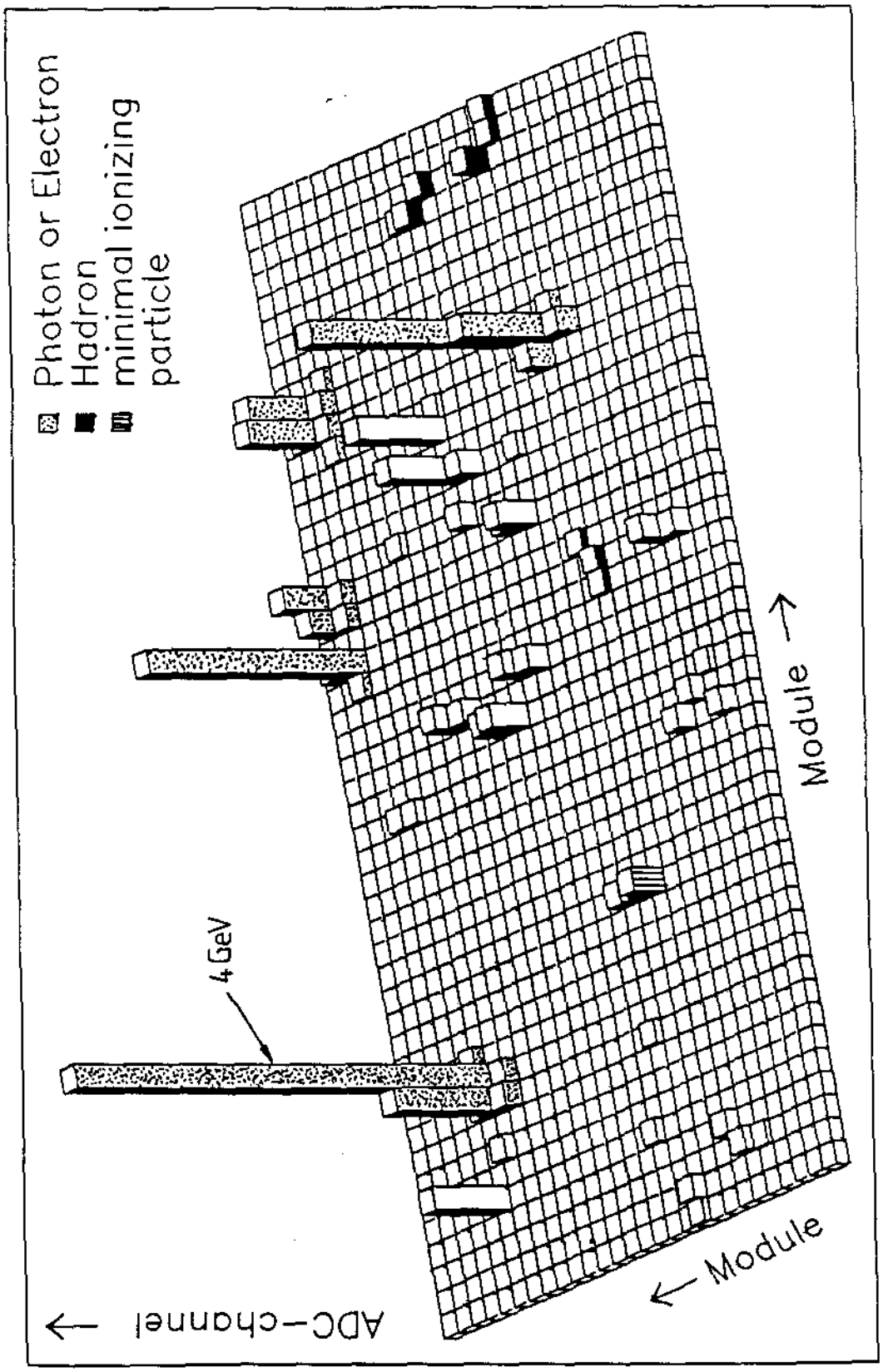
Photon or Electron
Hadron
minimal ionizing particle
4 GeV
Module →
← Module
← ADC-channel

Fig 8

Fig 8

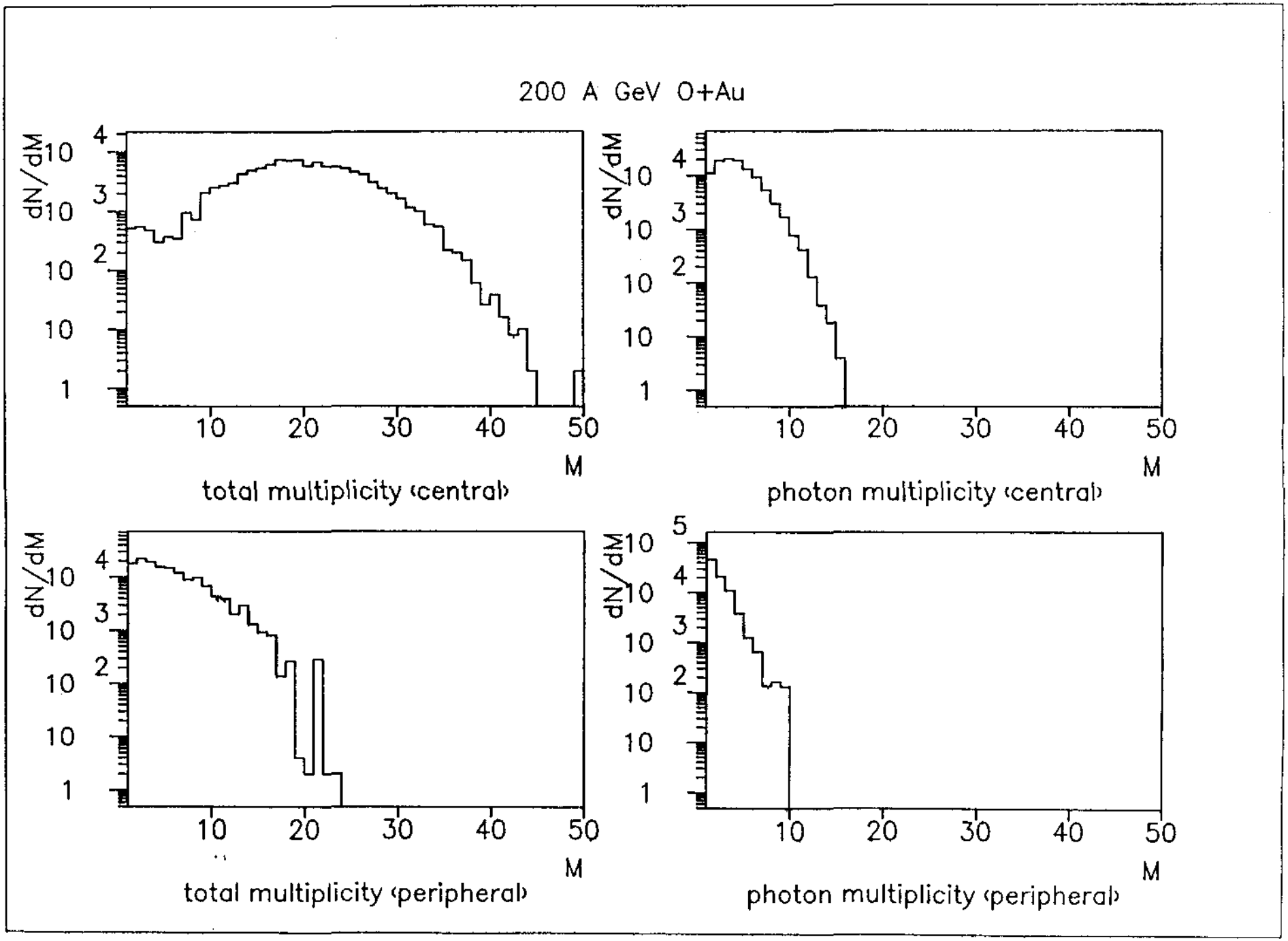
200 A GeV O+Au
dN/dM
M
total multiplicity ‹central›
photon multiplicity ‹central›
total multiplicity ‹peripheral›
photon multiplicity ‹peripheral›

F.. 4

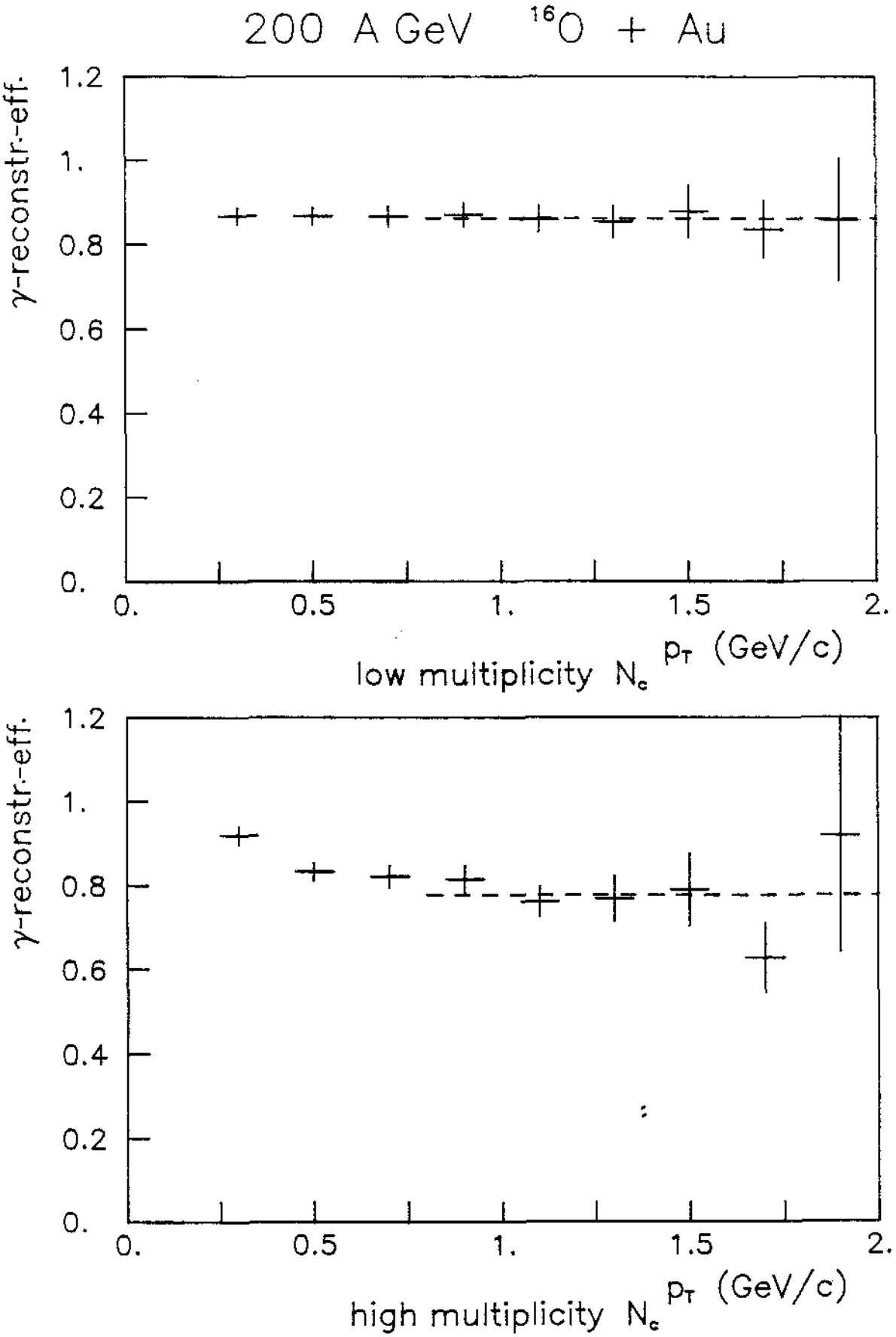
200 A GeV ^{16}O + Au
γ-reconstr.-eff.
1.2
1.
0.8
0.6
0.4
0.2
0.
0.
0.5
1.
1.5
2.
p_T (GeV/c)
low multiplicity N_c
γ-reconstr.-eff.
1.2
1.
0.8
0.6
0.4
0.2
0.
0.
0.5
1.
1.5
2.
p_T (GeV/c)
high multiplicity N_c

Fig. 10

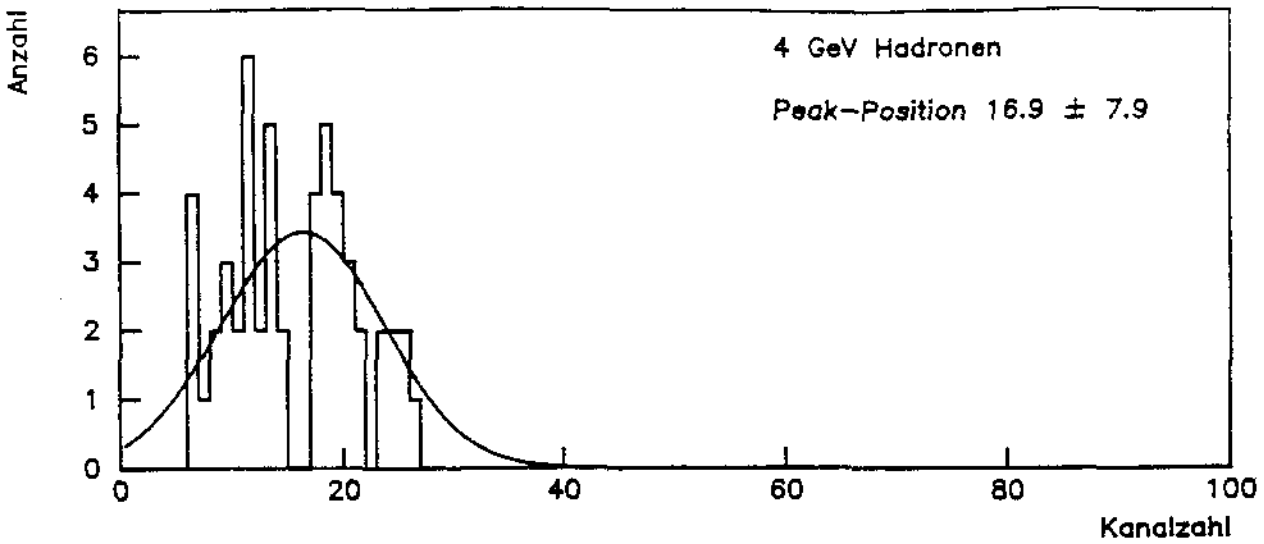

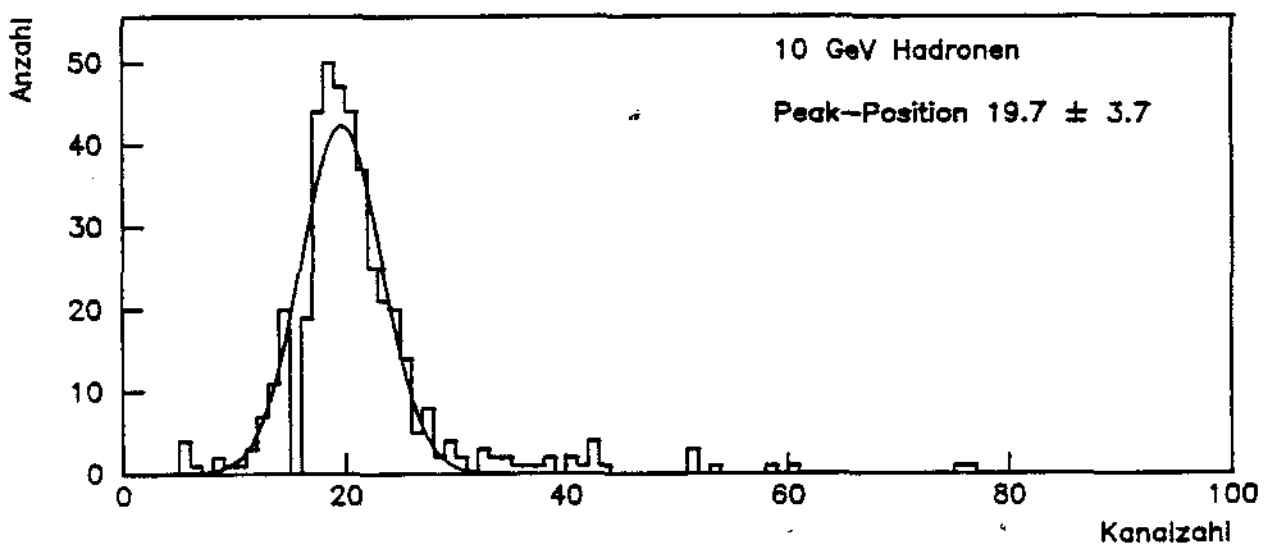

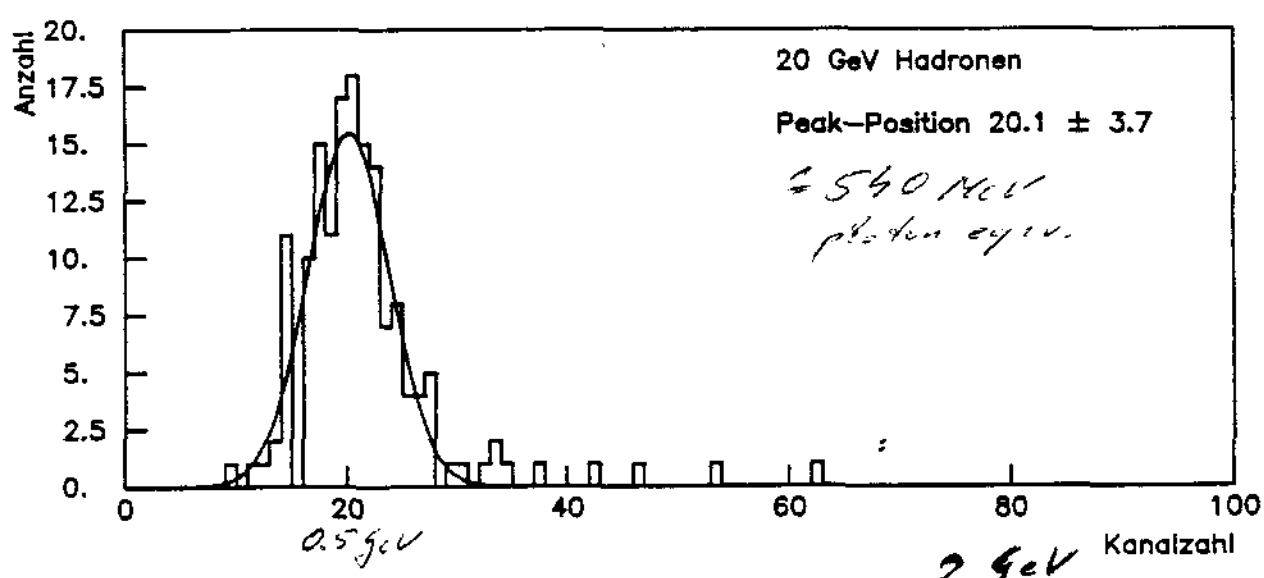

Abbildung 31. minimal-ionisierende Teilchen

SPS X1 spectrometer

Fig. 11

Hadron contamination of photons

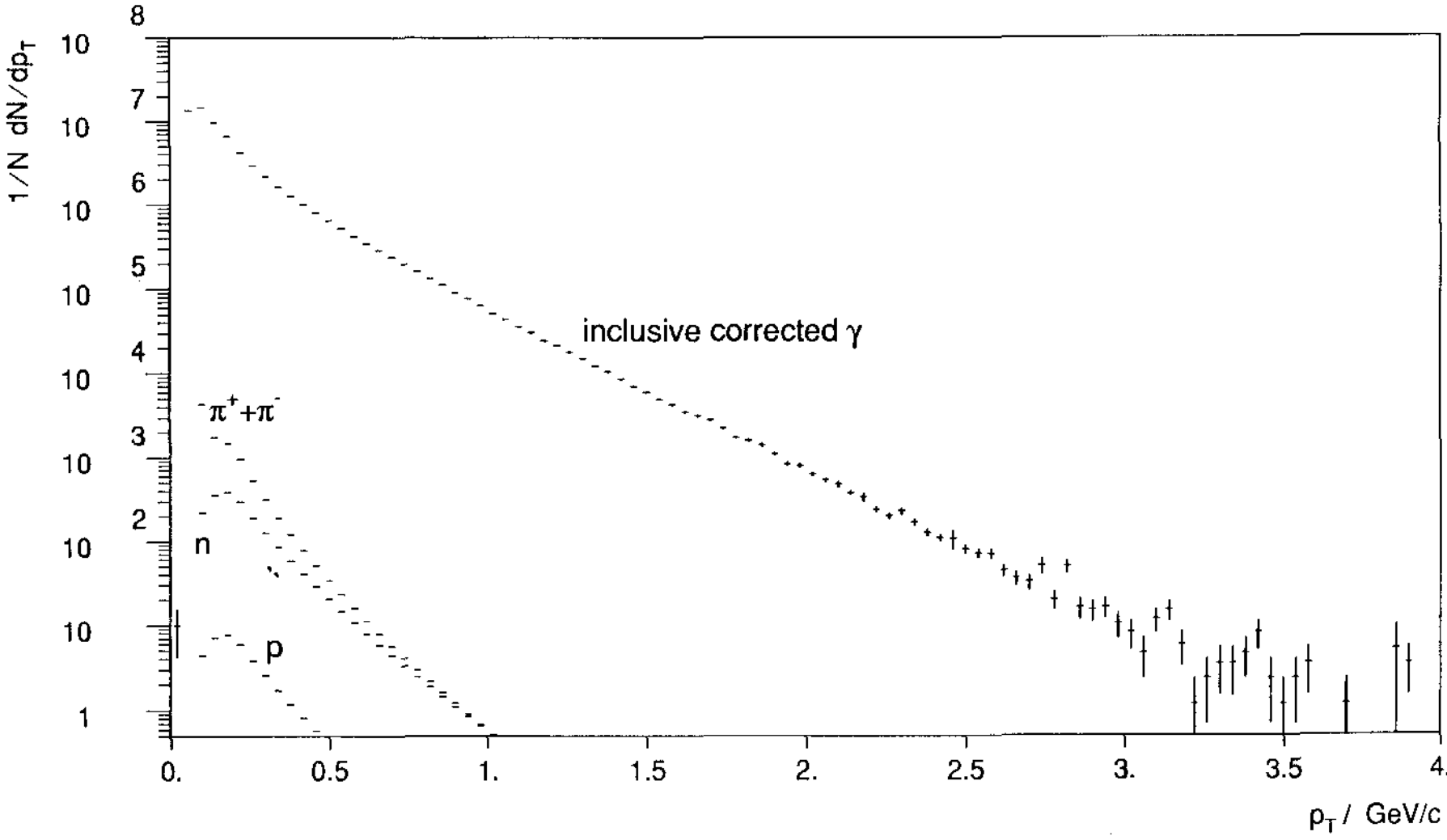

Fig 12

Fig 12

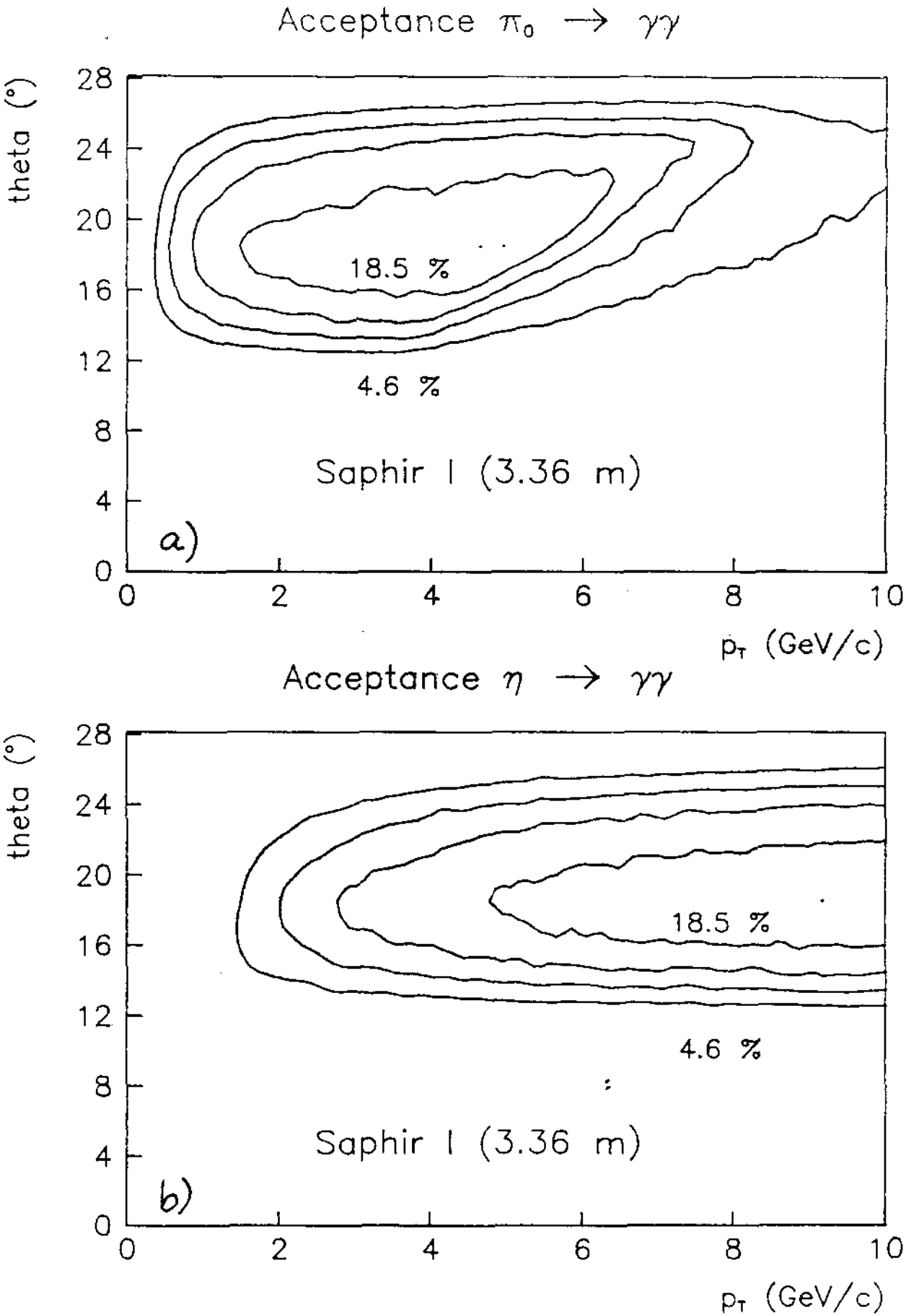
Acceptance $\pi_0 \rightarrow \gamma\gamma$
theta (°)
28
24
20
16
12
8
4
0
18.5 %
4.6 %
Saphir I (3.36 m)
a)
0
2
4
6
8
10
p_T (GeV/c)
Acceptance $\eta \rightarrow \gamma\gamma$
theta (°)
28
24
20
16
12
8
4
0
18.5 %
4.6 %
Saphir I (3.36 m)
b)
0
2
4
6
8
10
p_T (GeV/c)

Fig 13

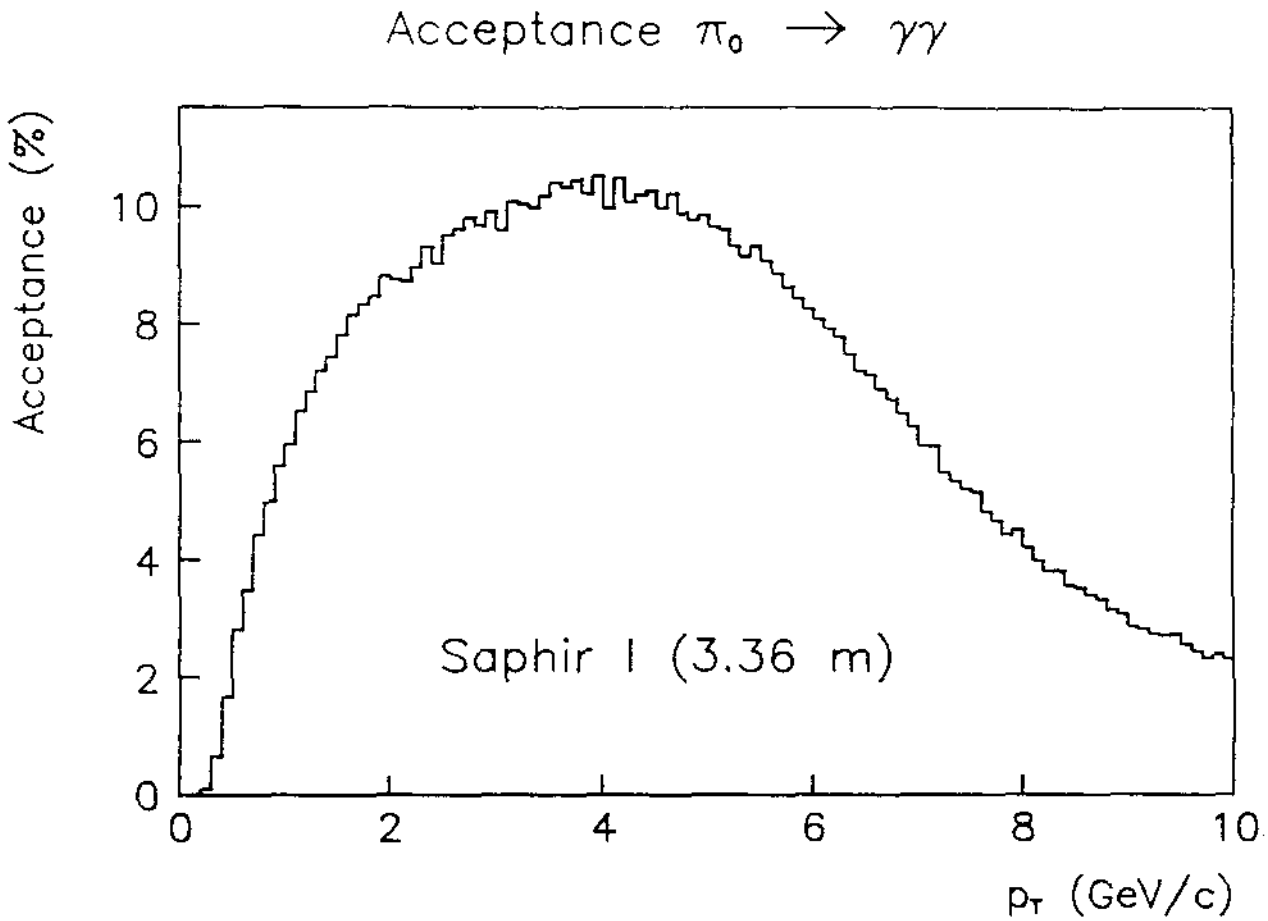
Acceptance $\pi_0 \rightarrow \gamma\gamma$
Acceptance (%)
10
8
6
4
2
0
0
2
4
6
8
10
Saphir I (3.36 m)
p_T (GeV/c)

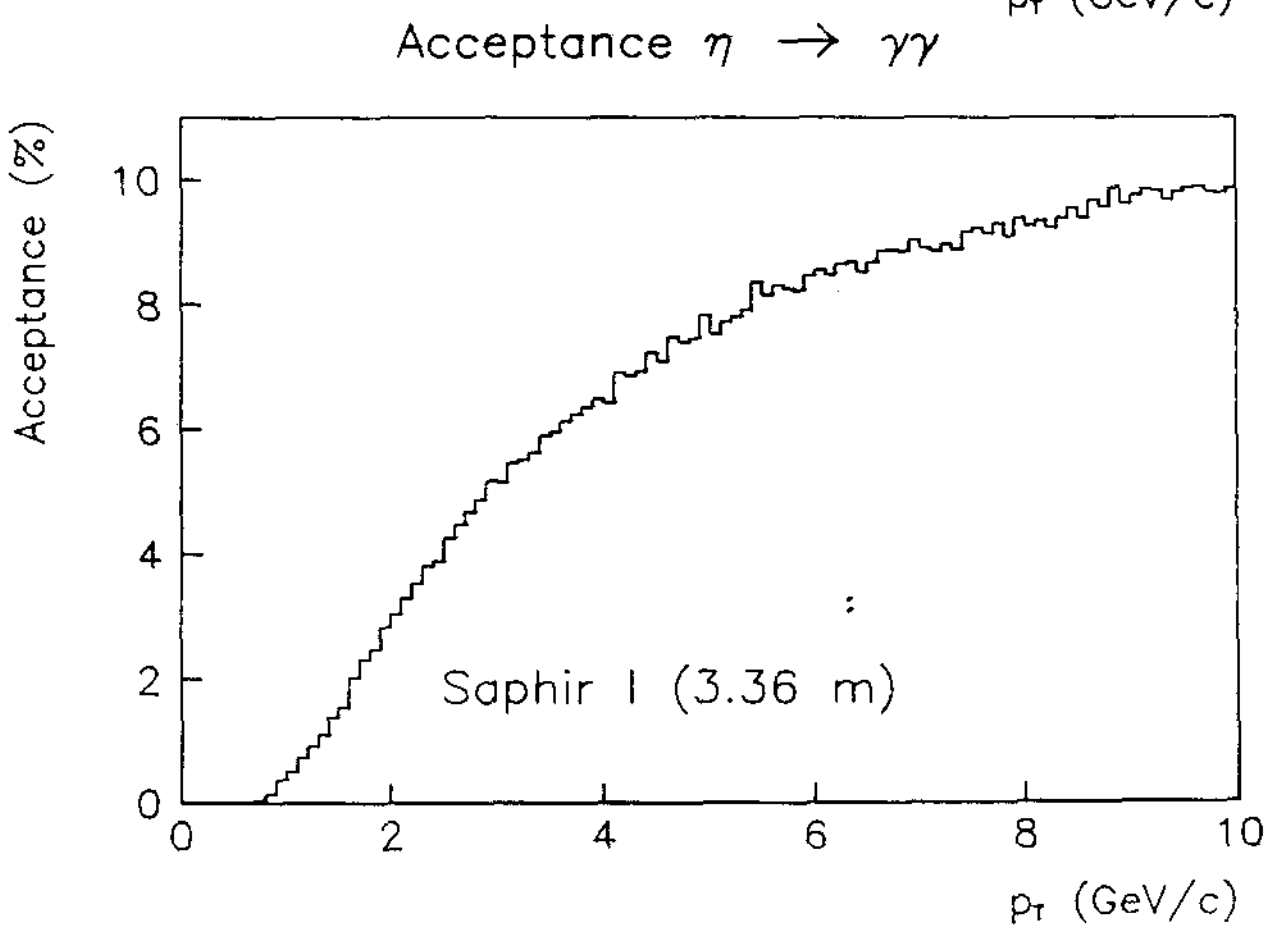
Acceptance $\eta \rightarrow \gamma\gamma$
Acceptance (%)
10
8
6
4
2
0
0
2
4
6
8
10
Saphir I (3.36 m)
p_T (GeV/c)

Fig 13 c

SAPHIR-I acceptance (Y=1.8)

All - accepted - rejected for E ≤ 0.4 GeV

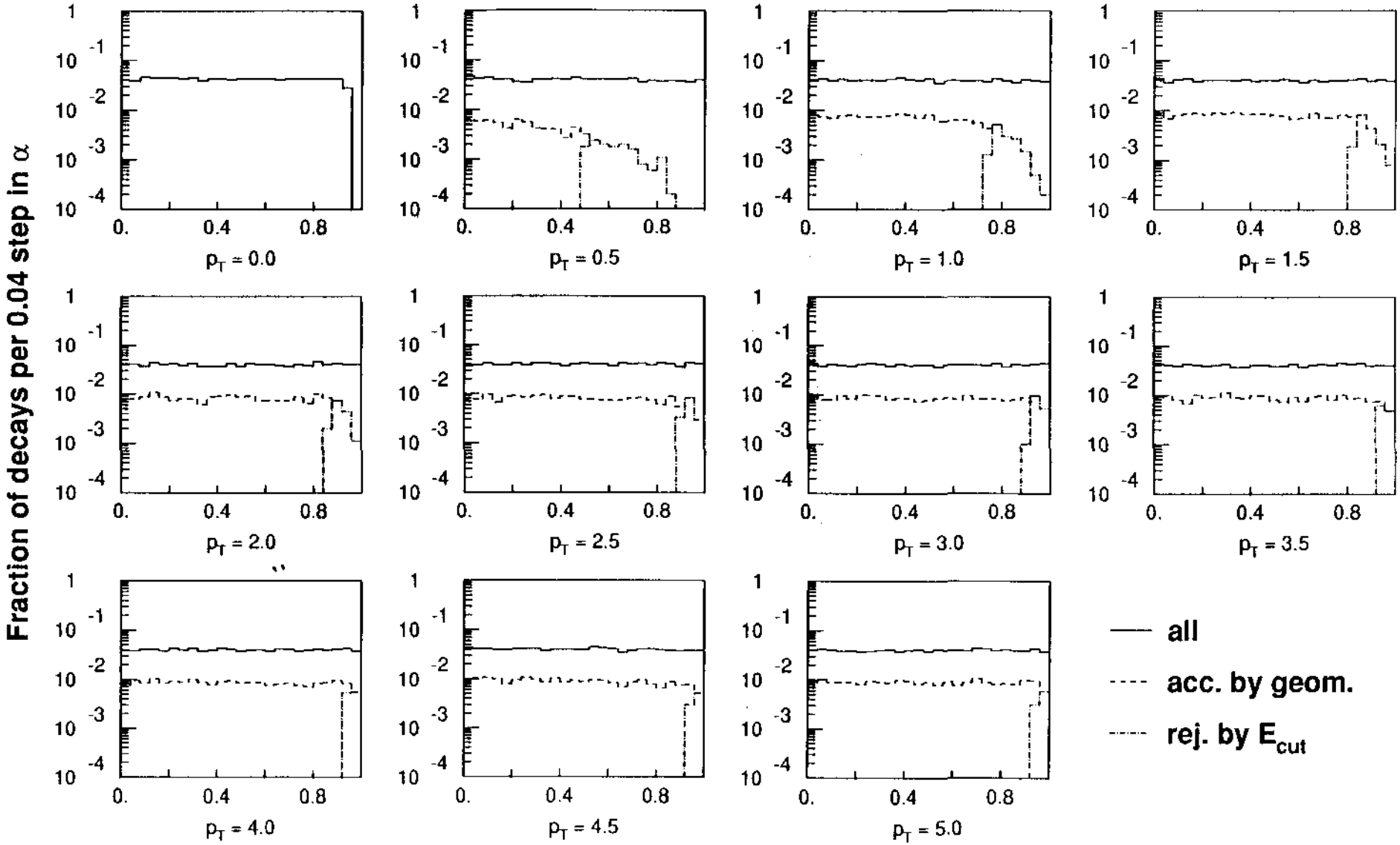

Fig 14

Fig 14

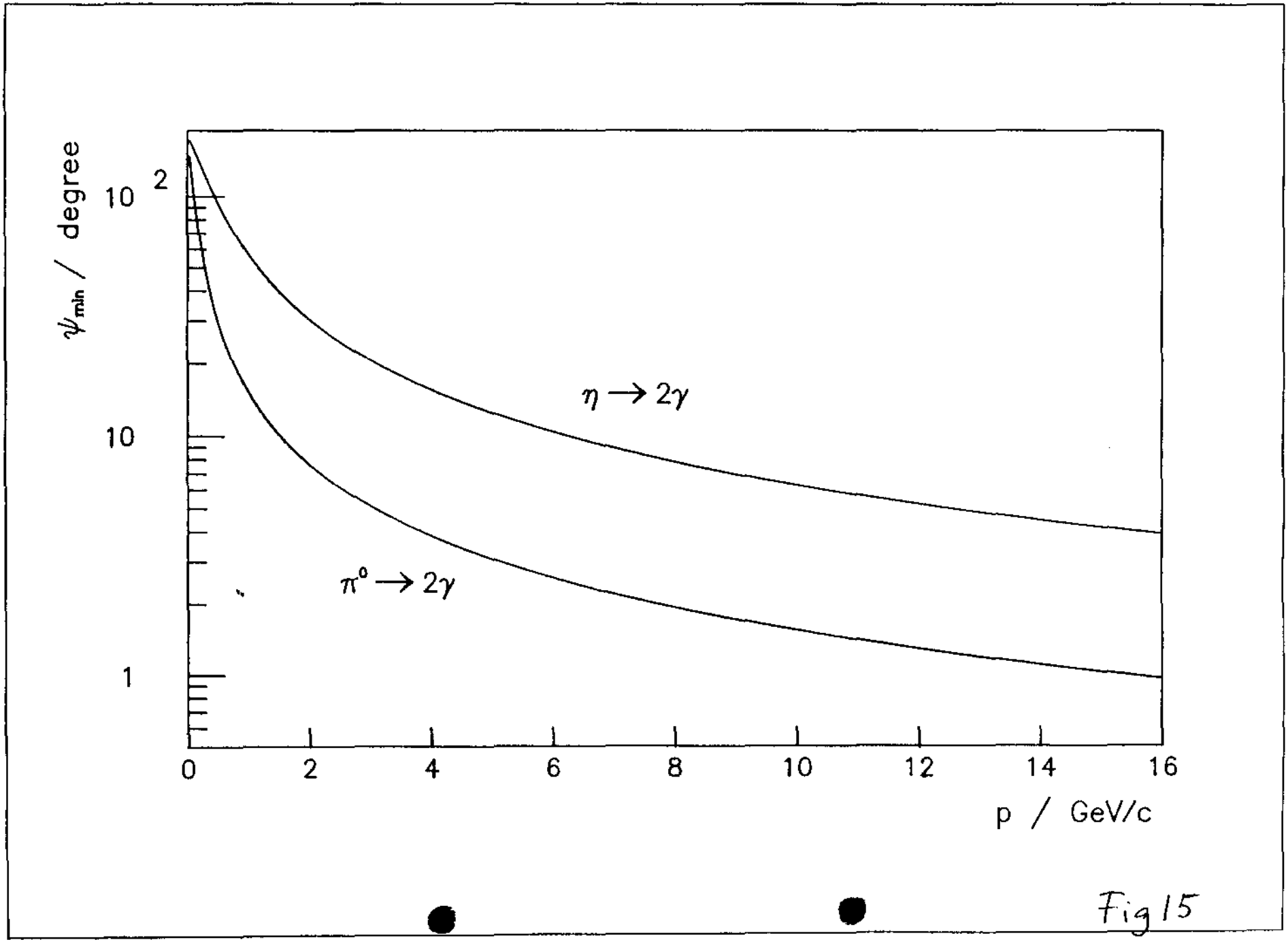
ψ_{min} / degree
2
10
10
1
$\eta \rightarrow 2\gamma$
$\pi^0 \rightarrow 2\gamma$
0
2
4
6
8
10
12
14
16
p / GeV/c

Fig 15

Fig 15

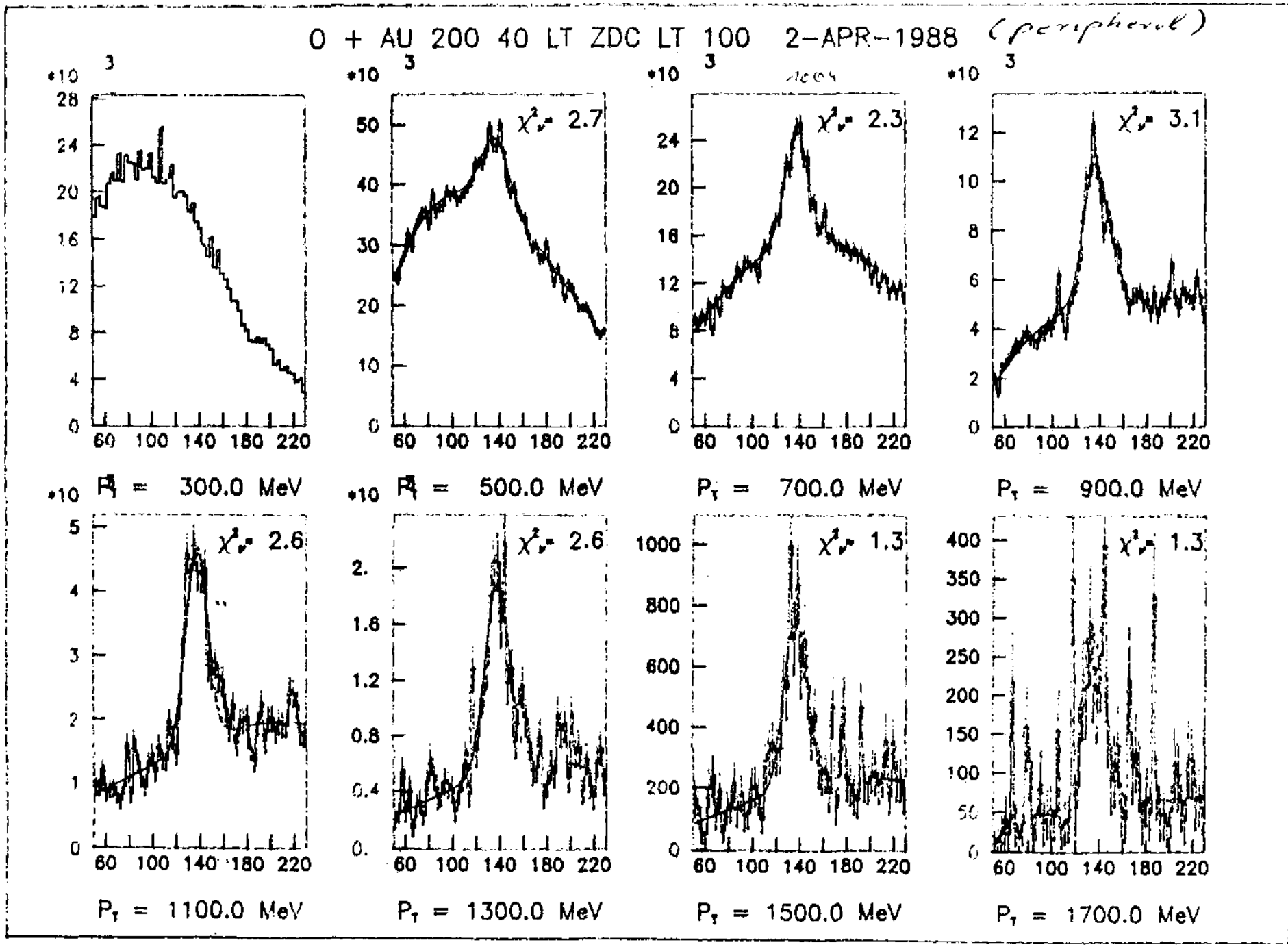
O + AU 200 40 LT ZDC LT 100 2-APR-1988 (peripheral)
χ^2_ν = 2.7
χ^2_ν = 2.3
χ^2_ν = 3.1
P_T = 300.0 MeV
P_T = 500.0 MeV
P_T = 700.0 MeV
P_T = 900.0 MeV
χ^2_ν = 2.6
χ^2_ν = 2.6
χ^2_ν = 1.3
χ^2_ν = 1.3
P_T = 1100.0 MeV
P_T = 1300.0 MeV
P_T = 1500.0 MeV
P_T = 1700.0 MeV

Fig 16a

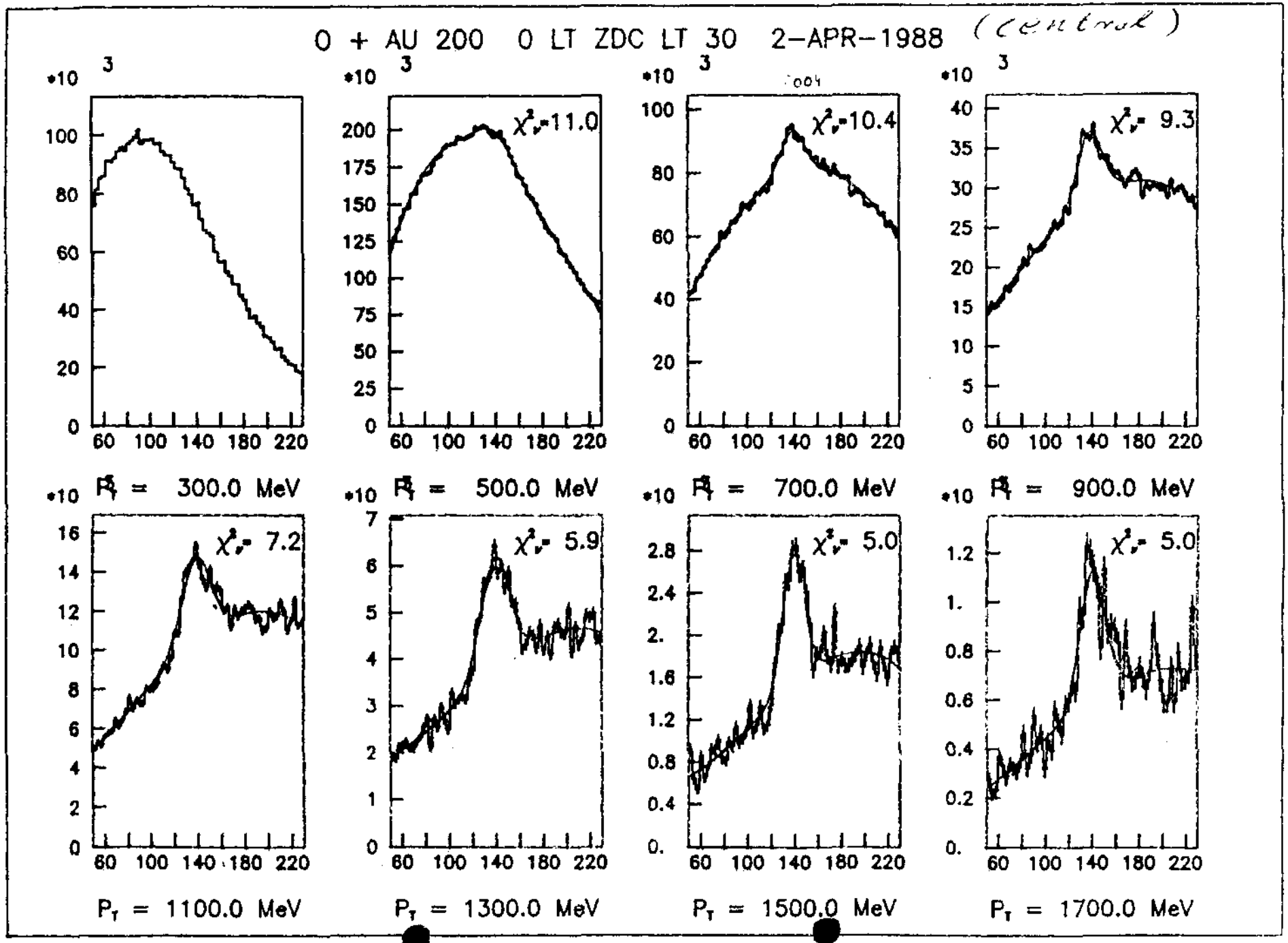
0 + AU 200 0 LT ZDC LT 30 2-APR-1988 (central)
*10 3
χ^2_ν=11.0
χ^2_ν=10.4
χ^2_ν= 9.3
P_T = 300.0 MeV
P_T = 500.0 MeV
P_T = 700.0 MeV
P_T = 900.0 MeV
χ^2_ν= 7.2
χ^2_ν= 5.9
χ^2_ν= 5.0
χ^2_ν= 5.0
P_T = 1100.0 MeV
P_T = 1300.0 MeV
P_T = 1500.0 MeV
P_T = 1700.0 MeV

Fig 16

200 A GeV O + Au

minimum bias

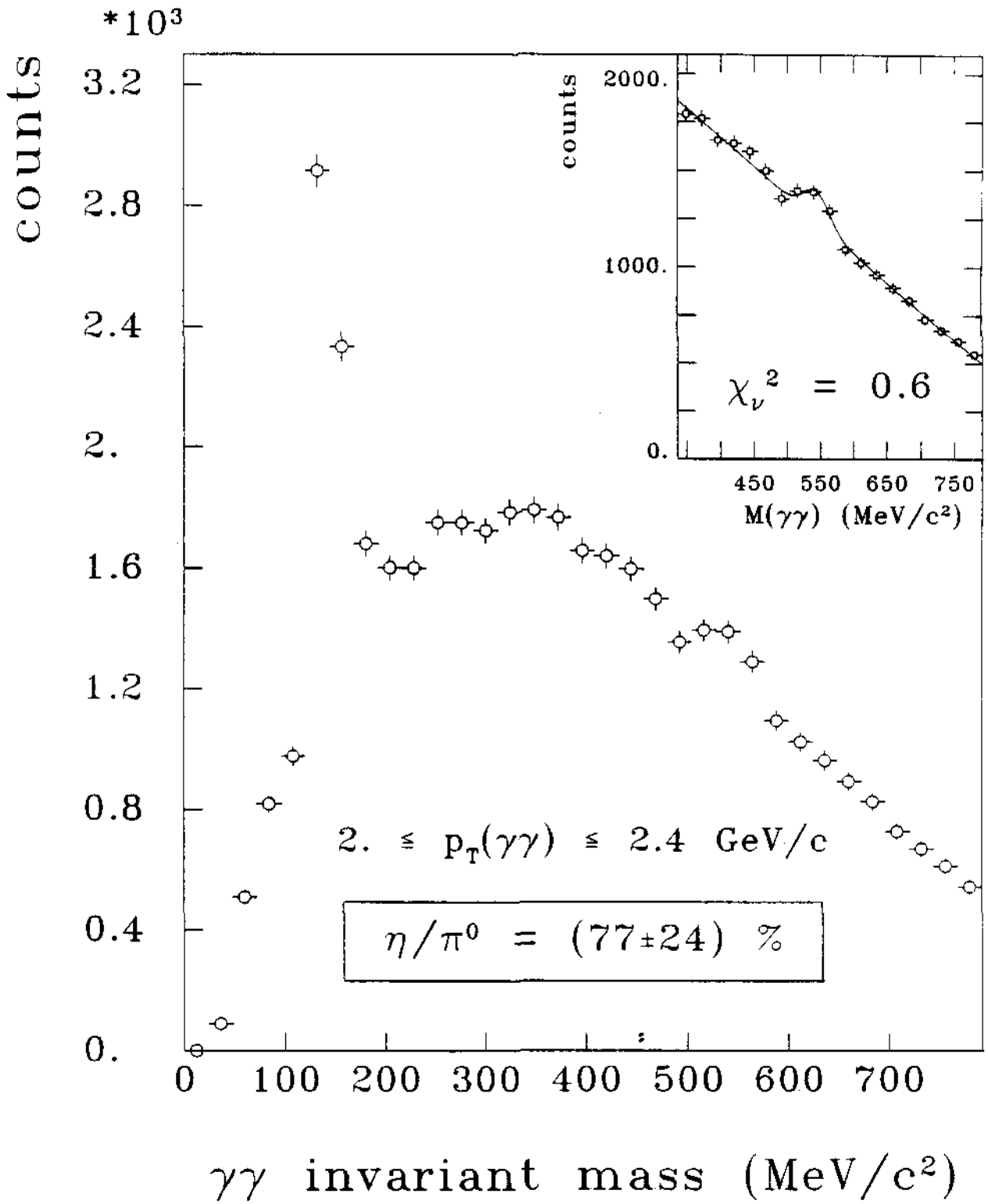

Fig 17

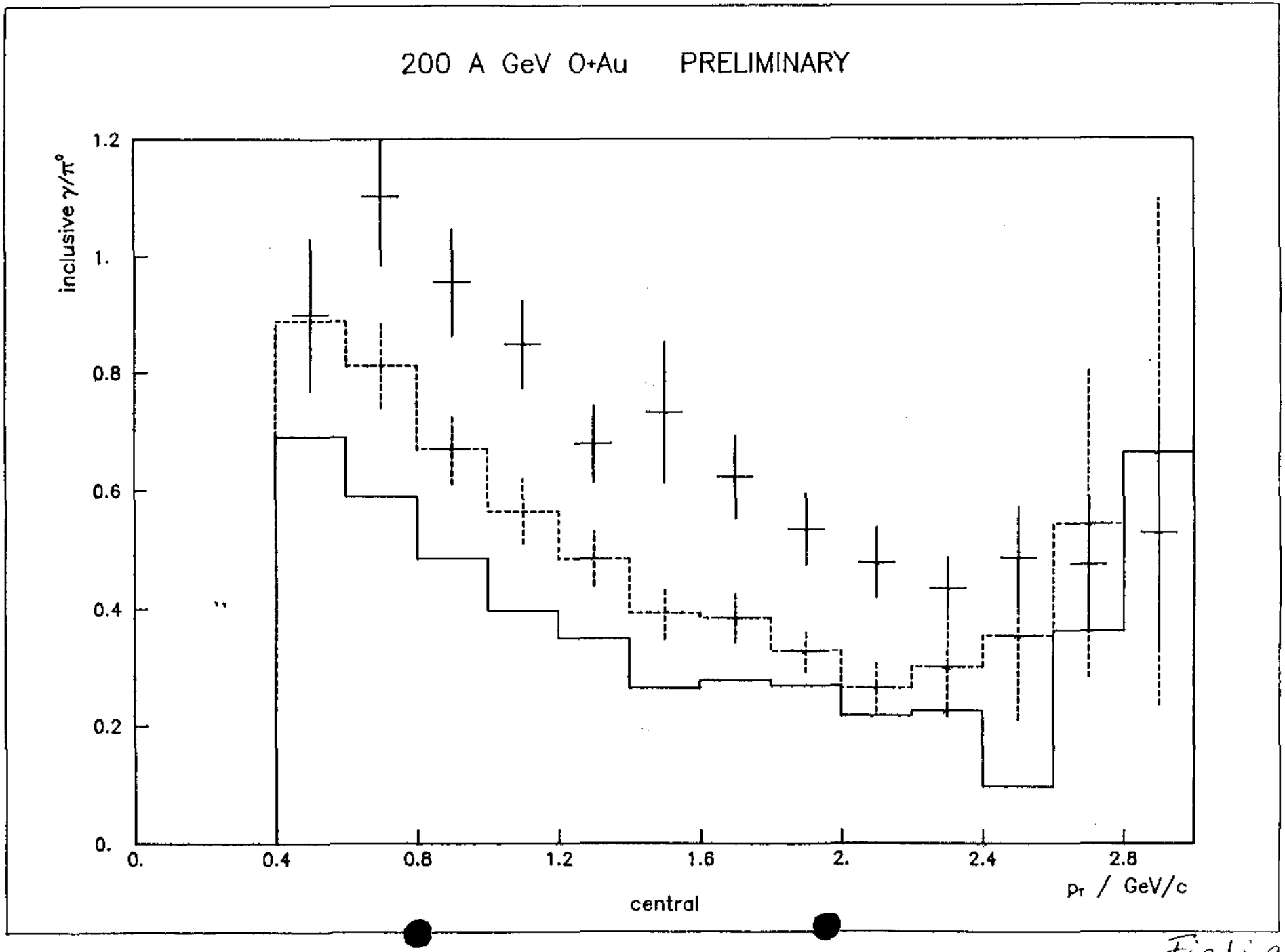

Fig 18a

Figlia

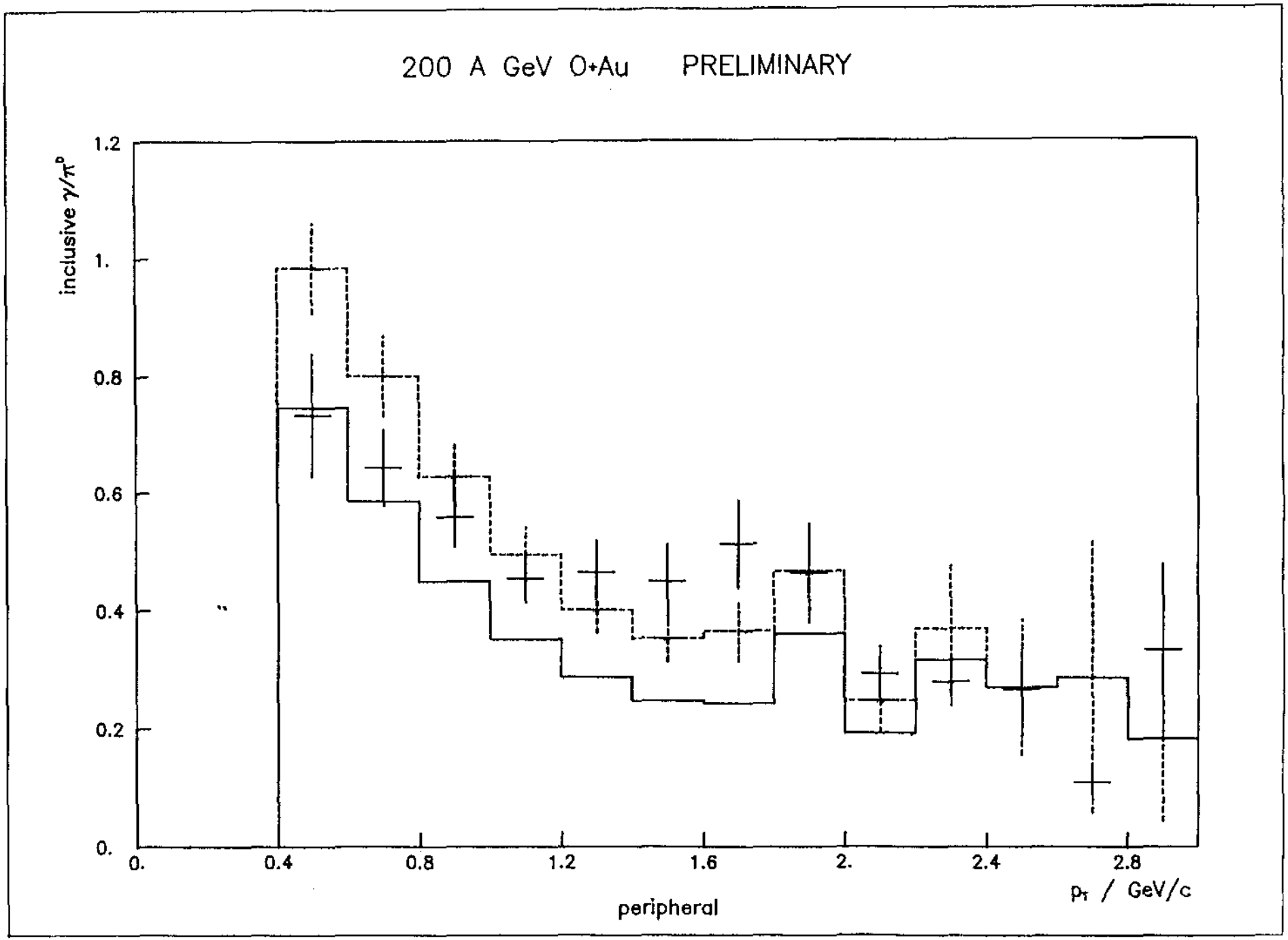

Fig 18a

Fig 18b

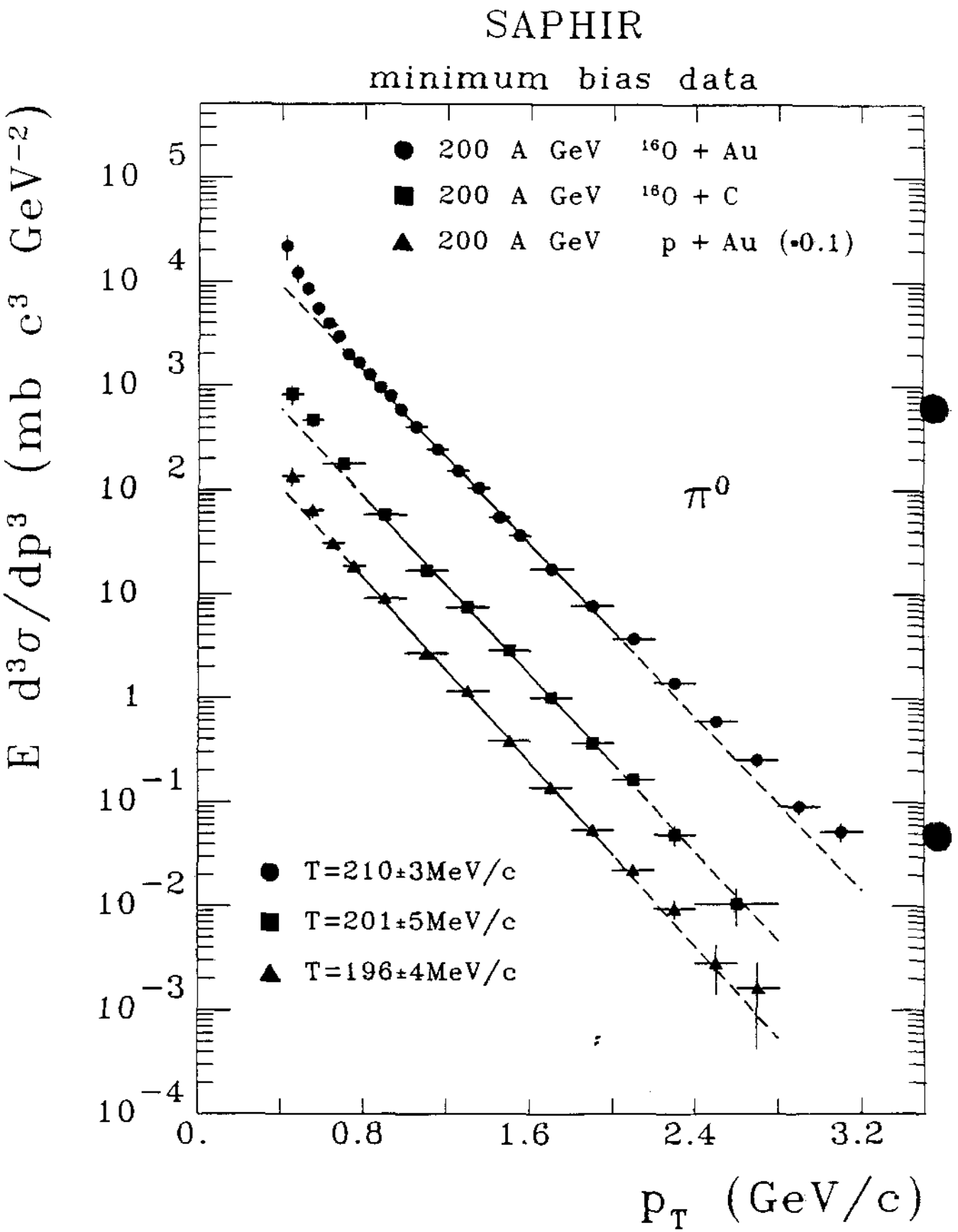
SAPHIR
minimum bias data
200 A GeV ^{16}O + Au
200 A GeV ^{16}O + C
200 A GeV p + Au (•0.1)
π^0
T=210±3MeV/c
T=201±5MeV/c
T=196±4MeV/c
E d$^3\sigma$/dp^3 (mb c^3 GeV^{-2})
10^5
10^4
10^3
10^2
10
1
10^{-1}
10^{-2}
10^{-3}
10^{-4}
0.
0.8
1.6
2.4
3.2
p_T (GeV/c)

Fig 19a

200 A GeV O + Au

ZDC-dependence

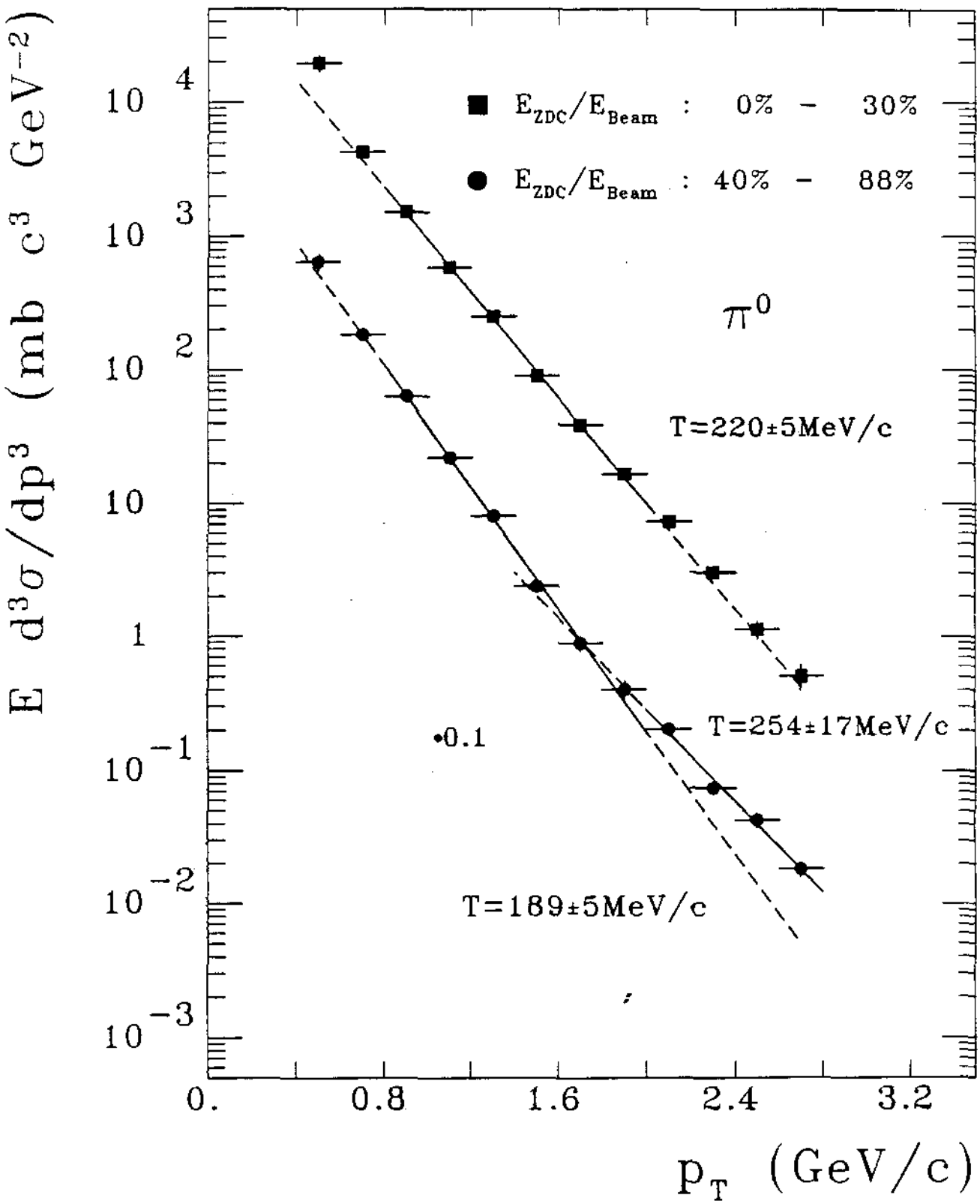

Fig 19 b

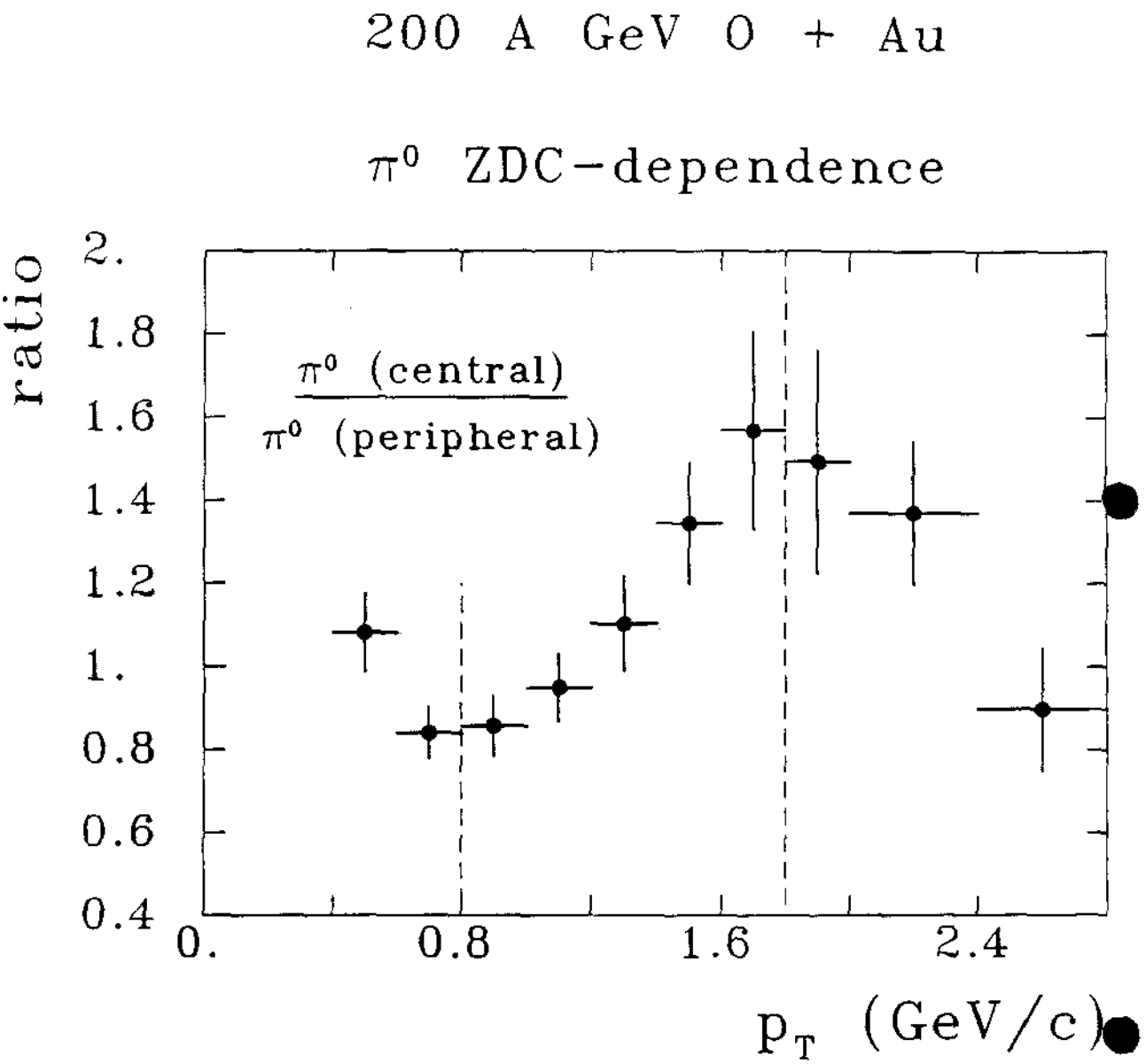
200 A GeV O + Au
π⁰ ZDC-dependence
ratio
2.
1.8
1.6
1.4
1.2
1.
0.8
0.6
0.4
π⁰ (central)
π⁰ (peripheral)
0.
0.8
1.6
2.4
p_T (GeV/c)

Fig 20

SAPHIR: Target-in vs Target-out

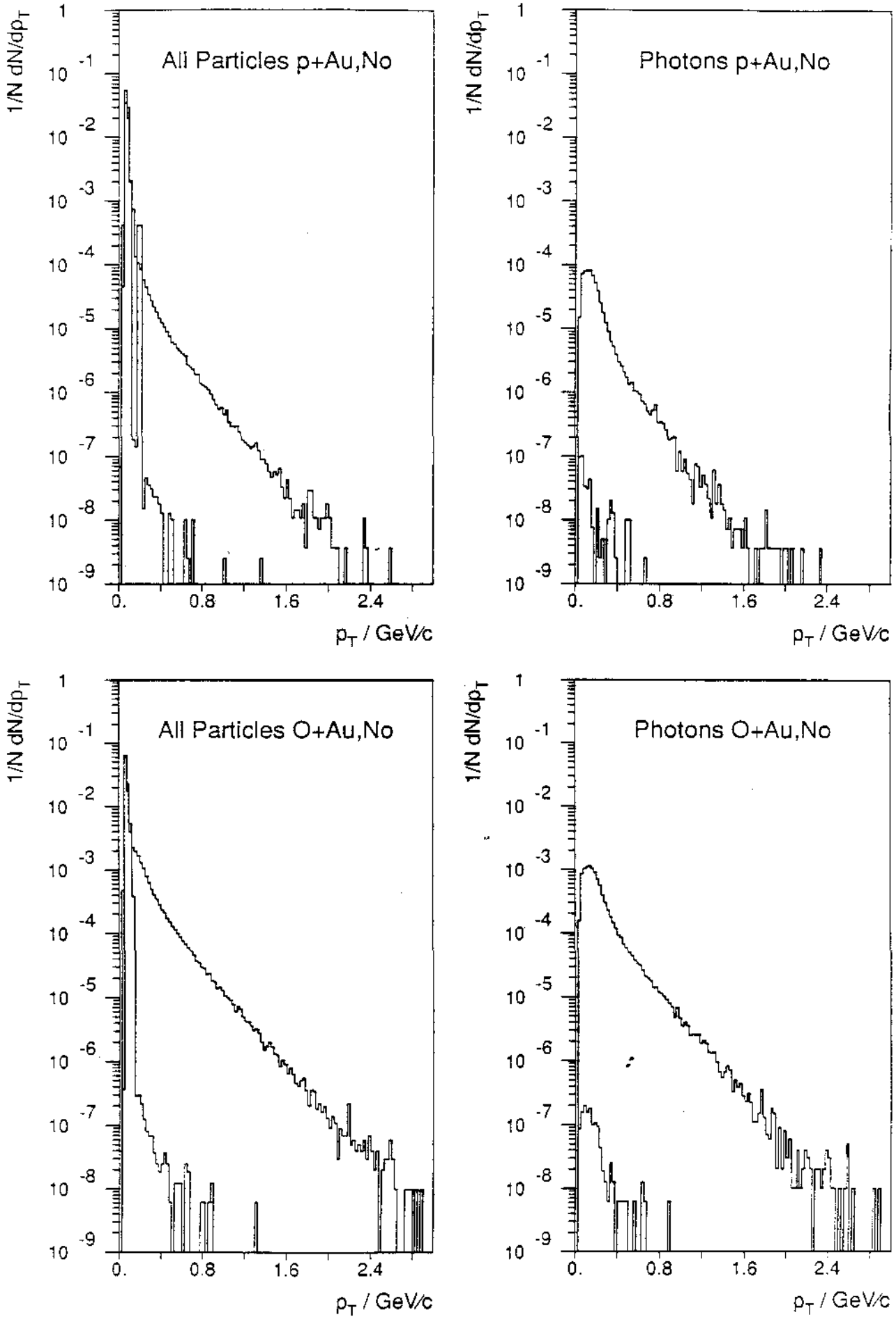

Fig 21

SAPHIR I+II setup

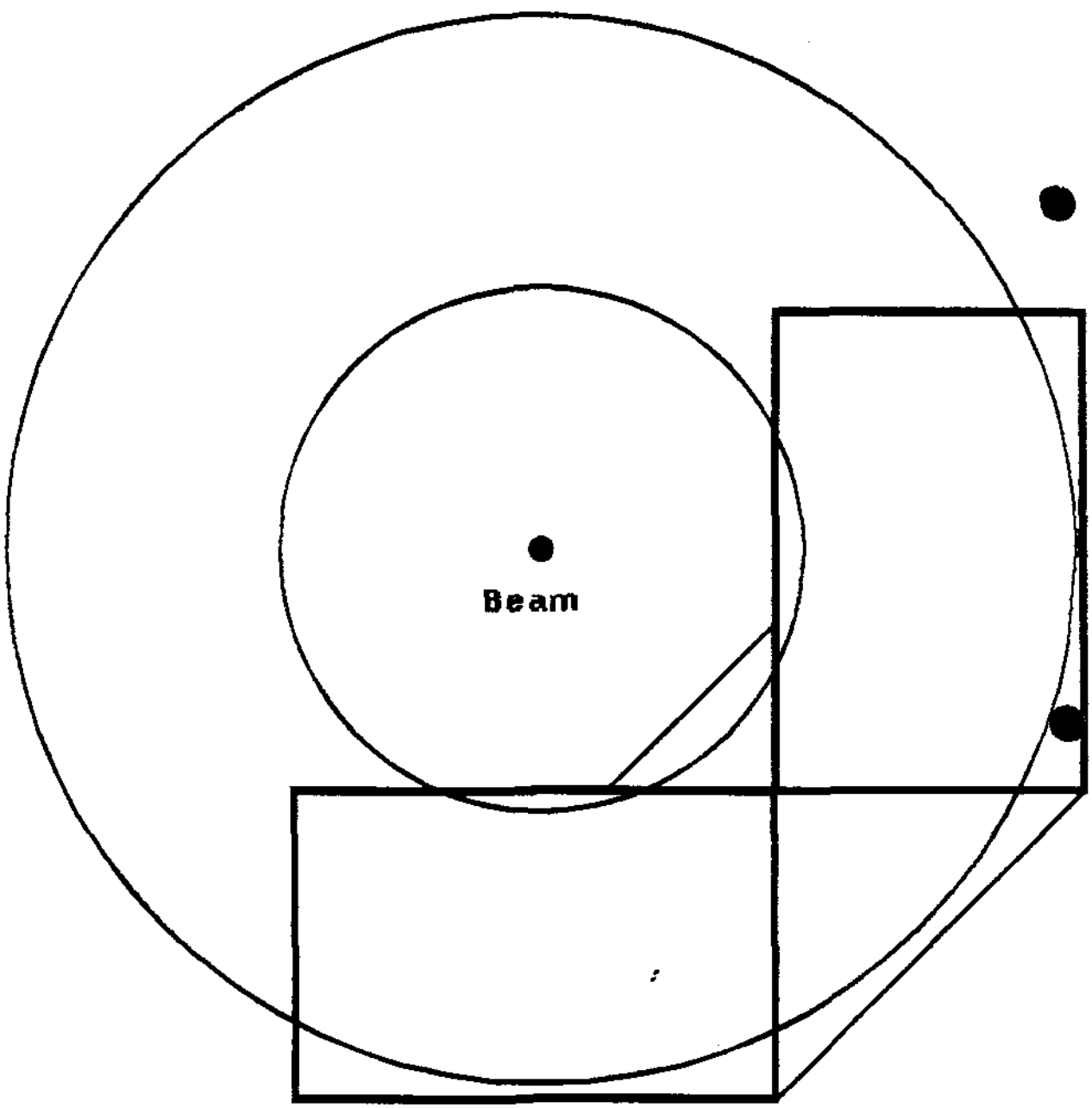

Fig 22

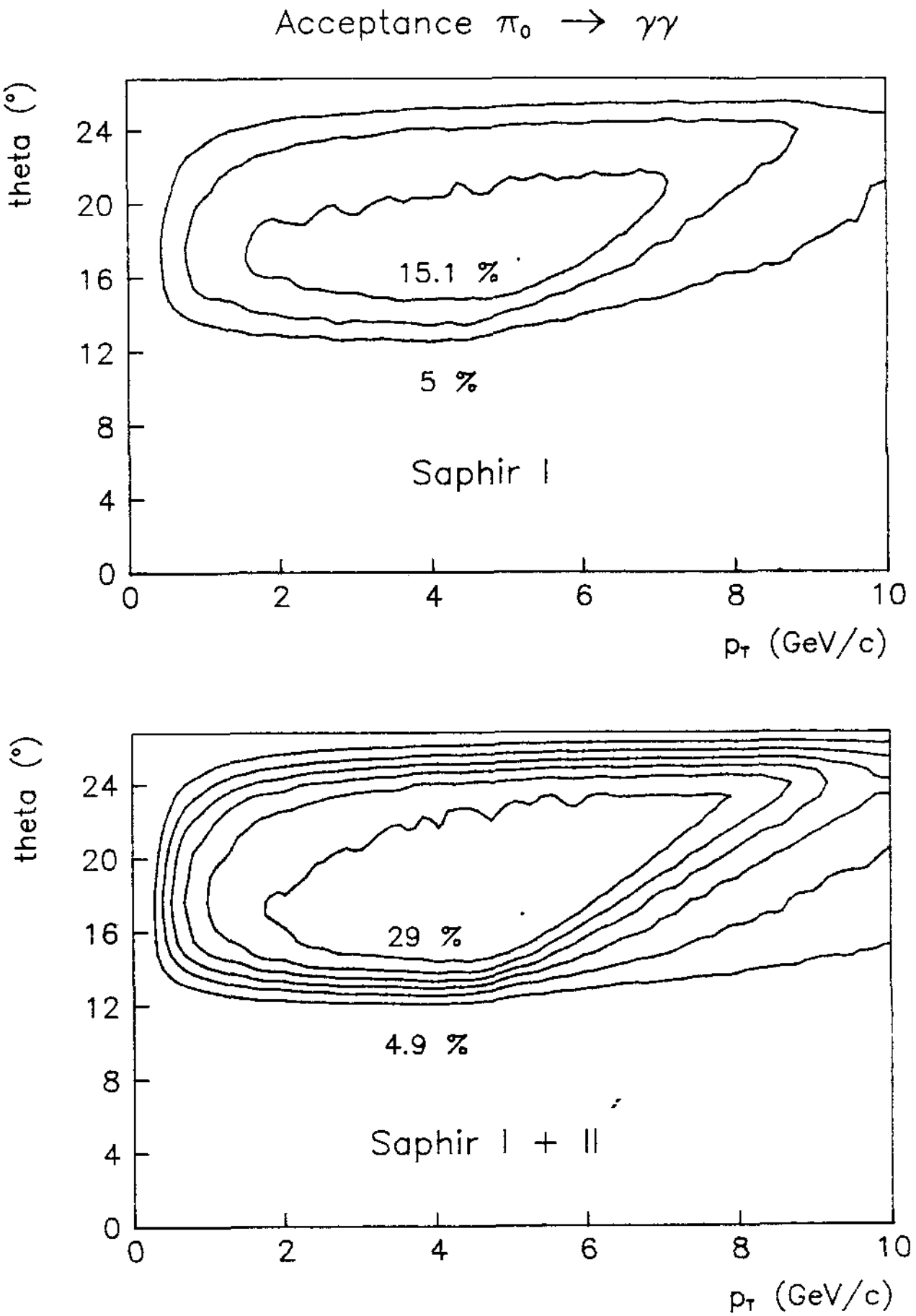
Acceptance $\pi_0 \rightarrow \gamma\gamma$
theta (°)
24
20
16
12
8
4
0
15.1 %
5 %
Saphir I
0
2
4
6
8
10
p_T (GeV/c)
theta (°)
24
20
16
12
8
4
0
29 %
4.9 %
Saphir I + II
0
2
4
6
8
10
p_T (GeV/c)

Fig 23a

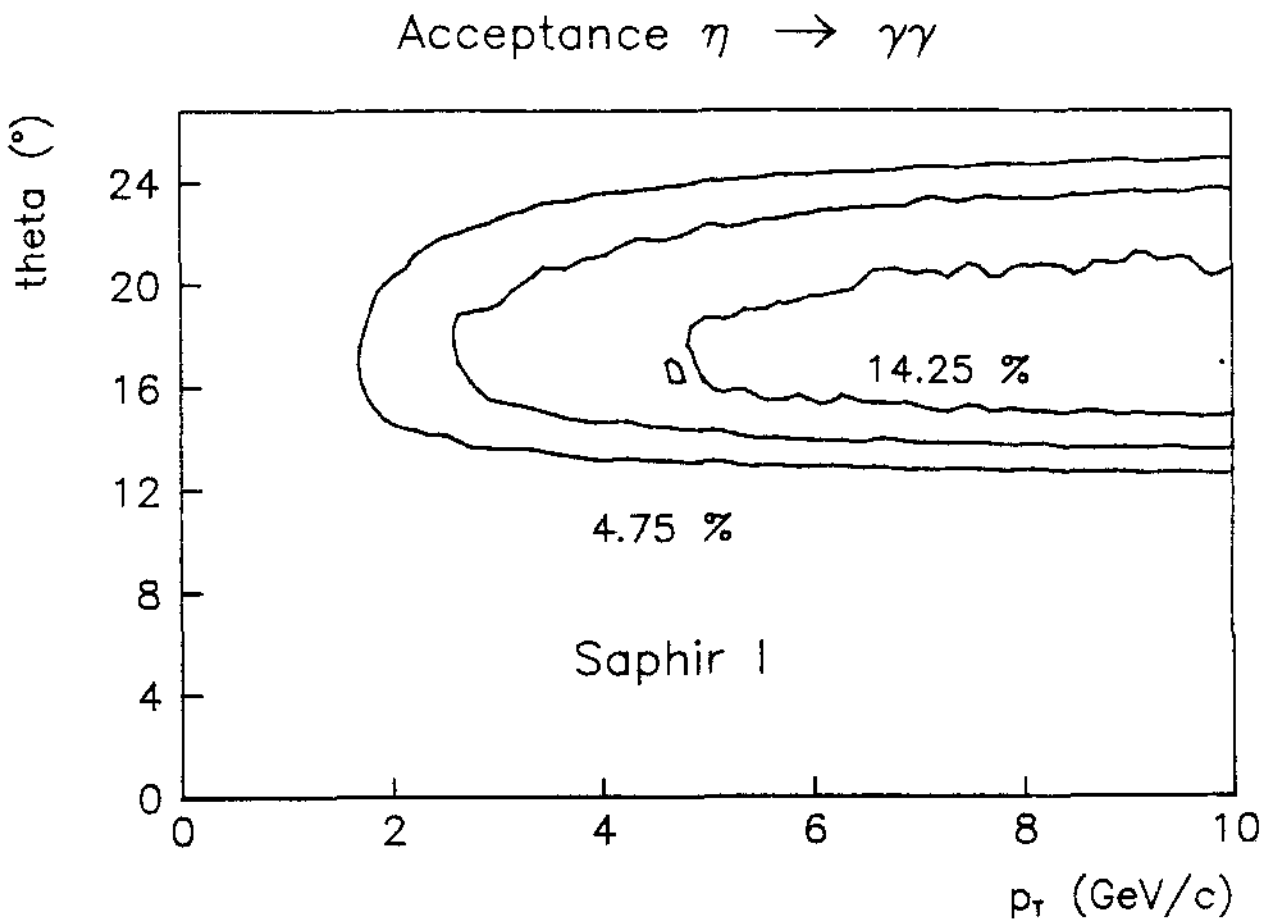
Acceptance $\eta \rightarrow \gamma\gamma$
theta (°)
24
20
16
12
8
4
0
0
2
4
6
8
10
p_T (GeV/c)
14.25 %
4.75 %
Saphir I

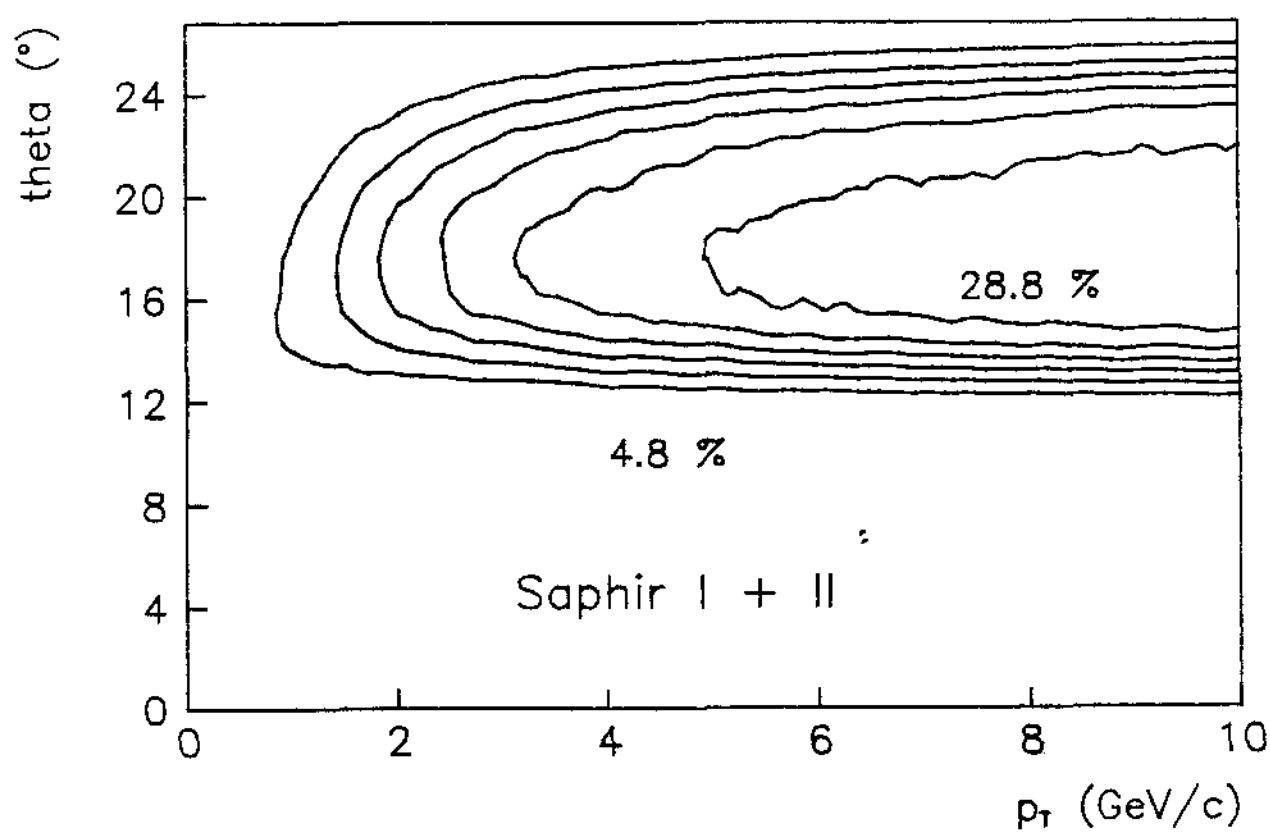
theta (°)
24
20
16
12
8
4
0
0
2
4
6
8
10
p_T (GeV/c)
28.8 %
4.8 %
Saphir I + II

Fig 23b

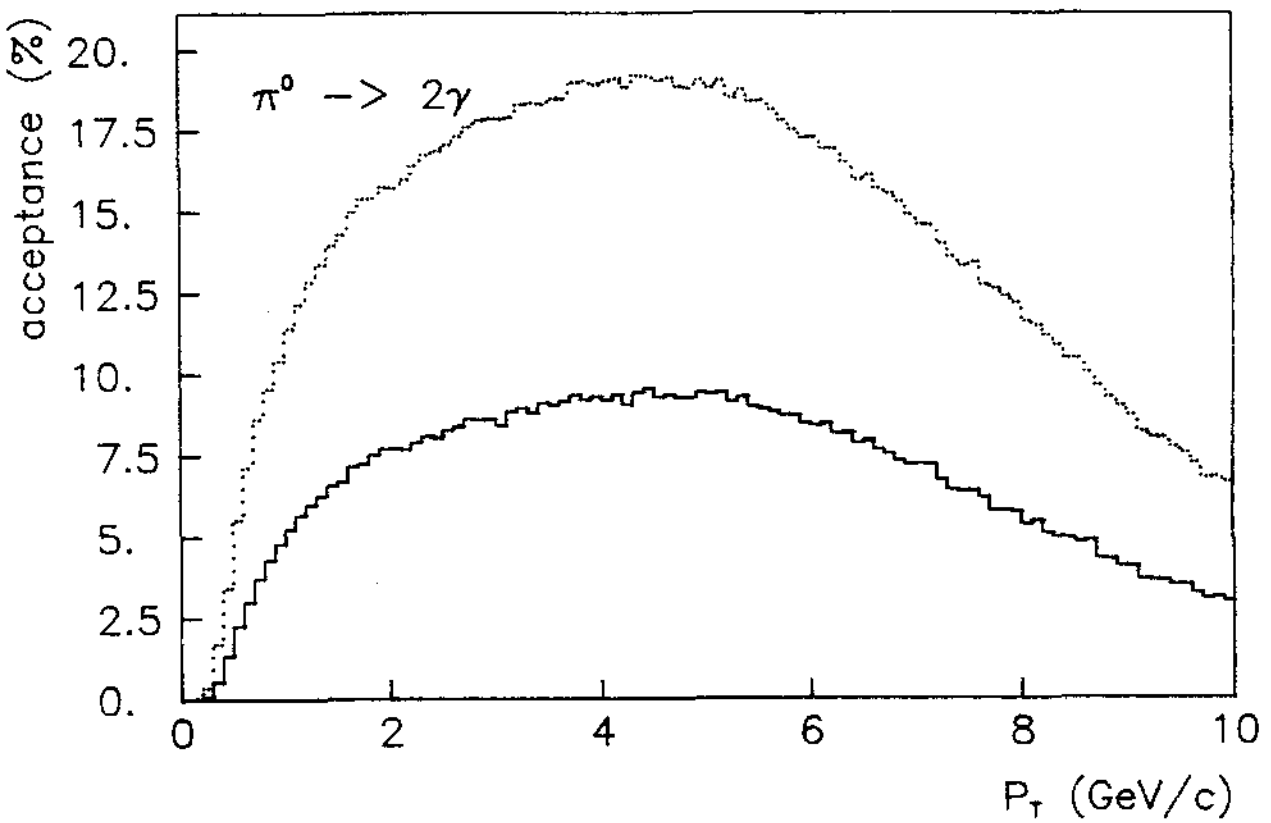
acceptance (%)
20.
17.5
15.
12.5
10.
7.5
5.
2.5
0.
π^0 -> 2γ
0
2
4
6
8
10
P_T (GeV/c)

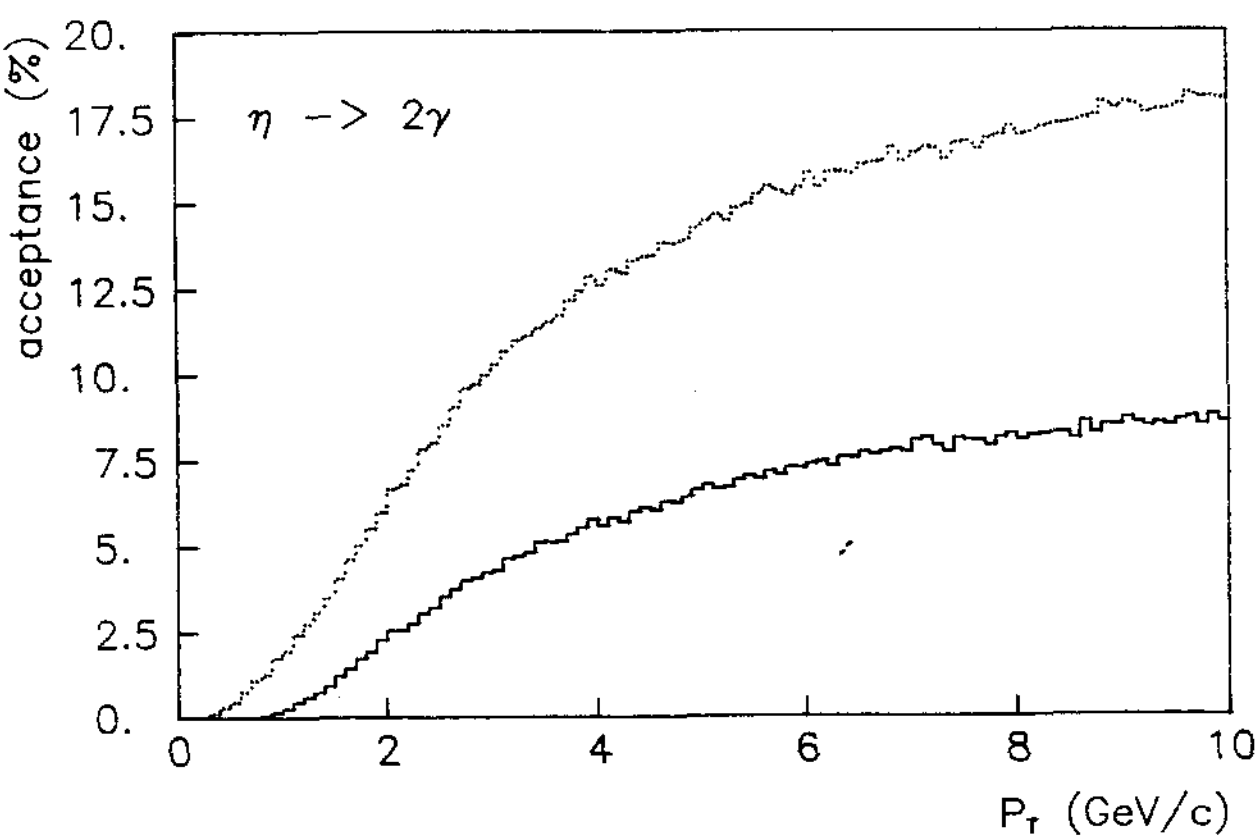
acceptance (%)
20.
17.5
15.
12.5
10.
7.5
5.
2.5
0.
η -> 2γ
0
2
4
6
8
10
P_T (GeV/c)

Fig 24

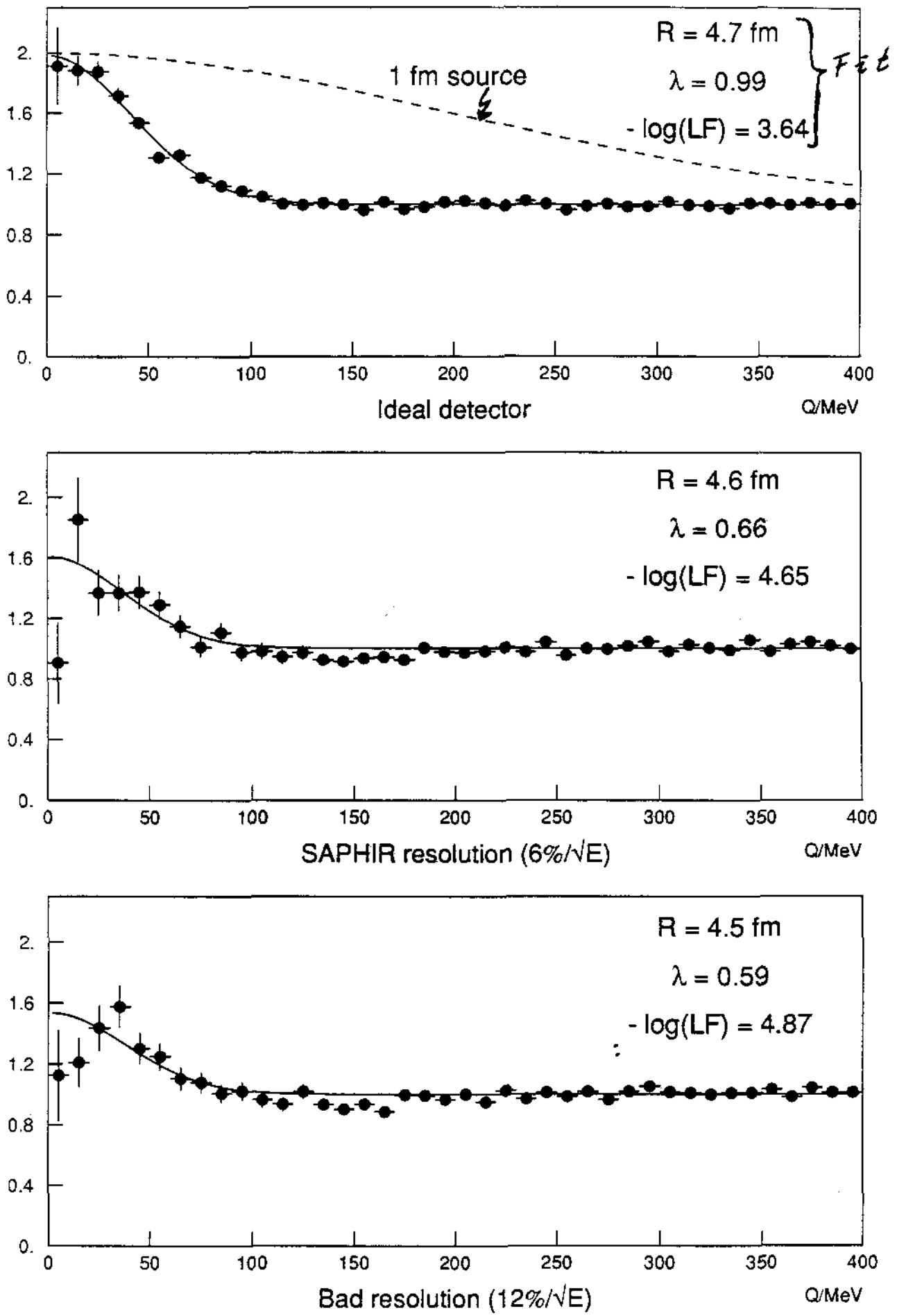
SAPHIR: π^0-π^0-correlations
R = 4.7 fm
λ = 0.99
- log(LF) = 3.64
Fit
1 fm source
Ideal detector
Q/MeV
R = 4.6 fm
λ = 0.66
- log(LF) = 4.65
SAPHIR resolution (6%/√E)
Q/MeV
R = 4.5 fm
λ = 0.59
- log(LF) = 4.87
Bad resolution (12%/√E)
Q/MeV

Fig 25

WA 80

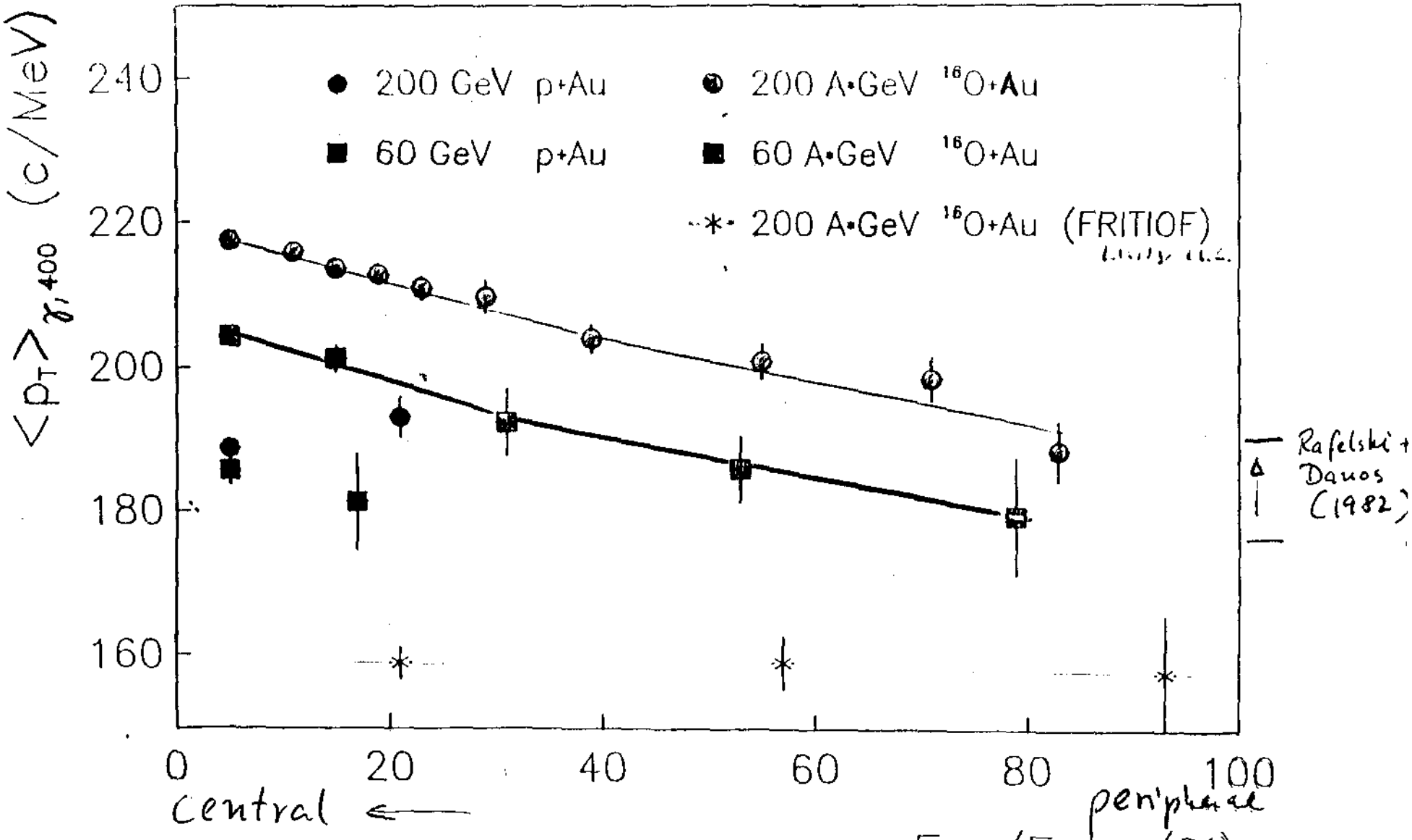
200 GeV p+Au
60 GeV p+Au
200 A·GeV ^{16}O+Au
60 A·GeV ^{16}O+Au
200 A·GeV ^{16}O+Au (FRITIOF)
$\langle p_T \rangle_{\gamma,400}$ (c/MeV)
240
220
200
180
160
0
20
40
60
80
100
central ←
peripheral
E_{ZDC}/E_{Beam} (%)
Rafelski + Danos (1982)

Fig 26